

Copyright  
by  
Gang Qiang Li  
2008

**The Dissertation Committee for Gang Qiang Li Certifies that this is the approved  
version of the following dissertation:**

**THE EXPRESSION OF MUSCARINIC ACETYLCHOLINE  
RECEPTORS ON THE AVIAN VESTIBULAR HAIR CELLS AND  
THE MODULATION EFFECTS ON KIR2.1**

**Committee:**

---

Manning J. Correia, Ph.D., Supervisor

---

Malcolm S. Brodwick, Ph.D.

---

Joseph C. Holt, Ph.D.

---

Golda A. Leonard, Ph.D.

---

Robert B. Leonard, Ph.D.

---

S.V. Penelope Jones, Ph.D.

---

Thomas G. Wood, Ph.D.

---

---

Dean, Graduate School

**THE EXPRESSION OF MUSCARINIC ACETYLCHOLINE  
RECEPTORS ON THE AVIAN VESTIBULAR HAIR CELLS AND  
THE MODULATION EFFECTS ON KIR2.1**

**by**

**Gang Qiang Li, M.D.**

**Dissertation**

Presented to the Faculty of the Graduate School of  
The University of Texas Medical Branch  
in Partial Fulfillment  
of the Requirements  
for the Degree of

**Doctor of Philosophy**

**The University of Texas Medical Branch**

**December, 2008**

## **Dedication**

I would like to use this opportunity to thank my parents who greatly supported my dream to study in the USA; my lovely wife, Jian W. Fu, who has stood by my side all these years and gives me courage; and my family members, all my friends and others who helped me during my Ph.D. studies.

## **Acknowledgements**

Acknowledgements - I thank Claudia Starr for her expert help in preparing thin sections for TEM. This work was supported in part by NIH Grants DC01273 to MJC and DC04070 to GAK<sup>1</sup>

---

<sup>1</sup> Li GQ, Kevetter GA, Leonard RB, Prusak DJ, Wood TG, Correia MJ (2007) Muscarinic acetylcholine receptor subtype expression in avian vestibular hair cells, nerve terminals and ganglion cells. *Neuroscience* 146: 384-402.

# **THE EXPRESSION OF MUSCARINIC ACETYLCHOLINE RECEPTORS ON THE AVIAN VESTIBULAR HAIR CELLS AND THE MODULATION EFFECTS ON KIR2.1**

Publication No. \_\_\_\_\_

Gang Qiang Li, M.D., Ph.D.

The University of Texas Medical Branch, 2008

Supervisor: Manning J. Correia

The major neurotransmitter released from the vestibular efferent terminals onto hair cells is acetylcholine (ACh). Two types of acetylcholine receptors (AChRs) have been suggested to be located on hair cells (HCs). They were nicotinic receptors (nAChRs) and muscarinic receptors (mAChRs). Even though pioneering physiological and pharmacological studies have shown evidence of mAChR located on the HCs, the protein expression and the role of muscarinic acetylcholine receptor (mAChR) in HCs have not been carefully studied. Our preliminary data indicated that the activation of mAChRs on pigeon vestibular type II HCs produced an inhibitory effect on an inward rectifier potassium channel, Kir2.1. Using immunohistochemical, immunocytochemical, and Western blot techniques, we demonstrated for the first time, the expression and co-expression of mAChR subtypes M1-M5 on the peripheral vestibular structures, including hair cells, supporting cells, ganglion, and other neural elements. To better understand the modulation effects of mAChR activation on Kir2.1 channels, the heterologous expression system (HES) was used to express a single mAChR subtype and Kir2.1. The expression plasmids for M3 or M5 mAChR subtype were co-transfected with pKir2.1 into the mammalian cell line tsA201 cells and electrophysiological studies including whole cell voltage clamp and current clamp were performed. Muscarinic receptor agonist (CCh) application to the tsA201 cells transfected with M3&pKir2.1 or M5&pKir2.1 exhibited concentration- and time- dependent facilitatory and/or inhibitory effects on the pKir2.1 channels. These effects depolarized or hyperpolarized the cell membrane potential, respectively. Further electrophysiological experiments were performed on native isolated

avian (pigeon) vestibular HCs. Whole cell patch clamp on both type I and type II HCs indicated that mAChR activation decreased both inward and outward current (type I & type II) which consequently produced hyperpolarization (type II) and depolarization (type I & type II). We also noticed that nAChR activation increased the outward current (type I & type II) and inward current (type II) which hyperpolarized the membrane potential (type I & type II) or depolarized the membrane potential (type II). In conclusion, mAChR played a role in the control of membrane potentials by modulating the ionic channels. The mechanism of mAChR induced effects is still unknown.

## Table of Contents

List of Tables (1-7) .....	xi
List of Figures (1-30) .....	xii
 <b>THE EXPRESSION OF MUSCARINIC ACETYLCHOLINE RECEPTORS ON THE AVIAN VESTIBULAR HAIR CELLS AND THE MODULATION EFFECTS ON KIR2.1</b>	
<b>Introduction</b>	
Acetylcholine receptors on vestibular hair cells .....	1
Muscarinic receptores .....	3
Inward rectifier potassium channel Kir2.1 .....	4
Significance .....	5
 <b>Chapter 1 Muscarinic Acetylcholine Receptor Subtype Expression in Avian Vestibular Hair Cells, Nerve Terminals and Ganglion Cells.....</b>	
Introduction .....	8
Experimental procedures .....	10
Animals .....	10
Electrophysiology .....	11
Transmission electron microscopy .....	13
RT-PCR cloning of M2-M5 open reading frames (ORFs) .....	14
Pigeon M2-M5 sequence analysis .....	15
Frozen section tissue preparation.....	16
Isolated single cell preparation .....	17
Immunohistochemistry and immunocytochemistry.....	18
Western blotting.....	20
Antibodies .....	22
Negative controls .....	23
Anatomical nomenclature .....	24
Results .....	24
Patch clamp recordings .....	24



Electron microscopy .....	25
Molecular structure of muscarinic receptor isoforms .....	26
Frozen section immunohistochemistry .....	27
Negative controls .....	27
Positive controls.....	27
Muscarinic receptor subtype expression in the pigeon vestibular periphery .....	28
Muscarinic receptor subtype expression on myelin sheaths and Schwann cells.....	30
Isolated cell immunocytochemistry .....	31
Western blotting.....	32
Discussion.....	33
Chapter 2 Muscarinic Receptor Agonist Application Modulation of Pigeon Inward Rectifying Potassium Channel (pKir2.1) Expressed in Transfected tsA201 cells .....	55
Introduction .....	55
Experimental procedures .....	57
M3/M5 mAChR subtype & pKir2.1 plasmid preparation .....	57
Culturing and transfection of tsa201 cells .....	58
Confocal image of transfected tsA201 cells .....	59
Electrophysiology .....	60
Drug application.....	61
Results .....	62
Confocal microscopy .....	62
Electrophysiological studies of transfected tsA201 cells.....	63
Effects of CCh application to the transfected tsA201 cells .....	66
Cells transfected with M3&pKir2.1.....	66
Cells transfected with M5&pKir2.1.....	67
Membrane potential changes in transfected tsA201 cells at voltages other than the resting membrane potential (RMP).....	68
Discussion.....	70

Chapter 3 The Responses of Isolated Pigeon Vestibular Hair Cells to Acetylcholine	
Receptor Agonist Application.....	92
Introduction .....	92
Experimental procedures .....	95
Animals .....	95
Isolation of vestibular hair cells.....	96
Electrophysiology .....	98
Results .....	101
Type I and type II vestibular hair cells (VHCs).....	101
Pharmacological studies of type II VHCs.....	105
Voltage clamp at constant holding membrane potential of -60 mV	
.....	105
The negative-positive step voltage clamp.....	105
The negative-positive ramp voltage clamp.....	106
The current clamp at the resting membrane potential (RMP)...	108
Pharmacological studies of type I VHCs .....	109
Discussion.....	110
References.....	129
Vita .....	

## List of Tables

Table 1:	Antibodies and antigens used for mAChR subtype studies .....	42
Table 2:	Sequence pair identities of Clustal W analysis comparing human and pigeon muscarinic subtypes M2-M5.....	42
Table 3:	Summary of mAChR subtype expression on the peripheral vestibular neurons .....	43
Table 4:	Concentration of solutions (mM).....	117
Table 5:	Best fitted parameters for Boltzmann function fits of current traces for the four groups of dissociated type II HCs from the semicircular canal and otolith organs.....	118
Table 6:	Summary of inward and outward current amplitudes and RMPs of the four groups of dissociated type II HCs from the semicircular canal and otolith organs .....	119
Table 7:	A summary of the AChR activation induced responses in type I and type II dissociated vestibular HCs .....	119

## List of Figures

Figure 1:	Current traces and I-V plot of pigeon type II vestibular hair cells ..	44
Figure 2:	Transmission electron microscopy images of efferent synapses on type I and type II hair cells and afferent terminals.....	45
Figure 3:	Protein sequence alignment of human M5 with pigeon M2-M5 .....	46
Figure 4:	Fluorescence labeling of mAChR subtype expression on vestibular peripheral structures in the crista, utricle and ganglion .....	48
Figure 5:	DAB staining of semicircular canal crista and vestibular ganglion..	50
Figure 6:	Fluorescence labeling of mAChR subtype expression on isolated type I and type II hair cells as well as vestibular ganglion cells .....	52
Figure 7:	Western blotting results for excised vestibular ganglion, dissociated vestibular end organ epithelium and dissociated nerve fibers .....	53
Figure 8:	Summary of M1-M5 mAChR subtype expression in the pigeon vestibular periphery .....	54
Figure 9:	Cartoons of DNA vectors used for the transfection of tsA201 cells.	79
Figure 10:	Confocal image of the tsA201 cell transfected with pCMS M3&EGFP and pcDNA3 pKir2.1-mRFP1 .....	80
Figure 11:	Current traces of the endogenous currents present in nontransfected tsA201 cells and currents in cells transfected with pKir2.1-mRFP1	81
Figure 12:	Electrophysiological control studies on nontransfected tsA201 cells, cells transfected with EGFP, with pKir2.1, with M3&pKir2.1 and with M5&pKir2.1.....	82

Figure 13:	I-V plots of the tsA201 cells transfected with M3&pKir2.1 exposed to different concentrations and different durations of $[K^+]$ and $[Ba^{2+}]$ .83
Figure 14:	Raw current traces from tsA201 cells transfected with M3&pKir2.1 during application of CCh and TC .....84
Figure 15:	Overlaid I-V plots showing the effects of varying the duration of superfusion of CCh and TC onto tsA201 cells transfected with M3&pKir2.1 .....85
Figure 16:	A continuous trace of the membrane potential of a tsA201 cell transfected with M3&pKir2.1 during application of CCh and TC ...86
Figure 17:	Overlaid I-V plots showing the effects of varying the duration of superfusion of CCh and TC onto tsA201 cells transfected with M5&pKir2.1 .....87
Figure 18:	Current clamp traces of the effects of application of different concentrations of CCh plus TC on the membrane potential of a tsA201 cell transfected with M5&pKir2.1 .....88
Figure 19:	Current clamp recordings of membrane potentials of a nontransfected tsA201 cell and cells transfected with either pKir2.1 or M3&pKir2.1 during different amounts of current injection .....89
Figure 20:	The average values of the voltage levels to induce the overshoot depolarization in the tsA201 cell transfected with pKir2.1, M3&Kir2.1, and M5&pKir2.1 .....90
Figure 21:	NMDG, NFA, and BaCl <sub>2</sub> application to tsA201 cells under current clamp .....91

Figure 22:	Voltage protocols used to test currents in dissociated VHCs as drugs were applied .....	120
Figure 23:	Typical current traces of dissociated type I and type II VHCs and the average amplitude of the inward and outward currents for otolith and semicircular canal type I and type II HCs.....	121
Figure 24:	The mean RMPs for dissociated type I and tpe II HCs from semicircular canals and otoliths.....	122
Figure 25:	Four types of current traces observed from dissociated type II VHCs	123
Figure 26:	Current traces from a dissociated type II VHC during drug application with its membrane potential held at -60 mV .....	124
Figure 27:	Current traces from different type II VHCs using the negative-positive step voltage protocol while drugs were applied.....	125
Figure 28:	Current traces from a dissociated type II VHC using the negative-positive ramp voltage protocol during drug application .....	126
Figure 29:	Membarne potential recordings from dissocated type II VHCs during various AChR agonist and antagonist application .....	127
Figure 30:	Voltage clamp and current clamp recordings from dissociated type I VHCs during drug application .....	128

# **THE EXPRESSION OF MUSCARINIC ACETYLCHOLINE RECEPTORS ON THE AVIAN VESTIBULAR HAIR CELLS AND THE MODULATION EFFECTS ON KIR2.1**

## **INTRODUCTION**

### **Acetylcholine receptors on vestibular hair cells**

The major transmitter released from vestibular efferent terminals is acetylcholine. This was demonstrated by measuring acetylcholinesterase and choline acetyltransferase activities in vestibular efferent fibers (Godfrey et al., 1984; Lopez and Meza, 1988; Khan et al., 1993) and histochemical studies of vestibular efferent neurons and endings (Hilding and Wersall, 1962; Gacek et al., 1965; Nomura et al., 1965; Iurato et al., 1972; Cohen, 1987; Khan et al., 1991; Ishiyama et al., 1994; Kong et al., 1994). In addition, pharmacological and physiological studies have provided sufficient evidence (Bernard et al., 1985; Guth et al., 1986; Guth et al., 1994) to show that the neurotransmitter released from vestibular efferent terminals is acetylcholine. For example, Guth et al. used frog isolated whole labyrinths and isolated semicircular canals to demonstrate changes in afferent nerve activity while applying acetylcholine, cholinomimetics and cholinergic antagonists in the bath (Guth et al., 1986).

Application of acetylcholine produced both facilitatory and inhibitory changes in afferent firing rates. The facilitatory effect could be mimicked by muscarine and carbachol and the inhibitory effect was blocked by strychnine. Loss of vestibular efferent neurons didn't change the effects of acetylcholine; however, substitution of a low  $\text{Ca}^{2+}$ /high  $\text{Mg}^{2+}$  abolished the effects. This indicated that acetylcholine acted directly on vestibular sensory hair cells. If acetylcholine is responsible for both facilitatory and inhibitory effects, the most likely mechanism is that there are two separate ACh receptors

located on vestibular hair cells (VHCs). In fact, there are two distinguishable broad classes of ACh receptors: muscarinic (mAChRs) and nicotinic receptors (nAChRs). Muscarinic and nicotinic receptors belong to two separate gene superfamilies and each of them is represented by multiple subtypes. Muscarinic receptors belong to the metabotropic receptor subfamily, which is composed of five family members, M1-M5; whereas the nicotinic receptors are ionotropic receptors and each subunit may be different. For example, at least 10 different nicotinic receptor  $\alpha$  subunits have been found (Lustig et al., 2001; Elgoyhen et al., 2001). Even though muscarinic receptors and nicotinic receptors have different pharmacological properties (e.g. different agonists and antagonists), they are both activated by the same ligand, acetylcholine.

The literature further suggests that acetylcholine application induces two opposite effects on VHC membrane conductance: both depolarization and hyperpolarization of hair cells. Hair cell membrane depolarization facilitates vestibular afferent firing, whereas membrane hyperpolarization inhibits afferent firing. Atropine, a relatively selective muscarinic receptor antagonist, selectively blocked the facilitatory effects (Guth et al., 1986; Norris et al., 1988; Housley et al., 1990). Strychnine, a potent antagonist of several nicotinic receptors, blocked the inhibitory effects (Norris et al., 1988; Sugai et al., 1992; Guth et al., 1994). These results suggest the presence of both muscarinic receptors and nicotinic receptors on vestibular hair cells. The intracellular mechanisms of the hyperpolarization induced by ACh receptor activation is much better understood than depolarization (Guth and Norris, 1996). It is believed that the activation of an AChR located on the hair cell membrane permits a  $\text{Ca}^{2+}$  influx that opens calcium activated potassium channels, which then hyperpolarizes the cell. Even though both nAChR and mAChR could mediate the hyperpolarization, the activation of metabotropic muscarinic



receptors plays a dominant role in depolarizing the hair cell membrane potential and facilitating afferent firing (Guth et al., 1986; Norris et al., 1988; Housley et al., 1990). The intracellular mechanism for mAChR depolarization of hair cells is still unknown. Until now, little work has been done to study muscarinic acetylcholine receptor subtypes which are located on vestibular hair cells.

### **Muscarinic receptors**

Muscarinic receptors belong to G-protein coupled receptors. When these receptors are activated, they can either directly activate potassium channels (Kir3 subfamily) by G $\beta\gamma$  subunits binding to either the N- or C-terminal regions of the channel (Logothetis et al., 1987; Reuveny et al., 1994; Krapivinsky et al., 1995; Kofuji et al., 1995; Inanobe et al., 1995; Huang et al., 1995), by directly binding G $\alpha$  subunits to the channel (Schreibmayer et al., 1996), or by activating a G protein-linked intracellular secondary messenger system to modulate ion channels. Thus, activation of muscarinic receptors could induce both depolarization (Guth et al., 1986; Norris et al., 1988) and hyperpolarization (Steinacker and Rojas, 1988; Ohmori, 1990; Yoshida et al., 1994) of hair cells with an increase or decrease in afferent firing. Application of a muscarinic receptor agonist to chicken cochlear hair cells increased intracellular Ca<sup>2+</sup> concentration and hyperpolarized the cell membrane potential (Shigemoto and Ohmori, 1990). The same results were also observed in frog vestibular hair cells (Ohtani et al., 1994) and guinea pig cochlear hair cells (Doi and Ohmori, 1993; Evans et al., 2000). Shigemoto and Ohmori (1991) speculated that the inhibitory effect was probably due to activation of the muscarinic receptor, G-protein and IP<sub>3</sub> (Shigemoto and Ohmori, 1991). Guth and Norris (1996) concluded that the musarinic receptor induced hyperpolarization used the

following cascade: muscarinic receptor, G protein, activation of PLC, increased level of IP<sub>3</sub>, increased intracellular Ca<sup>2+</sup> concentration, and Ca<sup>2+</sup> activated K<sup>+</sup> channels as the effector (Guth and Norris, 1996). However, the mechanism for depolarization of hair cells by muscarinic receptor activation is still unknown.

Based on the intracellular signaling pathway and the sensitivity to pertussis toxin, the five mAChR family members are generally divided into two groups: an odd numbered group and an even numbered group. In recent years, genes for several muscarinic receptor subtype have been cloned from mammalian (Kubo et al., 1986; Braun et al., 1987; Bonner et al., 1987; Peralta et al., 1987a; Shapiro et al., 1988; Bonner et al., 1988; Kashihara et al., 1992) and avian tissue (Tietje et al., 1990; Gadbut and Galper, 1994). Comparison of their amino acid sequences provides specific antibody epitopes that permit detection of their expression on vestibular hair cells.

### **Inward rectifier potassium channel Kir2.1**

Kir (inwardly rectifying K<sup>+</sup>) channels are a class of potassium channels composed of a tetrameric arrangement of one-pore/two-transmembrane helix protein subunits. Kir channels have been studied in RBL-2H3 cells (Jones et al., 1991a; Jones, 1997), *Xenopus* oocytes (Kunkel and Peralta, 1995; Bard et al., 2000), AtT-20 cells (Dousmanis and Pennefather, 1992; Jones, 1992), and tsA201 cells (Jones, 1996; Firth and Jones, 2001; Jones, 2003) with the coexpression of muscarinic receptor subtypes. Kir channels are involved with control of heart rate, neuronal firing patterns, vascular smooth muscle tone, secretion of hormones, and activation of immune response cells. They are also involved with cell generation, proliferation, growth, and differentiation. Moreover, Kir channels are ubiquitous in many cell types because they play an important role for modulating cell

excitability, being involved in depolarization of action potentials, setting the resting potential of the cell near the potassium equilibrium potential and contributing to potassium homeostasis. Activation of these channels will hyperpolarize the cell membrane potential, whereas inhibition of these channels will move the cell membrane potential to a more positive active state, where cells are more easily depolarized.

There are seven sub-family members (Kir1-Kir7) of inwardly rectifying potassium channels. Kir2.1 is a strong inward rectifier. It is constitutively active (Stanfield et al., 2002b), and sensitive to phosphorylation and intracellular second messengers (Fakler et al., 1994; Henry et al., 1996; Wischmeyer et al., 1998; Liu et al., 2001). Kir 2.1 is clinically important also since inactivation through point mutations (mostly in the PIP<sub>2</sub> binding domain) produces cardiac arrhythmias, dysmorphisms and dystonias (Plaster et al., 2001). To study this channel thoroughly, we have cloned, sequenced, expressed this channel in tsA201 cells and shown that the ion channel that carries the Kir current in pigeon vestibular hair cells is a member of the Kir2.1 subfamily (Correia et al., 2004). As shown in the same paper, pKir2.1 contributes strongly to setting the resting membrane potential of pigeon vestibular hair cells. Blockage of pKir2.1 depolarized the resting membrane potential from ~-90 mV to ~-60 mV.

We hypothesize that muscarinic receptors located on the vestibular hair cell membrane could modulate the cell membrane potential through an inward rectifier potassium channel (Kir2.1).

### **Significance**

It is thought that vestibular hair cells spontaneously release the neurotransmitter glutamate and cause vestibular primary afferents (which synapse upon the hair cells) to

maintain a spontaneous activity in the resting state. This spontaneous activity is increased or decreased by changes in transmitter release from the hair cell due to depolarization or hyperpolarization of the hair cell's resting membrane potential resulting from deflection of the cilia of the hair cell in opposite directions. Thus modulation will consequently change vestibular afferent firing rate. The vestibular efferents originating from the brain terminate on vestibular hair cells or/and on afferent terminals. The function of efferents is thought to modulate the afferent firing rate. The efferent mediated modulation could be direct, through axo-dendritic contacts with boutons or calyces; or indirect, through depolarization or hyperpolarization of the hair cells, which in turn modulates the firing rate of afferent fibers. However, the cellular and molecular mechanisms of the interactions between vestibular efferents, hair cells, and afferents are still unclear. Our work provides one possible explanation of the indirect efferent modulation.

Why are the mAChRs important? Muscarinic receptors are metabotropic receptors and are part of the G- protein coupled receptor family. As such, these receptors operate on the timescale of minutes to hours and mediate a wide variety of cellular processes. These features add greater flexibility to the cell signaling pathways by complementing the signaling capability of nicotinic AChRs which operate on the millisecond time scale and involve more direct receptor-effector cellular processes. Moreover, mAChRs add the capability of certain autocrine functions to the neural processes upon which they reside (See discussion in Chapter 1).

Why do we study the pKir2.1 channel? This channel contributes substantially to the resting membrane potential (RMP) by holding RMP close to  $E_K$  and away from the activation range of the voltage dependent  $Ca^{2+}$  channel where hair cell neurotransmitter release occurs. The pKir2.1 channel clamps the hair cell membrane potential preventing

large unwanted hyperpolarizations (Holt and Eatock, 1995; Correia et al., 2004); and it may be the ion channel effector of activated mAChR. Blockage of the pKir2.1 channel shifts the hair cell membrane potential more positive, making it more sensitive to external stimuli. In addition, since the pKir2.1 channel is present in both type I and type II hair cells, supporting cells, and afferent fibers, it may determine the K<sup>+</sup> environment in the calyceal cleft of the type I hair cells (Rennie and Correia, 2000) and at the basement membrane of the epithelium by controlling K<sup>+</sup> ion exchange between supporting cells and the hair cells (Masetto and Correia, 1997a). This channel is also probably involved in controlling the interspike interval of action potentials in vestibular afferents by modulating the final repolarization phase of action potentials. It may also contribute to electrical tuning of hair cells. And it has been shown (Plaster et al., 2001) that Kir2.1 channels also play a role in developmental signaling.

Our study of the modulation of K<sup>+</sup> channels found in hair cells by muscarinic acetylcholine receptors will provide information about the mAChR activation pathways where therapeutic pharmacological agents can modify the signaling cascades involved in hair cell depolarization and consequently primary afferent excitation. This is important because it will potentially help us find a way to benefit patients with dysfunction of vestibular system.

A total of three sets of experiments were performed to test our hypotheses: including mAChR protein identification in vestibular hair cells; electrophysiological studies of mAChR induced response of Kir2.1 in heterologous expression system (HES); and electrophysiological studies of mAChR induced current and voltage responses in isolated native avian (pigeon) vestibular hair cells. In the following sections, each set of experiments is presented as a separate chapter.

## **Chapter 1: Muscarinic Acetylcholine Receptor Subtype Expression in Avian Vestibular Hair Cells, Nerve Terminals and Ganglion Cells**

### **INTRODUCTION**

Two decades ago, the first muscarinic acetylcholine receptor subtype (mAChR) was successfully cloned (Kubo et al., 1986). The cDNAs from the four other known subtypes were subsequently cloned (Kubo et al., 1986; Bonner et al., 1987; Peralta et al., 1987a; Peralta et al., 1987b; Bonner et al., 1988). Muscarinic receptors belong to the G-protein coupled receptor family. The receptors have seven transmembrane domains. The residues in the third intracellular loop of the protein contribute to the structural diversity among the 5 different mAChR subtypes (Hulme et al., 1990; Wess, 1996; Wess et al., 1997). Based on their sensitivity to pertussis toxin, biochemical characteristics and intracellular cascades (Caulfield, 1993; Eglen and Nahorski, 2000), the five subtypes can be subdivided into two groups. The first group is composed of M1, M3 and M5. These subtypes are sensitive to pertussis toxin and they are coupled to  $G\alpha_q/11$  to activate phospholipase C and downstream intracellular cascades. The second class consists of M2 and M4. These subtypes are not sensitive to pertussis toxin and they are preferentially coupled to  $G\alpha_i/o$  proteins to inhibit adenylate cyclase and influence subsequent downstream pathways.

All five muscarinic receptor isoforms are widely expressed throughout the central and peripheral nervous system. Transgenic mice lacking genes that encode for each of the mAChR subtypes have provided some useful generalizations about their function (Wess et al., 2003b). The M1 receptor appears to be associated with locomotor function and higher cognitive processes such as learning and memory (Wess, 1996; Miyakawa et al., 2001). M2 receptors contribute to skeletal and smooth muscle contraction, analgesia

(Wess et al., 2003a) and thermal regulation (Stengel et al., 2000). M3 receptors are involved in smooth muscle contraction, glandular secretion, food intake and weight control (Caulfield, 1993; Matsui et al., 2000; Yamada et al., 2001b). M4 receptors contribute to locomotor activity and ACh release in the striatum (Gomeza et al., 1999; Zhang et al., 2002b). M5 receptors modulate dopamine release in the central nervous system and they are involved in vasculature vasodilatation (Vilaro et al., 1990; Weiner et al., 1990; Yamada et al., 2001a; Basile et al., 2002; Yamada et al., 2003; Fink-Jensen et al., 2003; Wess et al., 2003b).

In birds, preliminary pharmacological studies indicate that mAChRs located in the central nervous system are associated with vision, homing, navigation, metabolism and central thermoregulation (Chawla et al., 1975; Kohler et al., 1996; de Azevedo et al., 2002). However, the role of each of the mAChR subtypes has not been clearly established in either the central or peripheral nervous systems (Dietl et al., 1988; Kohler et al., 1995). Muscarinic receptor subtypes have been shown to be expressed in cochlear neurons, supporting cells (Drescher et al., 1992; Wangemann et al., 2001; Khan et al., 2002) and central auditory neurons (Chen et al., 1995). While mRNA for mAChR subtypes has been demonstrated in peripheral vestibular neurons (Wackym et al., 1991; Wackym et al., 1995; Wackym et al., 1996; Anderson et al., 1997; Ishiyama et al., 1997), protein expression has not been shown previously. Acetylcholine is the major neurotransmitter released from vestibular efferent terminals, the endings of fibers coursing centrifugally from the brain to synapse on sensory hair cells and afferent nerve terminals (Gacek et al., 1965; Iurato et al., 1971; Goldberg and Fernandez, 1980).

Pioneering physiological studies using the application of cholinergic agonists in the isolated labyrinth or the isolated semicircular canal of frogs produced both inhibitory

and facilitatory effects on primary afferent activity (Bernard et al., 1985; Guth et al., 1986; Norris et al., 1988). Subsequent patch clamp studies of dissociated individual frog vestibular hair cells indicated that “atropine-preferring” (Norris et al., 1988) or ‘muscarinic-like’ (Guth and Norris, 1996) receptors were expressed on the vestibular hair cell membrane (Housley et al., 1990; Yoshida et al., 1994).

We demonstrate here that the application of carbachol reduces Kir2.1 currents in pigeon vestibular hair cells. In a previous study (Correia et al., 2004), it was shown that inhibition of Kir2.1 currents depolarized the hair cell membrane potential. Furthermore, we demonstrate for the first time, the expression and co-expression of M1-M5 in supporting and neural cells of the pigeon vestibular periphery. Understanding the functional role of each receptor subtype in isolation or in combination will be the challenge of future experimentation.

Partial preliminary results were published as an abstract (Li et al., 2005).

## **EXPERIMENTAL PROCEDURES**

### **Animals**

Adult (6-40 wk old) white king pigeons (*Columba livia*) (Double T Farms, Glenwood, IA) of either sex were used for the present studies, including electrophysiology, vestibular peripheral anatomy and RT-PCR analysis. Studies of each muscarinic receptor subtype (M1-M5) were performed using frozen sections (immunohistochemistry, IH), dissociated single cells (immunocytochemistry, IC), and Western blotting (WB). The number of animals/subtype used: 4-7 for IH studies, 3-7 for IC studies, and 4-10 for WB studies. In no case did fewer than 3 animals provide data for



each subtype and each method. The experimental procedures used in this study were approved by the Institutional Animal Care and Use Committee at UTMB.

### **Electrophysiology**

Pigeons were anesthetized using Nembutal, 40 mg/kg iv, and ketamine, 60 mg/kg IM (supplementary doses as needed). While deeply anesthetized, the vestibular end organs were removed as described previously (Correia et al., 1989), placed into a D-MEM-PIPES solution (pH 7.4, osmolarity = 320 mosmol/kg H<sub>2</sub>O) supplemented with (in mM): 24 NaHCO<sub>3</sub>, 15 PIPES and 1.5% fetal calf serum, and kept in an incubator at 37°C. The atmosphere inside the incubator was saturated with a 95% CO<sub>2</sub> / 5% O<sub>2</sub> mixture (Ricci et al., 1996b). The incubation environment prolonged hair cell life to 4-6 hours. After 1-2 hours in the incubator, the vestibular end organs were dissected, trimmed, oriented and embedded within 4% agar. The agar block containing the ampulla was placed in a partially frozen high Mg<sup>2+</sup> solution consisting of (in mM): 3 KCl, 145 NaCl, 0.1 CaCl<sub>2</sub>, 7.5 MgCl<sub>2</sub>, 15 HEPES, 10 glucose, 0.283 sodium ascorbate and 2 Na<sup>+</sup> pyruvate, and then sliced using a Vibratome® 1000 sectioning system (Ted Pella Inc., Redding, CA). The plane of the section was parallel to the long axes of the crista and the thickness of each slice was 150-250µm.

The individual slice was put in a recording chamber bathed with an oxygen saturated external solution comprised of (in mM): 3 KCl, 145 NaCl, 2 CaCl<sub>2</sub>, 1 MgSO<sub>4</sub>, 15 HEPES, 10 glucose, 0.283 sodium ascorbate and 2 Na<sup>+</sup> pyruvate and stabilized by a weighted nylon mesh net for electrophysiological recording (Masetto and Correia, 1997a). The slices were viewed using a Zeiss Axioskop compound upright microscope

and DIC optics including an Optovar magnifier and a 40X water-immersion objective. The temperature of the bath was 23°C and continuously changed at a rate of ~750 µl/min.

The patch pipettes contained (in mM): 140 KCl, 1 CaCl<sub>2</sub>, 2 MgCl<sub>2</sub>, 10 HEPES and 11 EGTA. The pipette solution was titrated to a pH of 7.4 with KOH/HCl and maintained at an osmolarity of 320 mosmol/kg H<sub>2</sub>O.

The borosilicate pipettes (0.75 ID, 1.50 OD, no. 1B150F-3; World Precision Instruments, Sarasota, FL) were pulled on a P-2000 puller (Sutter Instruments, Novato, CA), then firepolished on a MF-83 microforge (Narishige USA Inc., Greenvale, NY). Electrode capacitance was greatly reduced by the following procedure which obviated further pipette coating. The glass blanks containing a thin filament were initially washed with Chromerge (VWR International, Cat. # 21865-000, West Chester, PA), silanized with 5% dimethyldichlorosilane (Sigma, Cat. # 40140, St. Louis, MO) in chloroform (Fisher, Cat. # C298-500, Pittsburgh, PA), then subsequently washed multiple times with ddH<sub>2</sub>O and dry heat sterilized at 240°C. The whole cell recording electrode impedance was typically 2–5 MΩ.

Whole cell currents were amplified 1X using an Axopatch 200 amplifier (Axon Instruments/Molecular Devices, Sunnyvale, CA). The currents were filtered at 2 kHz using the amplifier's Bessel filter then sampled at 5 kHz. Series resistance and capacitance were compensated between 80 and 98% with a typical value of 95%. No online leak subtraction was performed. Subsequently, in some cases, leak subtraction was performed digitally. Current and voltage were measured and controlled through a DigiData 1200 Interface (AD/DA converter; Axon Instruments/Molecular Devices, Sunnyvale, CA). Resting membrane potential was measured as the zero-current voltage ( $V_z$ ) in current-clamp mode. Cell input resistance ( $R_m$ ) was calculated by measuring the

average current evoked by a series of seven depolarizing pulses (10 mV in amplitude and 250 ms in duration) from a holding potential of -60 mV (Figure 1). This voltage series yielded the largest  $R_m$ . Because no time-dependent currents were evident, we considered the current measured in response to the above protocol to be leakage current. This leakage current was subsequently subtracted from the current traces. Voltages were corrected for the liquid junction potential (~3 mV negative inside the pipette). Although current-voltage ( $I$ - $V$ ) plots were not corrected for the voltage drop across the residual series resistance, all values of peak ( $G_p$ ) and steady-state ( $G_s$ ) slope conductance were corrected for the residual series resistance.

The cholinergic agonist carbachol was superfused onto the cell using a pressurized computer-controlled superfusion system (model DAD-12; ALA Scientific Instruments, Westbury, NY). The superfusion pipette (100  $\mu$ m bore) was placed ~30  $\mu$ m from the cell; and the flow rate was ~20  $\mu$ l/min.

The patch clamp data were gathered using Clampex V8 (Axon Instruments/Molecular Devices, Sunnyvale, CA), and the figures were produced using Clampfit V8 and OriginPro v7.5 (OriginLab, Northhampton, MA)

### **Transmission electron microscopy**

Pigeons were anesthetized and perfused by pump driven *in vivo* transcardiac bilateral carotid catheterization (Eden and Correia, 1981). The perfusate was 2.5% glutaraldehyde in 0.1 M phosphate buffer (pH = 7.4). Following overnight submersion of the head in the same concentration of glutaraldehyde, the anterior ampullae were dissected free and post fixed for 1 hr in 1% osmium tetroxide (dissolved in ddH<sub>2</sub>O) (Correia et al., 1985). After 2X H<sub>2</sub>O rinses, the ampullae were stained with 1% uranyl

acetate for 2 hrs and then dehydrated through a graded series of ethanols (70% - 3X for 15 min each time (ET) , 95% - 1X for 30 min and 100% - 2X for 1hr ET). Then the tissue was immersed in propylene oxide (2X for 30 min ET) alone and then overnight in a 1:1 mixture with Epon. Subsequently, the tissue was blocked and oriented so that thin sections could be made through the long axis of the crista. The thin sections were viewed and photographed using a Philips 200 or a Zeiss 10 TEM.

### **RT-PCR cloning of M2-M5 open reading frames (ORFs)**

Total RNA from pigeon brain was isolated using guanidinium thiocyanate (Chomczynski and Sacchi, 1987). Synthesis of cDNA and PCR amplification of ORFs for M2-M4 were performed as described previously (Correia et al., 2004) using primers listed below. M1 ORF amplification and cloning was not performed due to the lack of M1 gene sequence of chicken from gene bank. The M5 ORF was initially amplified as separate 5' (824bp) and 3' (932bp) DNA fragments using conditions identical to those used for M2-M4 and the M5 primers (see below). The full length ORF was generated by annealing the purified DNA fragment followed by primer extension and then amplification using the 5' forward and 3' reverse M5 primers.

M2 Forward – 5'GAATTCATGAATAACTCAACGTACATAAACTCTTC 3'

M2 Reverse – 5'GTCGACTTACCTTGTTGCTCCTATATTCTTGTAAT 3'

M3 Forward – 5' AAGCTTCGATGCTGACACACTACCAGTTGTGTTTC 3'

M3 Reverse – 5' GTCGACTATGAAGCCTCCCTAGGGATCCG 3'

M4 Forward – 5'ATGCACAACCTCTCCGCGCAGCC 3'

M4 Reverse – 5' TTATCTGGCCGTGCCAATGTTCTTG 3'

M5 5' Forward – 5' ATGGAAGTAAATCTATTCAGCAATTCTAC 3'

M5 5' Reverse – 5' CGACTGGATGAAGACCAGGAAGCC

M5 3' Forward – 5' GAGACTGAGAAACGTACCAAGGACC 3'

M5 3' Reverse – 5' TTATGGCATTTCGAGTGTGCCCCTGC 3'

Primer design was based upon the nucleotide sequence of the respective chicken ORFs for M2-M5 (M73217, L10617, J05218 and AF201960, respectively). The PCR products for M2-M4 were cloned using PCR2.1 as a vector. The initial PCR products for M5 were cloned into a pUC vector digested with SmaI and treated with calf intestine phosphatase (CIP). The final full length M5 ORF was cloned into PCR2.1. The M2-M5 clones were confirmed by DNA sequence analysis. The GenBank accession numbers for the nucleotide sequences of pigeon M2-M5 are AY838767, AY838768, AY838766 and DQ357059, respectively.

### **Pigeon M2-M5 sequence analysis**

The epitope sequences of the commercial mammalian anti- M2, M3, M4 and M5 antibodies were obtained from the manufacturers and aligned (using clustal W analysis) for comparison to pigeon muscarinic receptor subtype sequences. The alignment was done using the Megalign module of DNASTar (DNASTar, Madison, WI). Pigeon and human M2-M5 sequences were clustered using clustal W and phylogenetic analyses (Accelrys Gene 2.0, Accelrys, San Diego, CA). The probability of serines, threonines, tyrosines and asparagines being phosphorylation and glycosylation sites was obtained for the sequence DQ357059 (Pigeon M5) using the website [www.cbs.dtu.dk/databases](http://www.cbs.dtu.dk/databases).

### **Frozen section preparation**

Pigeons were anesthetized as described above. While deeply anesthetized, each pigeon's chest was opened to expose the heart. Two cannulae (14 Gauge, Harvard Apparatus, Holliston, MA) were inserted into the left and right carotid arteries through the left ventricle (Eden and Correia, 1981). The right atrium was opened. About 200-300 ml of warm (36°C) 0.9% NaCl solution was perfused through the upper body. To improve the perfusion efficiency, about 10 mg NaNO<sub>2</sub> was added in the saline solution to dilate the arteries. Then, 500-600 ml cold (4°C) 4% paraformaldehyde solution (freshly made) was perfused (gravitationally driven) for one hour. The head of each pigeon was removed and submerged in fixative and stored at 4°C overnight after exposing a small part of the membranous semicircular canals of the vestibular end organs and the skull covering the brain. The next day, the membranous semicircular canals and utricles were excised and dissected apart. All ampullae and utricles were put into PBS w/ 20% sucrose until they sank. Then they were immersed in 3% gelatin w/ 20% sucrose for 15 seconds. Subsequently, the sensory receptors were embedded in 10% gelatin w/ 20% sucrose; chilled in the refrigerator for one hour; blocked, trimmed and fixed in 4% paraformaldehyde w/ 20% sucrose overnight in the refrigerator. The vestibular ganglia were also taken out and treated in the same way.

A sliding microtome (Model 860, American Optical Corp., Buffalo, NY) was used to cut sections 20 µm thick. Each of the well-fixed gelatin embedded ampullae, utriculi, Scarpa's ganglia and hippocampus tissue were oriented on the microtome stage and frozen using ground dry ice. The plane of the sections was parallel to the long axis of the crista, perpendicular to the long axis of the utricle and parallel to a horizontal section through the vestibular ganglion.

As positive controls, two gerbils and one rat were perfused with the same fixatives. Brains were dissected and 40  $\mu\text{m}$  sections through the hippocampus and striatum were cut and reacted concurrently with pigeon tissues.

### **Isolated single cell preparation**

As described previously (Correia et al., 1989), the membranous vestibular end organs were removed from anesthetized pigeons then immediately put into D-MEM/PIPES solution (pH 7.4, Osm=320 mosmol/kg  $\text{H}_2\text{O}$ ) supplemented with 24 mM  $\text{NaHCO}_3$ , 10 mM PIPES and 1.5% fetal calf serum, which was kept in an incubator whose atmosphere was maintained at 37°C and saturated with a  $\text{CO}_2/\text{O}_2$  mixture. The incubation environment prolonged hair cell life for 4-6 hrs, but killed supporting cells thereby facilitating dissociation (Ricci et al., 1996a). The end organs were dissected in 4°C low  $\text{Ca}^{2+}$  saline (containing in mM: 0.1  $\text{CaCl}_2$ , 110  $\text{NaCl}$ , 2  $\text{KCl}$ , 2  $\text{MgCl}_2$ , 3 D-Glucose and 10 HEPES at pH 7.25) to separate the cristae and utriculi (Hirono et al., 2004). The cristae and utriculi were put in low  $\text{Ca}^{2+}$  saline w/ 1 mM EGTA (Sigma, Cat. # E3889-25G, St. Louis, MO) for 15 min. During the EGTA/low  $\text{Ca}^{2+}$  incubation, the membrane overlying each crista and macula was opened to increase the efficiency of subsequent enzyme digestion. The end organs were then placed in protease XXIV (65  $\mu\text{g}/\text{ml}$  in low  $\text{Ca}^{2+}$  saline, Sigma, Cat. # P8038-250MG, St. Louis, MO) for 20 min. Protease XXIV facilitated removal of the otolithic membrane and cupula and therefore decreased the damage to the hair cell cilia (Ricci et al., 1996a). Parenthetically, it has been reported that protease XXIV used for hair cell isolation eliminates the  $\alpha 9$ -nicotinic acetylcholine receptor (nAChR) mediated response (Holt et al., 2001). However, it is not clear whether this effect is on the receptor (nAChR) or the effector (SK ion channel). No

proteolytic effects on mAChR subtypes have been reported to our knowledge. Next, the end organs were put in deoxyribonuclease I (100 µg/ml in low Ca<sup>2+</sup> saline, Worthington, Cat. # X5D8021, Lakewood, NJ) for 5 min, followed by bovine serum albumin (1 mg/ml in low Ca<sup>2+</sup> saline, Fisher, Cat. # BP1605-100, Pittsburgh, PA) for 5 min to attenuate the enzyme reaction. In a glass chamber containing 60 µl low Ca<sup>2+</sup> saline, a thin glass wisp was used to dislodge hair cells from the epithelia of the cristae and utriculi through gentle mechanical agitation. Following subsequent trituration, the hair cells were plated in a channel of µ-Slide (Ibidi GmbH Integrated BioDiagnostics, Cat. # 80601, München, Germany). The bottom of the channel (a slide) was coated with concanavalin A (5 mg/ml, Sigma, Cat. # C2010-250MG, St. Louis, MO). To fix the isolated hair cells, 2.25% formaldehyde (Electron Microscopy Sciences, Cat. #15682, 37%, Hatfield, PA) and 0.75% glutaraldehyde (Electron Microscopy Sciences, Cat. #16310, 50%, Hatfield, PA) in PBS (containing in mM: 137 NaCl, 2.7 KCl, 4.3 Na<sub>2</sub>HPO<sub>4</sub> and 1.4 KH<sub>2</sub>PO<sub>4</sub> at pH 7.4) was gently added and kept at room temperature (RT) for 30 min. Ganglion cells were isolated and treated in the same way.

### **Immunohistochemistry and immunocytochemistry**

Frozen sections were rinsed in phosphate-buffered saline (0.1 M pH 7.4 PBS; 0.9% NaCl) for 10 min before they were incubated for 1 hr in 3% normal goat serum diluted in the working buffer (PBS w/ 0.3% triton X-100 (Sigma, Cat. # T6878 [X100], St. Louis, MO). The sections were kept at 4°C for 36-48 hrs in primary antibody diluted in working buffer. Subsequently, the sections were incubated in one of the fluorescent tagged secondary antibodies diluted in working buffer for 2 hrs at RT. For double labeling, the sections were incubated with two different primary antibodies and appropriate secondary



antibodies. Between each step, the sections were rinsed 3X for 10 min ET in PBS. Once the reaction was finished, the sections were rinsed 2X for 10 min ET in PBS and 1X for 10 min in distilled water. Then, they were mounted on gelatin-coated glass slides. After the sections dried at RT overnight, they were cover-slipped.

For the diaminobenzidine (DAB) reaction, a biotinylated secondary antibody and VECTASTAIN<sup>®</sup> ABC reagents (Vectastain Elite, Vector Laboratories, Burlingame, CA) were used according to the manufacturer's protocol. Sections were rinsed 2X for 10 min ET with PBS and 1X for 10 min ET with acetate buffer. The immunoreactivity of mAChR subtypes was visualized using 0.05% DAB (3,3'-Diaminobenzidine tetrahydrochloride, Sigma, Cat. # D5637-1G, St. Louis, MO) dissolved in 0.1 M acetate buffer containing 1.75% nickel ammonium sulfate (Fisher, Cat. # N-48, Pittsburgh, PA) and 0.0003% H<sub>2</sub>O<sub>2</sub>. Sections were mounted on gelatin-coated microscope slides, dried overnight and cover-slipped with Permount\* mounting medium (Fisher, Cat. # SP15-500, Pittsburgh, PA).

In some cases adjacent sections were stained with 1% osmium tetroxide (OsO<sub>4</sub>) for one hour to stain myelin.

For IC using isolated vestibular hair cells and ganglion cells, samples were rinsed with PBS 3X for 10 min RT after fixation and blocked 1 hr at RT in the blocking solution (PBS, 3% goat serum and 10 mg/ml bovine serum albumin). The isolated hair cells and ganglion cells were then incubated 48 hrs at 4°C with primary antibodies diluted in the blocking solution. After rinsing 3X for 10 min ET in PBS, tissues were incubated with secondary antibodies in the blocking solution for 2 hrs at RT. Following 2X PBS for 10 min ET and 1X for 10 min distilled water rinses, mounting medium was applied to resist photobleaching and the slides were cover slipped. Two types of mounting medium were

used for fluorescent microscopy: one was VECTASHIELD<sup>®</sup> mounting medium (Vector Laboratories, Inc., Cat. # H-1400, Burlingame, CA), which was used mainly for the isolated cells and the second, Prolong<sup>®</sup> Gold antifade reagent (Invitrogen, Cat # P36930, Carlsbad, CA), was used mainly for the frozen sections.

The concentrations of the primary antibodies were 1:500 for anti-M1, 1:200 for anti-M2, 1:200 for anti-M3, 1:200 for anti-M4 and 1:400 for anti-M5. The concentrations of the secondary antibodies, which were conjugated with fluorescent probes (Alexa<sup>™</sup> probes; see above), were 1:500 for either Goat anti-Rabbit IgG or Goat anti-Mouse IgG.

Samples were viewed using either a confocal (LSM 510 Meta, Zeiss, Thornwood, NY) or a light microscope (Olympus BX51, Olympus, Tokyo, Japan). The Zeiss LSM Image Browser program (v 3.5.0.376) was used to process the optical sections of the frozen tissue slices and dissociated cells. The tissue and cells were excited with 488 nm and 543 nm wavelengths. Stacks and single optical sections (0.5 and 0.9  $\mu$ m thick) of the cells and tissue were stored on disk. Light microscopic images of DAB and OsO<sub>4</sub> stained sections were captured using an Olympus DP 70 camera and DP Controller 2.1.1.183 software (Olympus, Tokyo, Japan). No manipulations except minor adjustments to brightness and contrast were made to any of the captured images. Figures containing or based on photomicrographs (Figure 8) were made using Photoshop CS2 (v 9.0.1) and Illustrator CS2 (v 12.0.1) (Adobe Systems Inc, San Jose, CA).

### **Western blotting**

Four types of lysates were obtained. The first consisted of dissociated cells and tissues from the vestibular end organ's neuroepithelia (NE). This lysate contained mostly hair cells but possibly some supporting cells and nerve terminals (calyces and boutons).

The second lysate was from nerve fibers attached to the neuroepithelia of the end organs and nerve bundles peripherally connected to Scarpa's ganglia (NF). The third lysate consisted of dissociated ganglion cells from dissected vestibular ganglia (VG). The fourth lysate was from the hippocampus region of the pigeon brain (used as controls, H). After sample collection was done, each lysate was centrifuged at 2000g at 4°C for 5 min and the supernatant was removed. The RIPA buffer (see Millipore/Upstate protocol: RIPA Buffer: Preparation of Modified Radioimmunoprecipitation (RIPA) Buffer at the final concentrations (in mM): 50 Tris-HCl with pH adjust to 7.4 using HCl, 150 NaCl, 1 EDTA, 1 PMSF, 1 Na<sub>3</sub>VO<sub>4</sub>, 1 NaF, and 1% NP-40, 0.25% Na-deoxycholate, 1mg/ml aprotinin, 1 mg/ml leupeptin, 1 mg/ml pepstatin) was added and mixed with samples by vortexing the solution gently every 10 min for 30 min while keeping the samples on ice. Then, 8000g centrifugation was applied at 4°C for 20 min. The supernatants were transferred to clean tubes and total protein concentration was measured using Micro BCA Protein Assay Kits (Pierce Biotechnology, Inc., Cat # 23235, Rockford, IL) and an ELx800 Microplate Absorbance Reader (BioTek Instruments, Inc., Winooski, VT). The average concentration (mean±SD) of the total protein was: Neuroepithelium 0.59±0.1 µg/µl (60 µl, n=6); nerve fibers 0.55±0.16 µg/µl (60 µl, n=6); ganglion 0.56±0.1 µg/µl (75 µl, n=6) and hippocampus 3.4±0.38 µg/µl (500 µl, n=4). An aliquot of 8µg from each lysate was mixed with 6X sample buffer, boiled in a water bath for 10 min, then electrophoresed through a 10% Tris-HCl gel (at 40 mA for 80 min) (Bio-Rad, Cat # 345-0009, Hercules, CA). The protein product was transferred electrophoretically (at 100 V for 90 min) on to nitrocellulose membranes (Bio-Rad, Cat # 162-0145, Hercules, CA). The membranes were blocked with Tris-Buffered Saline Tween-20 (TBST, 25 mM Tris, 0.15 M NaCl and 0.05% Tween-20 at pH 7.2) containing 5% non-fat milk for 1 hr. at RT.

Blots were either incubated with the muscarinic receptor antibodies or the corresponding pre-adsorption control solutions overnight at 4°C. After washing 3X for 10 min ET with TBST, the blots were reacted with the appropriate horseradish peroxidase (HRP) conjugated IgG for 1 hr at RT. After rinsing the blots 3X for 10 min ET with TBST, they were incubated using SuperSignal® West Femto Maximum Sensitivity Substrate working solution (Pierce Biotechnology, Inc., Cat # 34095, Rockford, IL) for 5 min. Then, the excess solution was drained and the blots were covered with clear plastic wrap and were exposed to Hyperfilm™ ECL film (Amersham Biosciences UK Ltd, Cat # RPN1674K, Buckinghamshire, UK) for 15–60 seconds depending on the band intensities. The films were developed in an automatic developer and the resulting negatives were scanned using an EPSON Perfection model 4990 scanner. The resulting digital files were saved for further analysis. As with the IC and IH, primary antibody negative controls, secondary antibody negative controls and pre-absorption controls were performed.

All antibodies were diluted in 1% non-fat milk-TBST solution. The concentration of the anti-M1 was 1:1,000; the anti-M2 was 1:500; the anti-M3 was 1:500; the anti-M4 was 1:2,000; and the anti-M5 was 1:1,000. The goat anti-rabbit conjugated HRP IgG was diluted into 1:10,000. Goat anti-mouse conjugated HRP IgG was diluted into 1:20,000.

## **Antibodies**

The primary antibodies included rabbit anti-M1-mAChR polyclonal antibody (Bioscience International, Cat. # Q4A173R, Saco, ME), rabbit anti-M2-mAChR antibody (Alomone Labs Ltd., Cat. # AMR-002, Jerusalem, Israel), rabbit anti-M3-mAChR antibody (Alomone Labs Ltd., Cat. # AMR-006, Jerusalem, Israel), mouse anti-M4-mAChR monoclonal antibody (Chemicon International, Cat. # MAB1578, Temecular,

CA), and rabbit anti-M5-mAChR antibody (Biodesign International, Cat. # Q4A871R, Saco, ME). Control antigens for M2 and M3 antibodies from Alomone Labs were included with the purchase of the antibodies. Blocking peptides for M1 (Cat. # A4A730H) and M5 (Cat. # A4A738H) were purchased from Biodesign International. M4 purified protein, used as a blocking peptide (Cat. # sc-4505 WB), was purchased from Santa Cruz Biotechnology, Inc. Molecular and pharmacological properties of the antibodies are detailed in Table 1.

The secondary antibodies were purchased from Molecular Probes (Eugene, OR). They included Alexa<sup>TM</sup> 488 and Alexa<sup>TM</sup> 594 labeled Goat anti-Mouse IgG and Alexa Fluor<sup>®</sup> 488 and Alexa Fluor<sup>®</sup> 594 labeled Goat anti-Rabbit IgG. In Western blotting experiments, ImmunoPure<sup>®</sup> Peroxidase conjugated Goat Anti-Rabbit HRP and Goat Anti-Mouse HRP (Pierce Biotechnology, Inc. Rockford, IL) were used.

### **Negative controls**

Several kinds of controls were carried out for IH and IC immuno-reactions and Western blotting. First, absence of antibody was used to control for tissue or cell autofluorescence (for IH and IC reactions). Second, primary antibodies were replaced by normal serum, followed by the completion of the protocol. This controlled for nonspecific fluorescence. Third, secondary antibodies were deleted and the reaction completed. Fourth and most robust, pre-absorption controls were performed for IH and WB, antigens (M1, M2, M3 and M5) or pure protein (M4) were pre-incubated with the corresponding antibodies with the ratio of 6:1 (M2 and M3), 3:1 (M1 and M5) and 1:10 (M4) by weight and kept at 4°C for at least 24 hrs.

## **Anatomical nomenclature**

Based on anatomical features, types of hair cells present and the cadre of ionic currents in the hair cells, the pigeon crista and macula can be divided into zones (Masetto and Correia, 1997a; Masetto and Correia, 1997b; Weng and Correia, 1999; Kevetter et al., 2000). In the crista, when sectioned along its long axis, three zones naturally appear in each hemi-crista on either side of the eminentia cruciata. Zone 1 (I), containing type II hair cells, extends from the planum semilunatum to the zone 2 (II) where there are almost exclusively type I hair cells. Zone 3 (III) extends from the central apical region of the crista about 150  $\mu\text{m}$  and contains type II and type I hair cells. Zone 2 (II) is between zones 1 and 3 and contains mostly type I hair cells found singly or in multiples in calyxes. Zones are also present in the pigeon utricular macula. In the striolar region, a zone (S) of cells is present that is comprised of a band of type I hair cells bordered by several rows of type II hair cells only (Jorgensen and Anderson, 1973). In the remaining surface of the macula, the extrastriolar zone (ES), there are only type II hair cells. The zones from which data were obtained are identified in subsequent figures.

## **RESULTS**

### **Patch Clamp Recordings**

The application of carbachol, a cholinergic agonist, modulated (reduced) the ionic currents through an inward rectifier channel, Kir2.1, found in pigeon vestibular hair cells (Correia et al., 2004). Figure 1 shows typical traces from a type II hair cell in a vestibular epithelial slice. Figure 1Aa shows control traces. Figure 1Ab presents traces acquired following application of 2  $\mu\text{M}$  carbachol for 30 seconds. A reduction in the amplitude of

the inward currents by ~30% (Kir2.1) can be seen. The outward current traces do not show any reduction. Following a 9 min wash with normal saline solution the traces recovered (Figure 1Ac) to pre carbachol levels. The current (I) – voltage (V) plot illustrated in Figure 1B documents the effects of the cholinergic agonist. The outward current at voltages > -50 mV are due to activation of other channels found in pigeon type II vestibular hair cells (Lang and Correia, 1989). Next we determined the source of the acetylcholine signaling molecule in the vestibular neuroepithelium.

### **Electron microscopy**

Three hundred thirty eight photomicrographs obtained from thin sections through zones 2 and 3 of the epithelium of the pigeon's anterior semicircular canal crista were studied. The sections were cut in a plane parallel to the long axis of the epithelium. Previously, the photomicrographs had been used to characterize hair cell-afferent terminal synapses (Correia et al., 1985). In this study, the photomicrographs were examined for synaptic complexes containing: a vesiculated pre-synaptic bouton (efferent terminal), pre-synaptic electron density (or a synaptic cleft) and a post-synaptic cistern. These structures are the signature of vestibular efferent synapses (Wersall, 1956). Forty four synaptic complexes were found that met all of these criteria. Type I hair cells and their calyces, type II hair cells and primary afferent bouton terminals were identified. The following distribution was obtained. 61% (27/44) were synapses between efferent terminals and type II hair cells; 2% (1/44) were synapses between efferent terminals and type I hair cells; 25% (11/44) were synapses between efferent terminals and type I hair cell calyces; and 11% (5/44) were synapses between efferent terminals and primary afferent dendrites and terminals. Figure 2 illustrates each of these synaptic complexes.

## **Molecular structure of muscarinic receptor isoforms**

Having determined the distribution of efferent projections onto hair cells and afferent terminals, we systematically examined the distribution of muscarinic receptors in the vestibular periphery. The remainder of the chapter summarizes this work. First, we cloned and sequenced muscarinic receptor subtypes M2-M5 from pigeon brain total RNA. We were unable to clone M1. Figure 3A shows the protein sequence corresponding to the transmembrane portion of the receptors. Note that there is considerable identity between the pigeon receptor subtypes and between pigeon M5 and human M5. Figure 3B shows the third inner loop of the protein. It can be seen that there is considerable diversity in the amino acids in the  $i_3$  loop. This region contains the open reading frame of muscarinic receptor subtypes M2-M5 for pigeon. As a reference, the sequence for muscarinic receptor subtype M5 from human is also shown. The ruler and residue numbers are based on the human M5 sequence Genbank accession # NP\_036257 (Bonner et al., 1988). The pigeon sequences are #s AY838767, AY838768, AY838766 and DQ357059 for the M2, M3, M4 and M5, respectively.

Two features are evident from Figure 3. First, there is good identity between pigeon mACh receptor subtypes and between these subtypes and human M5 for transmembrane segments I-VII, inner and outer loops 1-2 and outer loop 3, but there is considerable heterogeneity for the inner loop 3. This large loop (227 amino acids) contains amino acids that are involved in G protein activation and coupling. Second, although the number of residues found inside and outside inner loop 3 are the same order of magnitude, there are 5.3 times ( $16/3$ ) the number of serine/threonine residues that have a 50% chance of being a phosphorylation site on inner loop,  $i_3$ .



Table 2 presents sequence identities for human muscarinic receptor subtypes M2-M5 compared to pigeon muscarinic receptor subtypes M2-M5. A comparison of probabilities indicates a novel result that human and pigeon muscarinic receptors of the same subtype have greater sequence identity than a comparison of the subtypes for the same species. A phylogenetic analysis of the comparisons shown in Table 2 (data not shown) confirms this conclusion.

### **Frozen section immunohistochemistry**

#### ***Negative controls***

We observed no significant autofluorescence (Del Castillo et al., 1989) in our tissue. We omitted primary or secondary antibodies when performing IH, IC and WB. These controls produced negative results. We pre-absorbed the antibody for each receptor subtype with a blocking peptide or a purified protein (in the case of M4). Compared to the non pre-absorbed condition, the labeling of receptor subtypes on structures in the neuroepithelia were either partially or completely blocked (data not shown).

#### ***Positive controls***

It has been reported that several mAChR subtypes are expressed in rat hippocampus (Rouse and Levey, 1996;Rouse and Levey, 1997;Hajos et al., 1998;Van der Zee and Luiten, 1999). Positive control experiments labeled areas of gerbil and rat hippocampus and striatum previously shown to express certain muscarinic receptor subtypes. Our results produced the same staining pattern as previous studies done with the monoclonal antibody M35 (Van der Zee and Luiten, 1999). The anti- M3 labeled the neuropil and produced the same pattern of immuno-reactivity described in a second

publication (Levey et al., 1995) (data not shown). Our positive and negative control studies indicate that the antibodies we used for mAChR receptor subtypes are selective and specific.

### ***Muscarinic receptor subtype expression in the pigeon vestibular periphery***

All five mAChR subtypes were expressed in the pigeon's ampullary and utricular neuroepithelia, nerve fibers and ganglia as shown in Figure 4. M1, M2, M3, M4 and M5 mAChR subtypes were expressed on different structures (such as supporting cells, hair cells, nerve fibers, ganglion cells, etc.), but in many cases they were co-expressed on the same element (e.g., M1-M5 on hair cells). There was no preferential expression in any region of semicircular canal crista (zones 1, 2 or 3) or utricular macula (S or ES regions).

*Subtype M1* - M1 was expressed in both types (type I and type II) of hair cells in the pigeon's crista and macula. Figure 4 A-1 and A-2 illustrate double labeling of M1 and M4 in the crista (zone 3) and in the macula (striolar region). Type II hair cells are shown labeled in zone 3 (A-1) and type I hair cells, found primarily in zone 2, are not shown. However, type I hair cells, found in the striolar region of the utricular macula, are shown labeled in Figure 4 A-2. Staining of the cuticular plates and cilia were found on the top of some hair cells. The supporting cells, which have their nuclei located near the basement membrane, were also labeled by M1. Figure 4 A-1 and A-2 also show that M1 and M4 are co-localized inside nerve fibers and nerve terminals. In some areas, this co-localization can be seen as yellow structures. But in other cases M1 labeling appears to surround nerve fibers where there is no M4 expression. Since the nerve fibers are myelinated after they exit the basement membrane, the M1 labeling could indicate expression on myelin sheaths. In the vestibular ganglion (A-3), both M1 and M4 were

expressed on both ganglion cells and nerve fibers. As in panels A1-2, M1 but not M4 was also expressed on tissue surrounding the ganglion cells and nerve fibers, which could be Schwann cells and/or myelin sheaths.

*Subtype M2* – M2 was expressed on hair cells and supporting cells in the ampullary (zone 2/3) and utricular neuroepithelium (Figure 4 B-1, B-2). On some hair cells staining was present on the cuticular plate. M2 and M4 were co-expressed in the ganglion cells (Figure 4 B-3). Their expression levels were not always uniform. Since M2 staining was weak compared with M4, it was hard to identify M2/M4 co-localization in the nerve fibers and nerve terminals. However, IH using DAB indicated that M2 was expressed on nerve fibers and nerve terminals (see Figure 5).

*Subtype M3* – M3 labeling are shown in Figure 4C. In the crista (zone 2/3) and the macula striolar region of the utricle (Figure 4 C-1 and C-2), M3 was expressed on hair cells especially at the super-nuclear regions and on the cuticular plates but supporting cells were negligibly stained, if at all. M3 labeled parallel lines stopped just beneath the neuroepithelium basement membrane where the dendritic axons (nerve fibers) are known to lose their myelin. In contrast, M4 labeled nerve fibers extended into the neuroepithelium and terminated on hair cells. In C-3, M3 is shown to be mainly located on the ganglion cell bodies. No obvious co-expression of M3 with M4 was observed in neural processes of the ganglion cells.

*Subtype M4* – The M4 receptor subtype was expressed on myelinated vestibular nerve fibers and unmyelinated nerve terminals in the neuroepithelia. M4 was present on the boutons en passant and calyces as well as the myelinated nerve fibers in zone 2/3 of semicircular canal crista (Figure 4 D-1). The same labeling was evident in the striolar zone of the utricular macula (Figure 4 D-2). M4 was also expressed on vestibular

ganglion cells as well as their dendrites and axons. No M4 labeling was seen on Schwann cells or myelin sheaths (Figure 4 D-3).

*Subtype M5* – Structures labeled by M5 antibodies were very similar to those labeled by M1. M5 was expressed on both types of hair cells and supporting cells, as shown in the cristae (zone 3; Figure 4 E-1) and utricular striolar region (Figure 4 E-2). M5 was also expressed on accessory structures such as the cuticular plate and cilia. M5, with M4, was co-expressed on nerve fibers and nerve terminals. Additionally, M5 co-localized with M4 on some ganglion somata and their neural processes. Finally, M5 was expressed on putative Schwann cells (Figure 4 E-3). The green labeling above the row of hair cells in utricle (especially in E2) is artifact induced by labeling the otoconial membrane which was not removed.

#### ***Muscarinic receptor subtype expression on myelin sheaths and Schwann cells***

Pigeon vestibular nerve fibers and ganglion cells are myelinated (Landolt et al., 1973; Landolt et al., 1975). To verify that some of the mAChR subtypes were expressed on myelin sheaths and Schwann cells of the peripheral vestibular nerve fibers, we used osmium tetroxide to stain myelin and compared this label to the DAB immunoreactivity of mAChR subtypes in both vestibular end organs and Scarpa's ganglion (Figure 5). Sections through the utricular macula had the same staining patterns as the semicircular canal crista and are not shown.

The data summarized in Figure 5 indicates that M2 and M4 are extensively expressed on ganglion cell bodies and nerve fibers but not on myelin sheaths or Schwann cells (Figure 5 B-2, B-4). On the other hand, M1, M3 and M5 subtypes are expressed on ganglion cells and both myelin sheaths and Schwann cells (Figure 5 B-1, B-3 and B-5).

In addition, all five subtypes stained nerve fibers, as shown in (A) the ampulla end organ region and (B) the Scarpa's ganglion area. The results of osmium tetroxide and DAB staining in the vestibular ganglion and peripheral end organs (crista and macula) are consistent with the fluorescent IH results.

### ***Isolated cell immunocytochemistry***

Dissociated hair cell and ganglion cell IC was used to confirm the results of tissue IH and to examine expression of the receptor subtypes on fine structures such as the cuticular plate and cilia.

Both types of hair cells (type I and type II) from both the crista and utricle were examined. No difference in staining patterns was found in the hair cells from either the crista or the utricle for each mAChR subtype. Type I and type II hair cells can be distinguished by the ratio of the neck width to cuticular plate width and the neck width to the body width (Ricci et al., 1997). All five mAChR subtypes were expressed on both types of hair cells and ganglion cells (Figure 6). However, there was differential expression of the subtypes on certain cellular structures, including the cilia and cuticular plates. Only M1 and M5 were expressed on the cilia while only M4 was not expressed on the cuticular plates.

M4 and M5 appear expressed mainly in the hair cell membrane, as expected. However, for the other subtypes mAChR labeling was found to be in the cell cytoplasm or in both the cytoplasm and plasmalemma. In no case, however, did the nucleus of the cells show label.

Table 3 summarizes the results derived from all the IH and IC studies using frozen sections and dissociated cells.

### ***Western blotting***

The results of the Western blotting studies presented below are consistent with the data presented in Table 3 above. The results for each mAChR are summarized in turn.

*Subtype M1* - Multiple bands were seen for all three lysates (VG, NE and NF) but the M1 pre-absorption control (H-) showed a partial blockage of the band corresponding to a molecular mass (Mr) of 57 kDa compared with the normal control (H) (Figure 7). At this position, each lysate showed the same protein band. The molecular mass for pigeon M1 is unknown but in human, the molecular mass of M1 is estimated to be 51 kDa.

*Subtype M2* - Consistent with the results of frozen section staining, M2 showed weaker signals for protein samples from VG and NF compared to NE (Figure 7). A protein band at 47 kDa was completely blocked with pre-adsorption. This value is close to the theoretical Mr of pigeon M2 protein which should be 51.4 kDa.

*Subtype M3* - We located two protein bands that were blocked using pre-absorption controls (Figure 7). One protein band was located at 73 kDa; the other band was at 48 kDa. Two protein bands shown in Figure 7 could be due to the breakage of proteins during sample preparation. This result is identical to the blot shown on the manufacturer's data sheet. The blockage of these two bands by the negative control antigen indicates that both bands are related to M3 protein (personal communication, Ofra Gohar, Ph.D, Alomone Labs, Ltd., Jerusalem, Israel). The Mr of pigeon M3 should be 72 kDa. At that Mr M3 was present in all three vestibular samples, but weak in the nerve fibers which was consistent with the IH fluorescent and DAB results.

*Subtype M4* - Only one protein band for M4 was clearly seen on the VG, NE and NF lanes (Figure 7). No matter whether we increased the boiling time for denaturing the sample proteins or used other protein samples, such as gerbil's heart muscle, striatum or

hippocampus, a single band for M4 protein was always located at 98 kDa (data not shown). However, the theoretical Mr of M4 from pigeon is 55 kDa. This difference in molecular mass may be the result of post-translational modification resulting in the increased molecular mass. Compared with the normal control (H), the M4 protein band was partially blocked in the pre-adsorption control (H-) indicating that this protein band was indeed M4.

*Subtype M5* - M5 control lanes had at least three protein bands, only the one located at 74 kDa could be blocked with excess antigen. This product was present in the VG and NE lanes but barely detectable for NF. The measured Mr of M5 is 74 kDa which is larger than that calculated from its gene sequence (59.9 kDa). Again this could be due to the post-translational modification (Note the numerous glycosylation and phosphorylation sites in the sequences presented in Figure 3).

## DISCUSSION

Patch clamp recordings from pigeon native hair cells show that carbachol, a cholinergic agonist, reduces the current through the inward rectifier Kir2.1 channel. Previously, we presented preliminary results (Li and Correia, 2005) that carbachol also reduced the current in tsA-201 cells transfected with a vector that included M3, enhanced green fluorescence protein (EGFP) and pKir2.1. The reduction in pKir2.1 current leads to a depolarization of the cell membrane and therefore modulates the cell's sensitivity (Correia et al., 2004). This important physiological function prompted us to seek the source of ACh in the pigeon vestibular neuroepithelium and describe the muscarinic receptor subtypes.

It has long been known that in mammals cholinergic synapses exist between efferent vestibular neurons, hair cells and afferent terminals (Gacek et al., 1965; Iurato et al., 1971). Moreover, it has been shown that, like mammals (Goldberg and Fernandez, 1980), the cell bodies of putative avian efferent neurons are present in the brainstem (Schwarz et al., 1981; Eden and Correia, 1982). Cholinergic synapses exist in the pigeon vestibular neuroepithelium with anatomical features (See Figure 2) like those seen for efferent synapses in mammals (Wersall, 1956). That is, there is a vesiculated pre-synaptic bouton (efferent terminal), a pre-synaptic electron density (or a synaptic cleft) and a post-synaptic cistern. Analysis of a sample of 44 synapses reveals that efferent boutons synapse on hair cells, both type I and type II as well as calyx and bouton afferent endings. The distribution of types of synapses show the synapses between type II hair cells and efferents are the most frequent whereas synapses between type I hair cells and efferents are the least frequent. However, the novel finding of a synaptic contact between a type I hair cell and an efferent terminal indicates that efferents can control type I hair cells via either the cell body and/or the calyx.

To determine the molecular sequence of pigeon mAChRs we cloned and sequenced M2-M5. We aligned the 4 pigeon mAChR sequences with human M5 and noticed that in both pigeon (M2-M5) and human M5 there is good homology in all domains of the protein, except in the inner loop 3 domain. The  $i_3$  loop domain in each subtype has considerable diversity. In addition, there is greater identity between comparable subtype isoforms in pigeon compared to man than between the 5 subtypes in each species.

The vast majority of proteins are subject to one or more post-translational modifications which are functionally relevant. The mAChRs can be modified at



glycosylation sites near the start codon of the ORF and/or at phosphorylation sites in the inner loop 3. It has been shown that protein glycosylation is required for transport of the mAChR to the cell surface (Liles et al., 1986), but these sites are not involved in cell surface localization or ligand binding (Van Koppen and Nathanson, 1990). The rich S/T<sub>i3</sub> domain in M1-M3 has been demonstrated to be responsible for mAChR internalization/sequestration leading to a reduction in binding sites (Lameh et al., 1992; Moro et al., 1993). Moreover, it has been suggested that phosphorylation of members of the mAChR family may underlie uncoupling of receptors from G-proteins and may be responsible for the rapid phase of receptor desensitization (Contrera et al., 1993; Hosey et al., 1995).

We obtained very consistent results using 3 different methods (IH, IC and WB) to identify the mAChRs on neural and accessory structures in the pigeon vestibular periphery. A schematic summarizing these results and indicating the distribution of mAChR subtype expression in the pigeon's vestibular neuroepithelia, afferent fibers, ganglion cells, and accessory elements is presented in Figure 8. Our results do not speak to the amount of expression of M1-M5 but do indicate that mAChRs are widely present and co-expressed on vestibular peripheral structures. Furthermore, we cannot dismiss the additional possibility of mAChR expression on efferent fibers and terminals forming autoreceptors. This possibility was not explored in this study because of the difficulty of separating afferent and efferent terminals morphologically at the light microscopic level.

The possible roles of the mAChR subtypes in the vestibular periphery may be surmised based on knowledge gained from studies of mAChRs in other physiological systems. In general, it is known that acetylcholine receptors serve autocrine and neuronal functions (Wessler et al., 1998). The autocrine functions include control of cell growth

and proliferation and control of the release of chemical mediators (Fritz et al., 1999; Fujii and Kawashima, 2001; Chi et al., 2002; Nomura et al., 2003; Kawashima and Fujii, 2004). These functions could obviously be important in hair cell regeneration or maintenance and replenishment of endolymph and perilymph (Wangemann et al., 2001). The expression of mAChR subtypes on supporting cells and Schwann cells may provide a non-neuronal cholinergic function (Eglen, 2006). However, the abundance of mAChRs on the neuronal elements in the peripheral labyrinth strongly suggests mAChR involvement in sensory transduction and signal modulation.

The hair cell cilia and the underlying cuticular plate are crucial structures for sensory transduction. The cilia consist of multiple stereocilia and a single kinocilium. Stereocilia possess mechanically gated channels (Hudspeth, 1989) while the kinocilium serves as a linkage to transfer the mechanical stimuli to the stereocilia (Hudspeth and Jacobs, 1979). In this study we determined that cilia, at least stereocilia, showed clear expression for the odd-numbered mAChR subtypes: M1 and M5. The major component of the stereocilia is actin (Flock and Cheung, 1977; Tilney et al., 1980; Shepherd et al., 1989), which is cross-linked by another filament protein, fimbrin (Flock et al., 1982; Tilney et al., 1989; Drenckhahn et al., 1991; Hofer et al., 1997). Stereocilia have a similar structure and protein composition to microvilli of the intestine (Mooseker and Tilney, 1975). The rootlets of microvilli are enmeshed in the terminal web which has fine filamentous networks of actin-associated cross-linkers, such as myosin, tropomyosin, fodrin and spectrin-like proteins (Mooseker et al., 1978; Glenney, Jr. et al., 1982; Glenney, Jr. et al., 1983; Burgess et al., 1987; Citi and Kendrick-Jones, 1991). Stereocilia are embedded in the cuticular plates which contain actin, alpha-actin, myosin, tropomyosin, fodrin, fimbrin, etc. (Sobin and Flock, 1983; Slepecky and Chamberlain,

1985; Scarfone et al., 1988; Hasson et al., 1997). When acetylcholine is applied to ciliated epithelial cells, the ciliary beat frequency (CBF) is increased in cultured ovine tracheal epithelial cells (Salathe and Bookman, 1995), cultured frog esophagus epithelium (Zagoory et al., 2001), cultured explants of *Rana pipiens* palate (Aiello et al., 1991) and cultured adenoid explants (Yang and McCaffrey, 1996). Selective M1 and M3 mAChR subtype antagonists significantly inhibited the ACh induced stimulation of CBF. A similar role for acetylcholine in hair cell stereocilia could be speculated.

In hair cells, the movement of the cuticular plate and stereociliary bundle plays a role in hair cell motile responses (Zenner, 1988). Furthermore, the control of hair cell motile responses may be due to phosphoinositide metabolism (Schacht J. and Zenner H.P., 1986; Schacht and Zenner, 1987), which changes the intracellular calcium level that in turn modulates actin polymerization and microfilament-based motility (Lassing and Lindberg, 1988). In rat cochlear hair cells, the activation of M3 is thought to increase the inositol phosphate cascade (Guiramand et al., 1990). Considering the intracellular signaling pathway and the molecules responsible for the modulation of ciliated epithelial movements, mAChR activation could regulate the mechano-electrical transduction of vestibular hair cells at least at three places: stereocilia, cuticular plate and soma. The expression of mAChR subtypes M1 and M5 on cilia, M1, M2, M3 and M5 on the cuticular plates and hair cell bodies and M4 on the hair cell body indicates that each mAChR subtype might play different roles to regulate the hair bundle sensory transduction and signal processing in the hair cell. Recent studies of hair cells indicate that hair bundle motility can occur spontaneously or be evoked (Martin and Hudspeth, 1999). Thus, the wide expression of mAChR on the vestibular hair bundle, cuticular plate and hair cell body could exercise regulatory control of hair bundle spontaneous or driven

motion and consequently improve or degrade (modulate) the efficiency of hair cell transduction. An interesting and perplexing question, however, is where are the ACh stores located that activate receptors on the cilia and cuticular plates? The cilia and cuticular plates are bordered by endolymph. They are separated from the neuroepithelium by the tight junctions between hair cells and adjacent supporting cells. It could be suggested that hair cells excrete ACh through the apical surface of the cuticular plate but this is unproven and needs future study.

The expression of all five mAChR subtypes on vestibular hair cells indicates that they probably play an important role in modulating ion channel activity involved in changing the hair cell membrane potential and regulating transmitter release from hair cells onto afferent terminals. The signaling molecule for this sequence of events would be the release of ACh by efferent terminals onto hair cells and nerve terminals. In isolated frog vestibular hair cells, application of the mAChR agonist carbachol stimulated the transmitter release from hair cells (Derbenev et al., 2005). Notably, carbachol decreases currents in Kir2.1 channels (Jones et al., 1991b; Jones, 1996; Pemberton and Jones, 1997; Firth and Jones, 2001) and decreases currents in KCNQ channels (Selyanko et al., 2000; Wei et al., 2005; Shen et al., 2005) and either increases (M4 acting on AtT-20 cells) or decreases (M1-M5 acting on NIH3T3 transfected cells) current in calcium L type channels (Pemberton and Jones, 1995; Pemberton and Jones, 1997). The above mentioned channels whose currents can be modulated by carbachol have been identified as being expressed on vestibular type II hair cells. These channels include Kir2.1 (Correia et al., 2004), putative KCNQ (Rennie et al., 2001) and L type  $\text{Ca}^{2+}$  channels (Lang and Correia, 1989).

Different AChR subtypes apparently modulate different ion channels in different polarizing directions. For example, the odd-numbered groups of mAChRs, mediated through  $G\alpha_q/11$  protein, can produce inhibitory effects on KCNQ and Kir2.1 channels and depolarize the hair cell membrane potential. On the other hand, it has been found that the cochlear hair cell membrane potential can be hyperpolarized by activating the  $Ca^{2+}$  activated  $K^+$  channel (Shigemoto and Ohmori, 1991). The even-numbered but not odd-numbered mAChRs, are responsible for increasing the conductance of the  $Ca^{2+}$  activated  $K^+$  channel (Kong et al., 2005). Again,  $Ca^{2+}$  activated  $K^+$  channels are present on pigeon vestibular hair cells (Lang and Correia, 1989).

Supporting cells in the pigeon vestibular neuroepithelium express Kir2.1 ion channels (Masetto and Correia, 1997a) and show M1, M2, M3 and M5 expression. They could communicate with hair cells through gap junctions and be modulated by ACh. However, the question again arises - where does the ACh transmitter come from? We were unable to visualize efferent terminals synapsing on supporting cells, using either light or TEM microscopy. There are only suggestions of such synapses. For example, electron microscopic analyses have demonstrated that labeled immature efferent axons were present among supporting cells of the greater epithelial ridge at P0 in the rat cochlea (Bruce et al., 2000) and in mouse cochlea efferents have extensive collaterals among supporting cells of the greater epithelial ridge from 16.5 days post coitum onwards (Bruce et al., 1997).

Scarpa's ganglion bipolar cells and their neural processes express all the mAChR subtypes. This result is consistent with earlier studies of mAChR message. Using RT-PCR mRNA analysis, rat vestibular peripheral end organ and Scarpa's ganglion cells expressed message for all five mAChR subtypes while in human message for only M1,

M2 and M5 was found (Wackym et al., 1996; Ishiyama et al., 1997). The expression of muscarinic receptors on vestibular ganglion cells and nerve fibers could be involved in the regulation of the axoplasmic transport (Kawakami et al., 1995), neurofilament expression and neurite growth (Small et al., 1995).

Vestibular ganglion cells and nerve fibers are enveloped by myelin sheaths formed by Schwann cells, (Landolt et al., 1973; Landolt et al., 1975; Samandari and Bogusch, 1981; Ona, 1993; Kido et al., 1993; Kido and Sekitani, 1994). Previous studies (Torskaia and Goloborod'ko, 1977; Haynes, 1983; Lan et al., 1996) have reported that glial cells demonstrate the presence of acetylcholinesterase and choline acetyltransferase which might indicate the existence of cholinergic receptors on the glial cells. Our results show that M1, M3 and M5 are expressed on both myelin sheaths and putative Schwann cells. It is known that K<sup>+</sup> channels play an important role in the formation, maintenance and proliferation of myelin (Wilson and Chiu, 1990; Sobko et al., 1998). M1, M3 and M5 may modulate K<sup>+</sup> ion channels in myelin and Schwann cells and therefore may assist in the initiation, repair and proliferation of myelin. Moreover, the activation of the intracellular signal effectors, such as mitogen-activated protein kinase might also participate in the controlling of cell growth and proliferation (Berkeley and Levey, 2000; Hamilton and Nathanson, 2001).

Finally, the mAChR subtypes that were grouped on different vestibular peripheral structures were not always the same (See legend of Figure 8). A similar heterogeneity of muscarinic receptor subtype co-expression has been found in other tissues e.g., salivary gland, ileum, lung and neuromuscular junctions (Dorje et al., 1991; Levey, 1993; Garcia et al., 2005). Similarities and differences also exist between mAChR subtype expression in the pigeon vestibular periphery and the rat cochlea. For example, the odd numbered

mAChRs are expressed on hair cells, supporting cells and ganglion cells in both systems. But, while M2 and M4 subtypes are expressed on both types of hair cells, nerve fibers (particularly M4) and ganglion cells in the peripheral vestibular system, their expression was not detected in cochlea (Khan et al., 2002).

In conclusion, based on previous work in other tissues and cell types, we have suggested possible roles of the mAChRs expressed in the pigeon vestibular periphery. The exciting challenge for future research will be to decipher the functional contribution of each mAChR subtype or groups of subtypes on each of the neural structures where we have found their expression. A second challenge will be the parceling out of the role of nicotinic receptor subtypes from those of muscarinic subtypes and vice versa in the vestibular periphery. To do this we will need much more specific mAChR and nAChR agonists and antagonists and robust supplementary electrophysiological techniques.

Table 1.

## Antibodies and Antigens Used for Muscarinic Receptor Subtype Studies

mAChR Subtypes	Item*	Cat. #	Host	Source	Company	Epitope	Identity to Pigeon	Pigeon Accession #
mAChR M1	Ab	Q4A173R	Rabbit		Biodesign	Amino acid		
	Ag	A4A730H		Human	International	451-460	---	---
mAChR M2	Ab	AMR-002	Rabbit		Alomone Labs	Amino acid	87/132	AY838767
	Ag	For AMR-002		Human		225-356	(65.9%)	
mAChR M3	Ab	AMR-006	Rabbit		Alomone Labs	Amino acid	17/19	AY838768
	Ag	For AMR-006		Rat		461-479	(89.5%)	
mAChR M4	Ab	MAB1578	Mouse		Chemicon	Amino acid	101/194	AY838766
	Protein	sc-4505 WB		Human	International	217-401	(52.1%)	
					Santa Cruz	Amino acid	92/184	
mAChR M5	Ab	Q4A871R	Rabbit		Biotechnology	220-394	(50%)	DQ357059
	Ag	A4A738H		Human	Biodesign	Amino acid	13/16	
					International	516-531	(81.3%)	

\* Ab, Antibody; Ag, Antigen.

Table 2.

Sequence pair identities of Clustal W analysis comparing human and pigeon muscarinic subtypes M2-M5. Percent identity for the same subtype but across species appears bolded in the cells. Note that these are the highest values.

HM2	HM3	HM4	HM5	PM2	PM3	PM4	PM5	
	46.5	59.0	43.9	<b>87.3</b>	46.3	63.4	44.5	HM2
		39.4	47.9	37.4	<b>80.3</b>	37.9	49.3	HM3
			43.8	57.8	45.3	<b>75.4</b>	44.1	HM4
				39.1	51.7	40.6	<b>74.8</b>	HM5
					45.3	63.3	39.5	PM2
						34.1	54.4	PM3
							41.0	PM4
								PM5



Table 3.

Summary of mAChR subtype expression on the peripheral vestibular neurons

	M1	M2	M3	M4	M5
Hair Cells	Yes	Yes	Yes	Yes	Yes
Cilia	Yes	No	No	No	Yes
Cuticular plate	Yes	Yes	Yes	No	Yes
Supporting cells	Yes	Yes	No	No	Yes
Nerve Terminals	Yes	Yes	No	Yes	Yes
Nerve Fibers	Yes	Yes	Yes	Yes	Yes
Myelin Sheath	Yes	No	Yes	No	Yes
Gang lion Cells	Yes	Yes	Yes	Yes	Yes
Schwann Cells	Yes	No	Yes	No	Yes

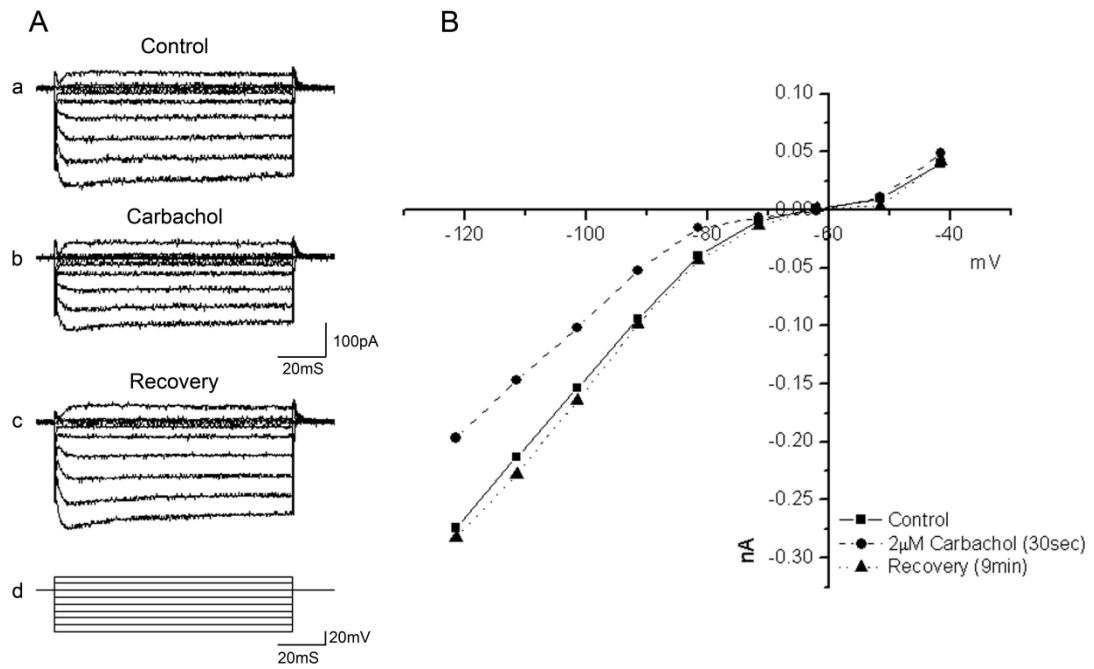


Figure 1. A. Traces of inward and outward currents produced by inward rectifier  $K^+$  channels (Kir2.1) in a pigeon type II vestibular hair cell. Traces are shown for the control (a), carbachol application (b) and recovery (c). As seen in the voltage protocol traces (Ad) the cell was held at -60 mV and voltage was varied in 10 mV increments from -120 to -40 mV. (B) An I-V plot showing the results of control (■), carbachol (●) and recovery (▲) responses.

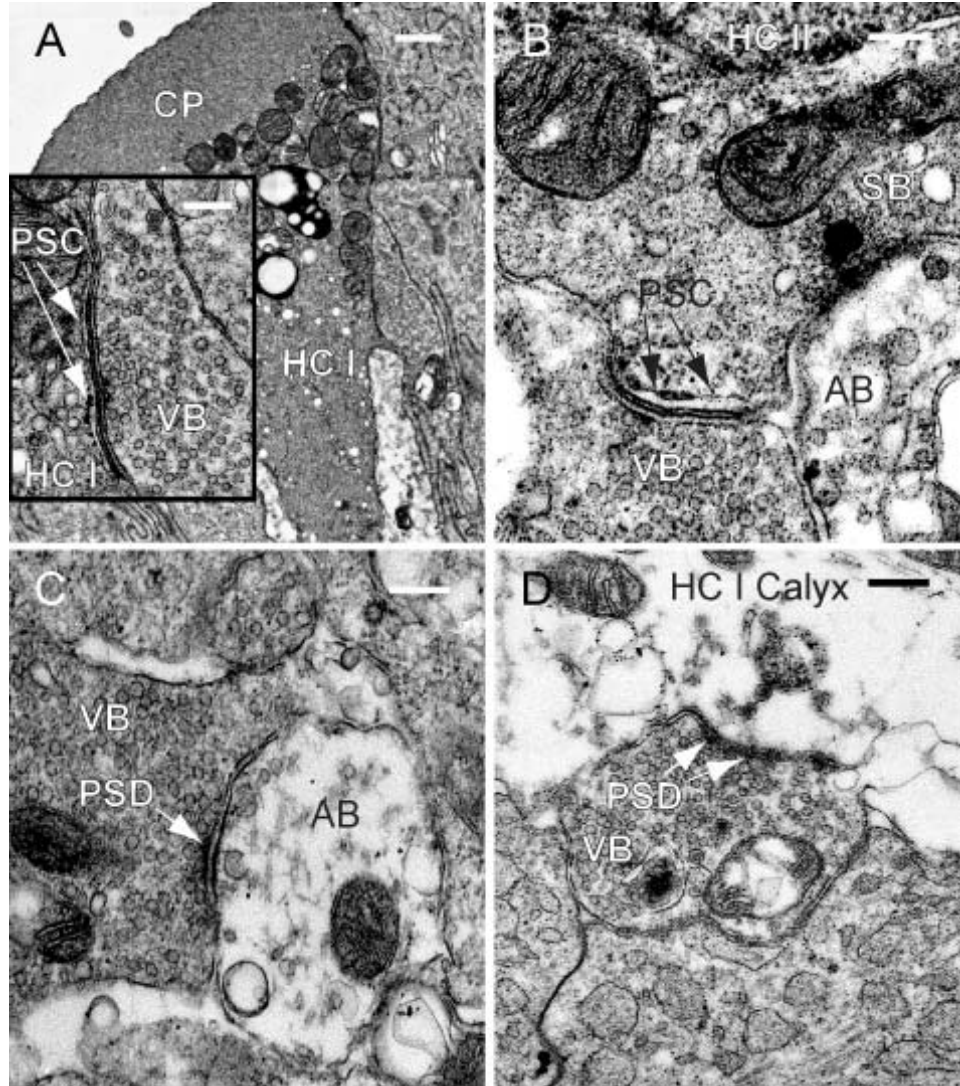
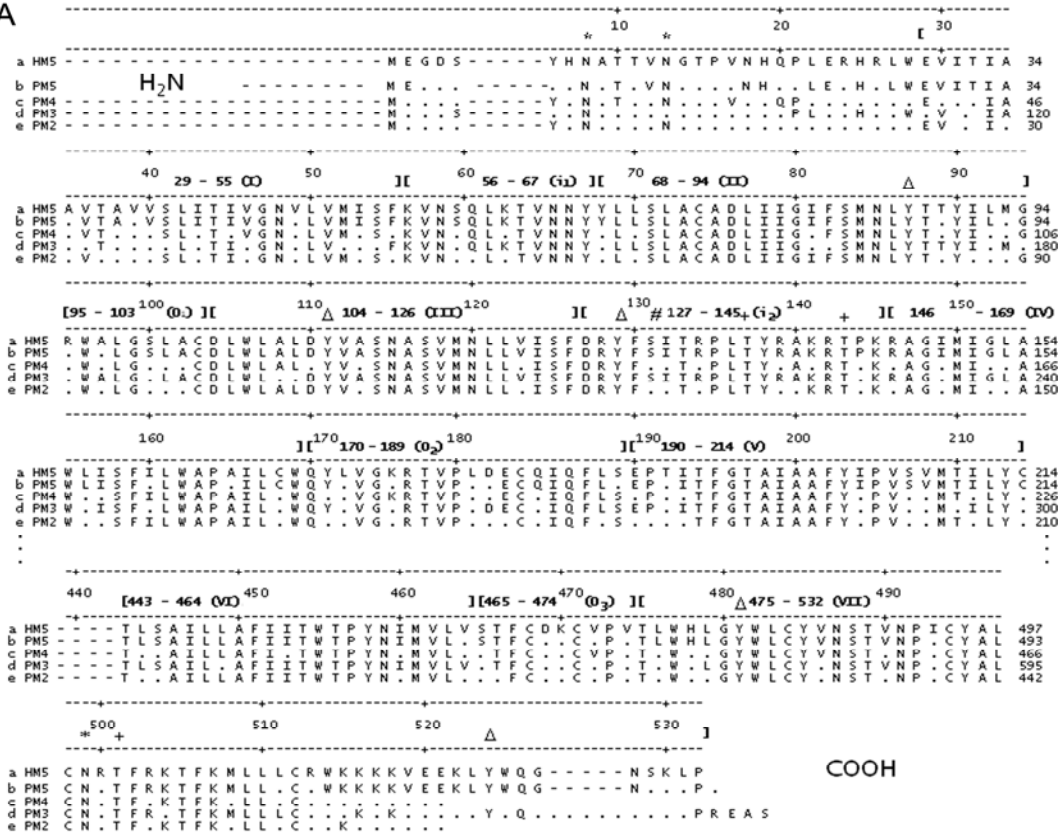


Figure 2. Efferent synapses on type I hair cell (A); type II hair cell; (B); afferent nerve fiber (C) and type I hair cell calyx (D). Inset in panel A shows enlarged view of synaptic contact between efferent terminal and type I hair cell. Abbreviations: cuticular plate (CP); post synaptic cistern (PSC); vesiculated bouton (VB-efferent); type I hair cell (HC I); type II hair cell (HC II); synaptic body (SB); afferent bouton (AB) and pre-synaptic density (PSD). Bars: inset in A = 20 nm; Fig. A = 5 μm; in B-D = 200 nm.

A



B

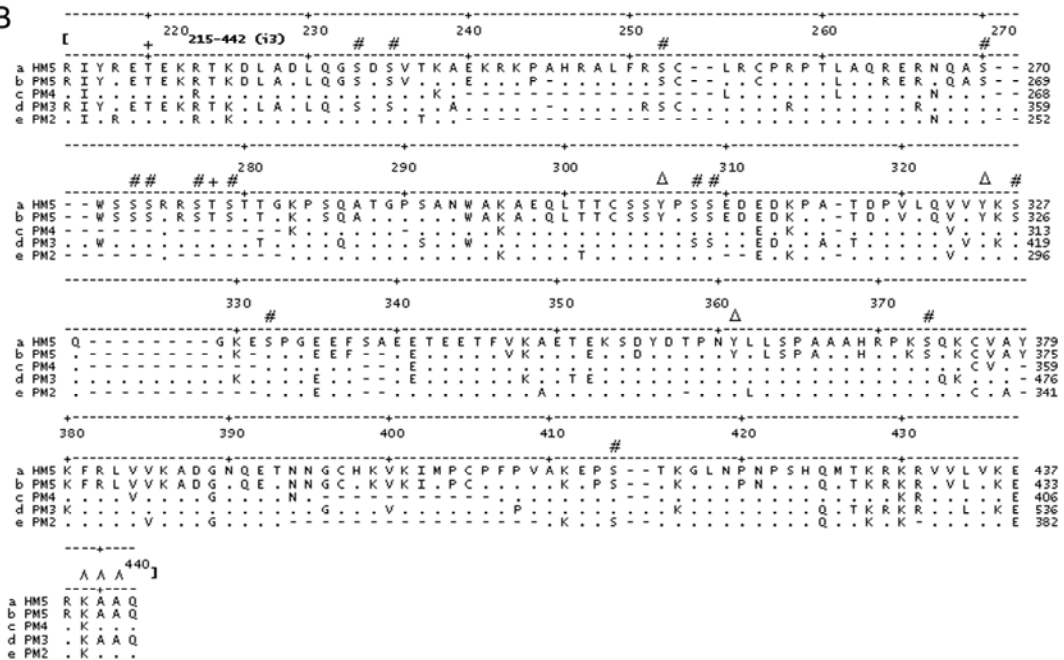


Figure 3. (A) Alignment of human M5 (HM5) with pigeon M2-M5 (PM2-PM5). Shown are all seven transmembrane segments and outer and inner segments 1-2. (B) Alignment of HM5 and PM2-PM5. Shown is the inner loop 3. This segment is believed to contain three amino acids (K339, A440 and A441) that are involved in G protein activation and coupling (Burstein et al., 1998). In the alignment in both A and B only identical residues are shown. The seven transmembrane segments are bracketed and labeled by roman numerals. The three inner and outer segments are labeled **i**<sub>1-3</sub> and **o**<sub>1-3</sub>. Within the brackets, the range of residues is given. Serine, threonine and tyrosine residues with a probability of  $P > 0.5$  of being a phosphorylation site are labeled with #, + and Δ, respectively. Glycosylation sites are identified by \*. The amino and carboxyl terminals are identified by H<sub>2</sub>N and COOH, respectively.

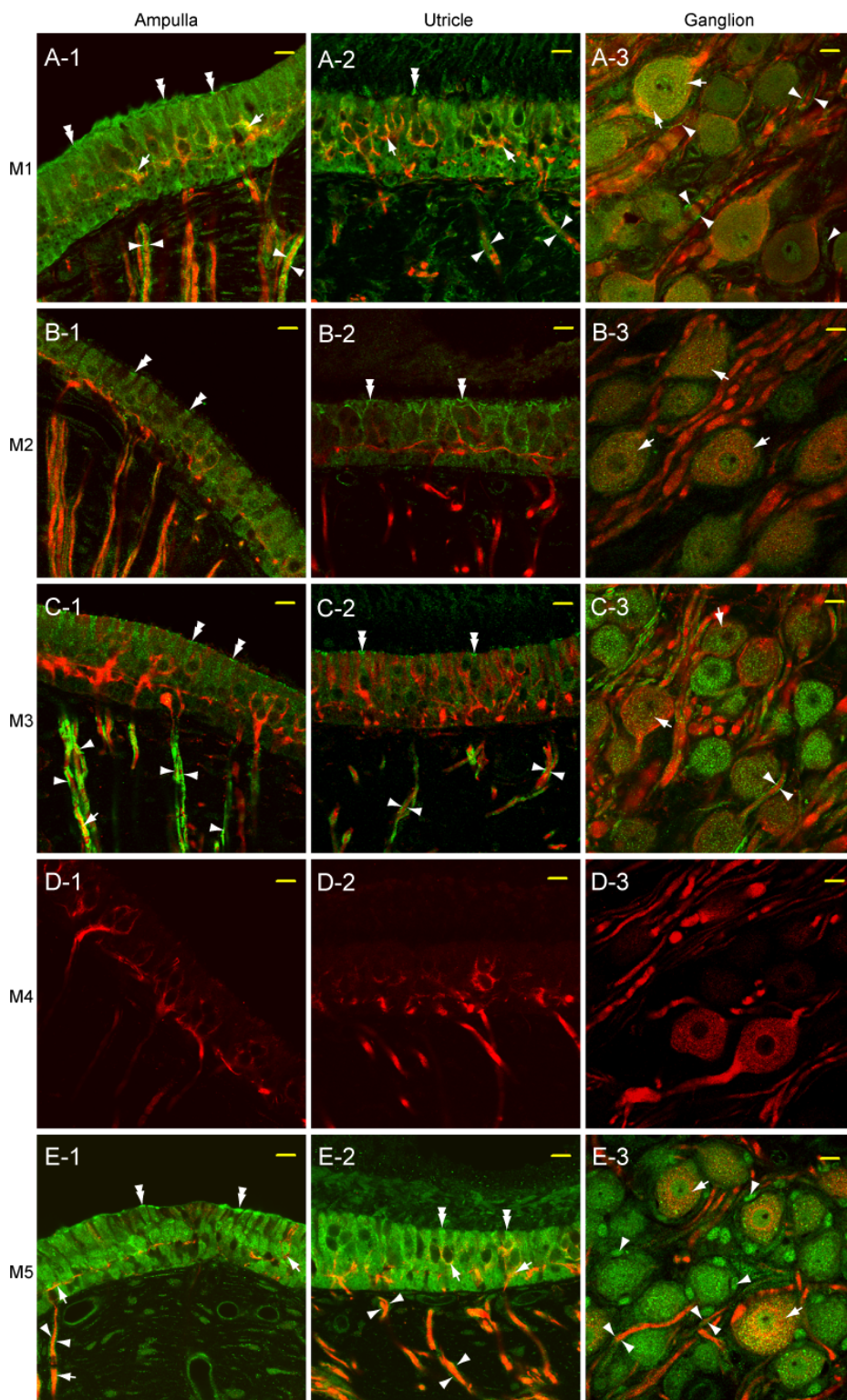


Figure 4. Fluorescent labeling of mAChR subtype expression on vestibular peripheral structures in the crista, utricle and ganglion. The results show anti-M4 antibody reacted with a red fluorescent secondary antibody while other mAChR subtypes are labeled with a green secondary antibody. No differences were found when the red/green fluorescent secondary antibodies were reversed. The co-expression of M4 with M1, M3 and M5 on nerve fibers, nerve terminals and ganglion cells are marked by arrows. Myelin sheaths and Schwann cells surrounding ganglion cells are indicated by single arrowheads. Cuticular plates w/ or w/o protruding cilia are indicated by double arrows. The labeling above the row of hair cells in utricle (especially in E2) is artifactual labeling of the otoconial membrane which was not removed. Scale bars = 10  $\mu$ m.



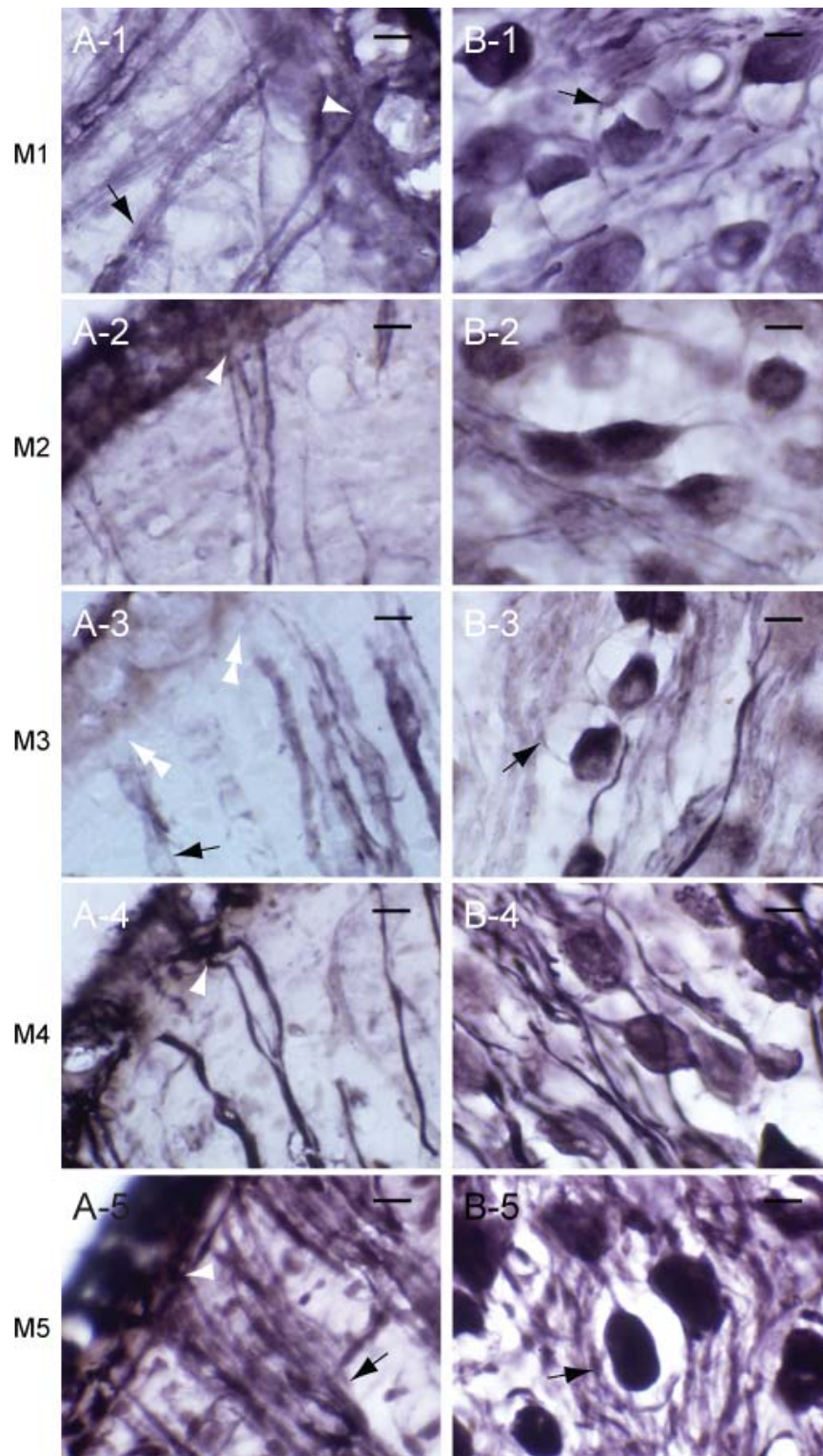




Figure 5. DAB staining of (A) semicircular canal crista and (B) vestibular ganglion. The number in each panel corresponds to the mAChR subtype number. Myelin sheaths and Schwann cells circumscribe the nerve fibers and ganglion cells (black arrows). Nerve fibers expressing M1, M2, M4 and M5 traverse the basement membrane and terminate in the neuroepithelium (arrowheads). There is no M3 expression on peripheral nerve terminals inside of the neuroepithelium. The myelin sheath staining stops just beneath the basement membrane (double arrowheads in A-3). Scale bars = 10  $\mu$ m.

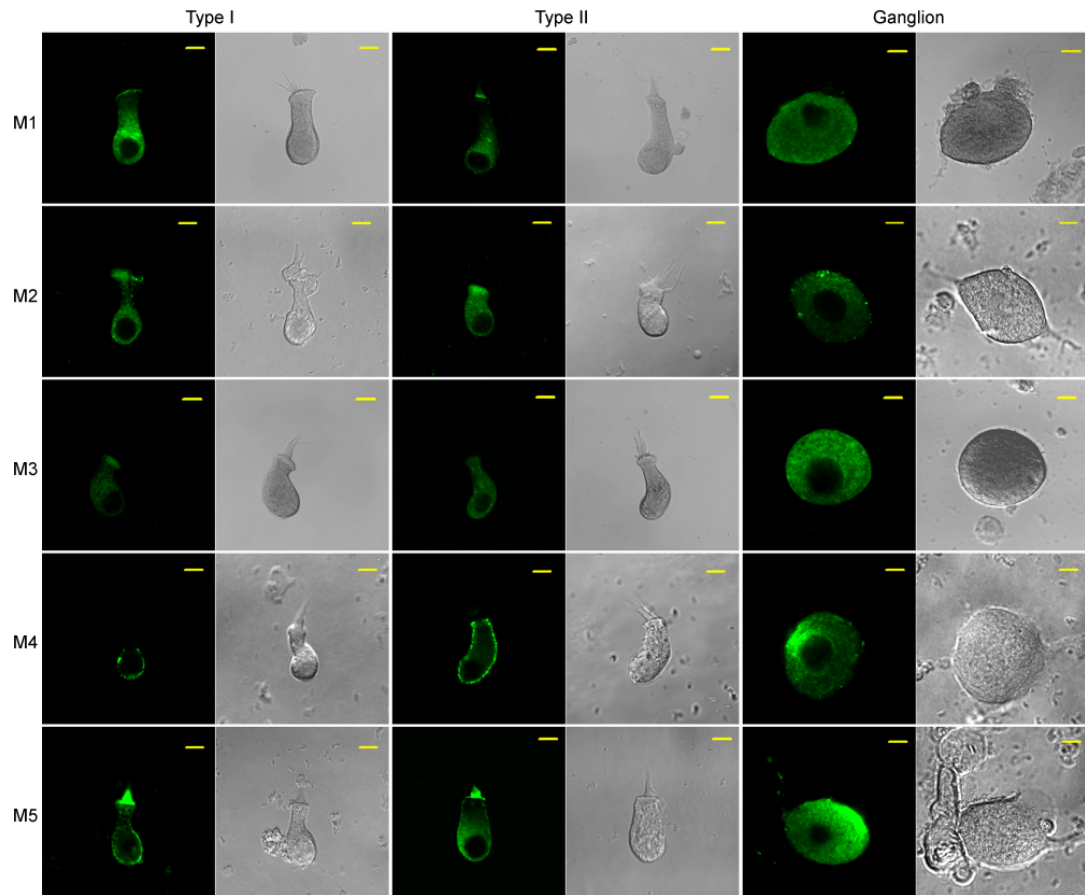


Figure 6. Isolated type I and type II hair cells from crista and utricle, as well as vestibular ganglion cells labeled with each of five primary antibodies. The primary antibodies were labeled with a green-tagged secondary antibody. Corresponding differential interference contrast (DIC) photomicrographs are shown in adjacent columns. Note that M1 and M5 are located on hair cells, cilia and cuticular plates; M2 and M3 are shown on hair cells and cuticular plates and M4 is expressed only on hair cells. All five mAChRs are expressed on ganglion cells (column 3). Scale bars = 5  $\mu$ m.

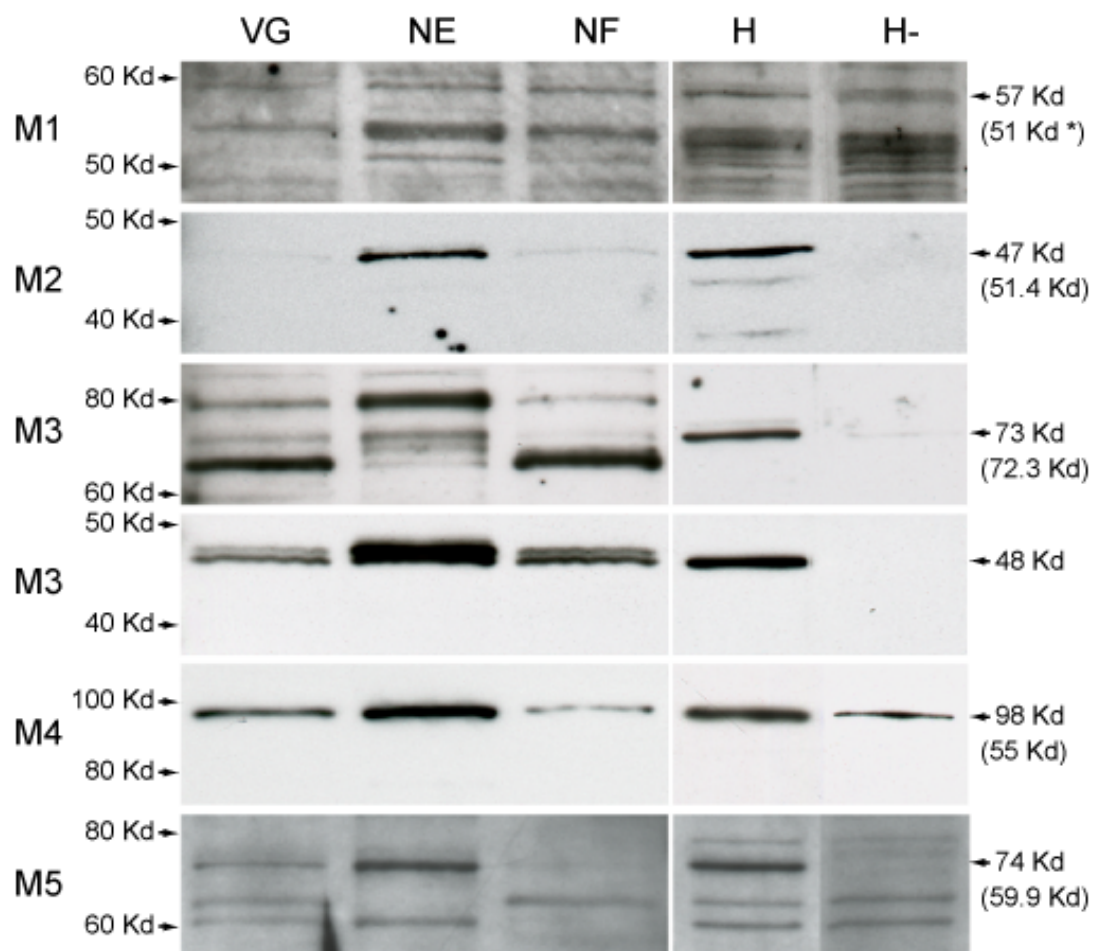


Figure 7. Western blotting results for excised vestibular ganglion (VG), dissociated vestibular end organ epithelium (NE) and dissociated nerve fibers (NF). Protein samples used for the normal controls (H) and pre-adsorption controls (H-) were from pigeon hippocampus. Molecular mass based on markers are indicated on the left. The measured and theoretical molecular masses (in parentheses) are shown on the right. Non stringent “Dirty” Western blot techniques were applied to help identify all mACHR subtype protein products. Molecular mass of M1 mACHR in human is marked by \*.

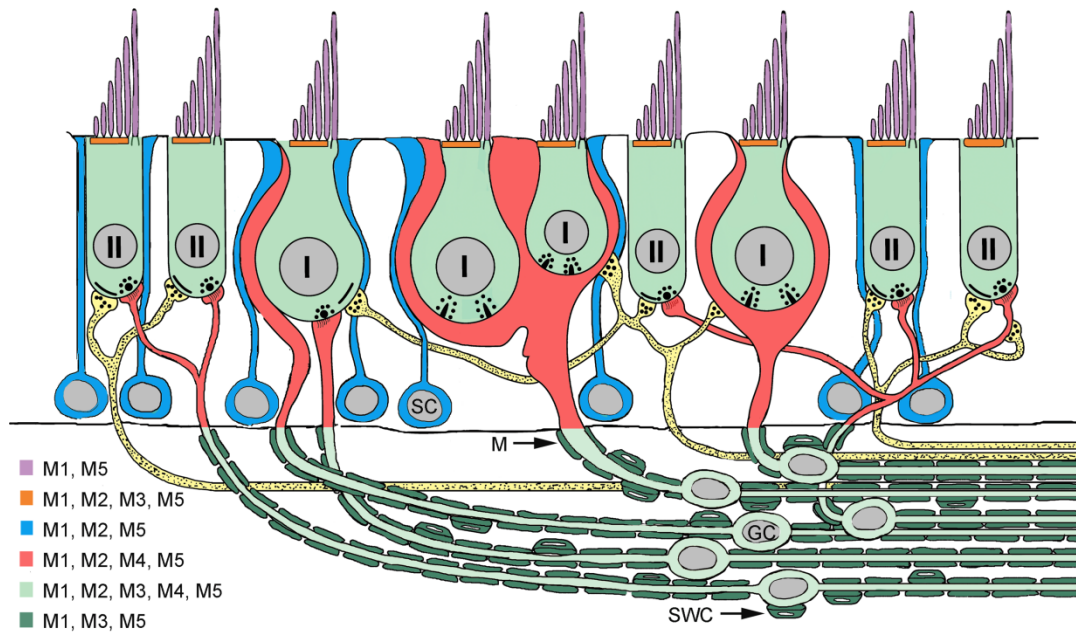


Figure 8. Summary of M1-M5 mAChR subtype expression in the pigeon vestibular periphery. Shown are the two types (I and II) of hair cells (light green); cuticular plates (orange); cilia (violet); supporting cells (SC, blue); afferent endings (calyxes and boutons, red); nerve fibers of ganglion cells and ganglion cells (GC, light green); myelin sheaths (M) and Schwann cells (SWC, dark green). Each color indicates the location of expression and the mAChR subtypes that were expressed. Although efferent fibers and efferent terminals (yellow) are shown for reference no attempt was made to determine mAChR subtype expression on these structures because of the difficulty of separating afferent and efferent terminals at the light microscopic level.

## **Chapter 2: Muscarinic Receptor Agonist Application Modulation of Pigeon Inwardly Rectifying Potassium Channel (pKir2.1) Expressed in Transfected tsA201 Cells**

### **INTRODUCTION**

Inward rectifier potassium (Kir) channels modulate cell excitability by repolarizing the cell membrane potential during action potentials; keep the cell membrane potential close to the resting potential; and contribute to K<sup>+</sup> homeostasis between the cell and surrounding extracellular fluids (Hille, 2001). Kir channels are a class of potassium channels composed of tetrameric proteins of one-pore/two-transmembrane domain subunits. There are seven sub-families of Kir channels, Kir1-7. The amino acid identity between individual members within each sub-family is ~60%, with ~40% identity between sub-families. Among the seven Kir members, Kir2 and Kir3 have the characteristics of “strong” inward rectification, which means that their currents rapidly decline at voltages positive to the cell’s reversal potential. The other four sub-family members display “weak” rectification and their currents decline gradually at voltages positive to the reversal potential. Kir2.1 (IRK1), a subtype of Kir2, is a strong inward rectifier, that is constitutively active (Stanfield et al., 2002a) and sensitive to phosphorylation and other intracellular messenger signals (Fakler et al., 1994; Henry et al., 1996; Jones, 1997; Wischmeyer et al., 1998; Liu et al., 2001). For example, the activation of PKC inhibits Kir2.1 channel function; while the increased level of intracellular cAMP would subsequently activate PKA, which enhances Kir2.1 current amplitude (Park et al., 2008).

Kir2.1 channels have been identified on pigeon vestibular hair cells. These channels are modulated by mAChR agonists. As shown in chapter 1, all five subtypes of mAChRs are expressed on pigeon vestibular hair cells (Li et al., 2007). However, no selective agonists are available to distinguish the mAChR subtypes. Therefore, it has become critical to express a single mAChR subtype in the heterologous expression system (HES) in order to perform electrophysiological studies on mAChR subtype modulation of Kir2.1 channels. Generally, there are two categories of protein expression systems: prokaryotic (*E. coli*) and eukaryotic (yeast, insect and mammalian cells). The advantages of the eukaryotic protein expression systems are that they have post-translational modification and yield more functional and more soluble proteins (Fernandez and Hoeffler, 1999).

In the present study, a mammalian tsA201 cell line was used as the host for the protein expression of both pKir2.1 and mAChRs. The tsA201 cell line is a transformed HEK293 cell line (an adenovirus-transformed derivative of human embryonic kidney cells, (Graham et al., 1977)) stably expressing simian virus 40 (SV40) temperature-sensitive large-T antigen (Rio et al., 1985; Heinzel et al., 1988; Margolskee et al., 1993). The large-T antigen is the viral-encoded protein that promotes the replication of any DNA that contains an intact SV40 origin sequence and a certain type of viral promoter, such as cytomegalovirus (CMV)-containing construct (Borowiec et al., 1990; de Chasseval and de Villartay, 1992; Soneoka et al., 1995; Arenal et al., 2004). Since the ORFs of pigeon Kir2.1 and most mAChR subtypes have been cloned, sub-cloned and their sequences confirmed (Correia et al., 2004; Li et al., 2007), the mammalian expression vectors, pCMS-EGFP (Clontech, Cat. # 6101-1, Mountain View, CA) and

pcDNA3 (Invitrogen, Cat. # V790-20, Carlsbad, CA), were used for the gene tranfection of M3/M5 and pKir2.1 in tsA201 cells correspondingly.

## **EXPERIMENTAL PROCEDURES**

### **M3/M5 mAChR subtype & pKir2.1 plasmid preparation**

We have successfully cloned, sub-cloned and confirmed the sequence of the open reading frames (ORFs) for pigeon M2, M3, M4, and M5 (Li et al., 2007). The ion channel that carries IKir in pigeon vestibular hair cells belongs to the Kir2.1 subfamily and has also been cloned and sequenced as described previously (Correia et al., 2004). Briefly, the procedure to clone the ORFs of mAChR subtypes and pKir2.1 involved the following steps. First, total RNA was collected from pigeon brain using guanidinium thiocyanate (Chomczynski and Sacchi, 1987). Second, SuperScript II reverse transcriptase (Invitrogen, Carlsbad, CA) was used to perform first-strand cDNA synthesis. Third, PCR amplification was performed with 100 pmol of each primer. The primers were designed based on the nucleotide sequence of the corresponding chicken ORFs. Finally, the PCR products, ORFs for M2-M5 and pKir2.1, were cloned into PCR2.1 vector and confirmed by DNA sequence analysis.

The M3 and M5 mAChRs' ORFs were inserted into a eukaryotic expression vector, pCMS-EGFP, at a multiple cloning site (MCS) and placed under the transcriptional promoter of the CMV promoter. The EGFP was under the transcriptional control of the SV40 promoter (Figure 9A). The ORF for pKir2.1 was fused inframe with a monomeric red fluorescent protein (mRFP1) and introduced into the pcDNA3 vector using CMV as the promoter (Figure 9B). The open reading frames for pKir2.1 and M3

and M5 are accessible in GenBank under accession numbers AF192507, AY838768, and DQ357059, respectively.

### **Culturing and transfection of tsA201 cells**

A human embryonic kidney tsA201 cell line (Gifted by University of Washington Medical School, Seattle, WA) was maintained in an incubator in T75 flasks containing 20 ml complete media (D-MEM (Cellgro, Cat. # MT10-014-CV, Manassas, VA) w/ 10% fetal bovine serum (Sigma, Cat. # F2442, St. Louis, MO), 1X non-essential amino acids (Sigma, Cat. # M7145-100ML, St. Louis, MO), and 1X PS antibiotics (Cellgro, Cat. # MT30-001-CI, Manassas, VA) in CO<sub>2</sub> incubator. The incubator maintained the temperature at 37°C, humidity at 75% RH, and CO<sub>2</sub> level at 5% tension. One day before transfection, tsA201 cells were treated with 0.05% trypsin/EDTA (Cellgro, Cat. # MT25-052-CI, Manassas, VA), diluted and seeded in 35 mm Petri dishes containing 2 ml complete media in each Petri dish with a concentration of  $1.0 \times 10^5$  cells per milliliter. After overnight incubation, cells in each Petri dish were transfected with plasmids encoding M3 (M5) mAChR subtype with EGFP (1 µg) and pKir2.1 with mRFP1 (0.2 µg). Briefly, the protocol for transfection was that plasmids were diluted with 100 µL D-MEM serum-free medium within the sterilized polypropylene microcentrifuge tubes (1.5 mL, Fisher, Cat. # S34890-3, Pittsburgh, PA). FuGENE<sup>®</sup> HD Transfection reagent (4.2 µl) (Roche Applied Science, Cat. # 04709705001, Indianapolis, IN) was added and mixed thoroughly. Finally, after 15 min RT incubation of the transfection complex, the mixture was added to cells in a drop-wise manner. The optimal ratio between the total amount of DNA (µg) and total volume of FuGENE<sup>®</sup> HD Transfection reagent (µl) had been titrated to be 2:7. This ratio resulted in a transfection efficiency of 54.4% ~ 63.8%



after 24 hrs incubation. The amount of pKir2.1 plasmid was kept at a low level (0.2 $\mu$ g) in order to keep the transfected cell in a healthy condition while maintaining reasonably high transfection efficiency.

The whole cell patch clamp experiments were performed at 24 ~ 48 hrs after transfection. On the day of the experiments, the Petri dish containing the transfected tsA201 cells was removed from the incubator; the complete media was removed and replaced with enzyme free cell dissociation solution (Millipore, Cat. # S-004-B, Billerica, MA). A sterilized glass tube with the fire-polished tip was inserted in the solution and air was rapidly pumped in and out through the pipette into the solution to physically remove the tsA201 cells from the bottom. After 15 ~ 20 times of titration, the cells were collected in a 15 ml centrifuge tube (Fisher, Cat. # 05-538-59A, Pittsburgh, PA); centrifuged at 2,000 RPM for 10 minutes; titrated completely in the normal external solution; put in a recording chamber coated with 0.5 mg/ml concanavalin A (Sigma, Cat. # 7275, St. Louis, MO) or 3 mM poly-D-lysine (Sigma, Cat. # P0296-10MG, St. Louis, MO), and allowed to settle for 15 minutes. Concanavalin A and poly-D-lysine helped tsA201 cells attach to the chamber bottom and prevented them from floating away during patch clamp and drug application. No differences in the electrophysiological properties of the cells attached to the chamber by either reagent were observed.

### **Confocal images of transfected tsA201 cells**

Mammalian tsA201 cells were split and seeded in a 35 mm Petri dish onto a sterilized cover slip (Fisher, Cat. # 12-545-101, Pittsburgh, PA). The complete media (2 ml) contained tsA201 cells at the concentration of  $1.0 \times 10^5$  cells/ml. After the dish was shaken several times to distribute tsA201 cells evenly within the media, it was saved in

the incubator. The transfection of pCMS M3 (M5)/EGFP and pcDNA pKir2.1-mRFP1 plasmids was performed on the following day as described above. After 24 hrs incubation (normally producing a 70 ~ 80% cell confluence and ~60% successful transfection efficiency), the cover slip was removed and the cells were covered with warmed D-MEM medium and observed with confocal microscopy (LSM 510 Meta) with two different excitation wavelengths: 488 nm (green) and 543 nm (red) at 63x. In addition, the DIC image was used to ascertain the health of cells and used to focus. Zeiss LSM Image Browser program (v 3.5.0.376) was used to process the images. No digital manipulations, except minor adjustments to brightness and contrast, were made to any of the captured images.

### **Electrophysiology**

The setup for the electrophysiological studies, including the amplifier, DigiData, Clampfit program, drug application system, etc., was the same as that described in Chapter 1. The only difference was that voltage clamp and current clamp studies were performed. The cells were continuously perfused (1.2 ml/min) with normal external solution. The normal external (NE) solution contained (in mM): 145 NaCl, 3 KCl, 1 MgSO<sub>4</sub>, 2 CaCl<sub>2</sub>, 10 glucose, 15 HEPES, 0.283 vitamin C and 2 Na pyruvate, with pH adjusted to 7.4 with NaOH/HCl and osmolarity to 320 mosmol/kg. The recording electrode was backfilled with the internal pipette solution (in mM): 140 KCl, 2 MgCl<sub>2</sub>, 10 HEPES, CaCl<sub>2</sub>, 11 EGTA. On the experimental day, 10 µl of 33.13 mM ZD7288 (Tocris, Cat. # 1000, Ellisville, MO), a stock solution kept at -80°C, was diluted in 10 ml internal pipette solution. ZD7288 is a selective blocker for *I<sub>h</sub>* channels (BoSmith et al., 1993)

which are present in pigeon vestibular hair cells (Masetto and Correia, 1997a). No endogenous  $I_h$  current has been reported in HEK293 cells.

In addition, several solutions were used to study the properties of pKir2.1 channel, including N-Methyl-D-Glucamine (NMDG, 145mM) (Sigma, Cat. # M2004-500G, St. Louis, MO), sodium replacement in the normal external solution; Niflumic acid (NFA, 100  $\mu$ M) (Sigma, Cat. # O6754-5MG, St. Louis, MO), a chloride channel blocker; and BaCl<sub>2</sub> (100  $\mu$ M) (Sigma, Cat. # 449644-5G, St. Louis, MO), a K<sup>+</sup> channel blocker.

A Newman-Keuls multiple comparison procedure was performed at the  $\alpha=0.05$  significance level to determine specific pairwise differences.

### **Drug application**

The drugs used to produce the pharmacological results described below included: the acetylcholine receptor agonist carbachol (CCh) (Sigma, Cat. # C4382-1G, St. Louis, MO), selective nicotinic receptor antagonist tubocurarine (TC) (Sigma, Cat. # T2379-100MG, St. Louis, MO), and general acetylcholine receptor antagonist atropine (Sigma, Cat. # A0132-1G, St. Louis, MO). The drugs (1000X) were prepared as stock solutions in double distilled water (CCh and TC) or 100% ethanol (atropine). They were kept at -20°C and diluted into the NE solution at the desired concentration on the day of experiment. The agonist CCh solution was mixed with TC and applied to the cells in order to only activate the mAChRs without any potentially confounding nAChR responses. The concentration of TC was 10  $\mu$ M because previous studies have shown that 1  $\mu$ M TC almost completely blocked the  $\alpha 9$  nicotinic receptor that induced firing in primary afferent nerve fibers of the frog saccule (Guth et al., 1994). TC at 10  $\mu$ M also completely antagonized the DMPP-sensitive nicotinic receptor in the frog saccule (Holt

et al., 2003). The antagonist atropine was mixed with the same concentration of TC (10  $\mu$ M) as that in the CCh solution. In this way, both the agonist (CCh and TC) and antagonist (atropine and TC) solutions were kept at the same concentrations. If application of the antagonist blocked the response of the agonist, it indicated that the response induced by CCh and TC was mediated through mAChRs, but not nAChRs.

In order to study the kinetics of the pKir2.1 channels expressed in tsA201 cells, two separate sets of experiments were performed. Either a high  $[K^+]$  (72 mM) solution or  $Ba^{2+}$  solution (500  $\mu$ M) was applied extracellularly. The high  $[K^+]$  solution was prepared by increasing KCl in the NE solution.

## **RESULTS**

### **Confocal microscopy**

The reporter genes of the plasmids, pCMS M3 (M5)/EGFP and pcDNA3 pKir2.1-mRFP1, were EGFP and mRFP1 respectively. They were used as a marker of transfection of tsA201 cells to determine whether plasmids were successfully transfected into the cells. Figure 10 is a confocal image of tsA201 cells transfected with pCMS M3/EGFP and pcDNA3 pKir2.1-mRFP1 (M3&pKir2.1) after 24 hrs incubation. Both reporter gene proteins, EGFP and mRFP1, of the plasmid vectors are present in the cells. The mRFP1 is mainly located on the membrane; EGFP is expressed within the cytoplasm.

When tsA201 cells were transfected with pCMS M5/EGFP and pcDNA3 pKir2.1-mRFP1 (M5&pKir2.1), the results of the confocal image were the same as those treated

with M3 with pKir2.1 plasmids. Native control tsA201 cells without plasmid transfection showed no fluorescence (not shown).

### **Electrophysiological studies of the native and transfected tsA201 cells**

The endogenous ion channels and receptors of tsA201 cells have not been identified. Control studies are important to prevent confounding results of nontransfected and transfected cells. Two types of control studies were performed. First, the endogenous currents of transfected and nontransfected tsA201 cells were compared. Second, immunocytochemical staining and pharmacological studies were performed to determine whether nontransfected tsA201 cells have endogenous mAChRs expression.

To study the pKir2.1 current properties, the voltage of tsA201 cells transfected with pKir2.1 was held at -60 mV and then changed from -120 mV to +40 mV in 10 mV increments (Figure 11B). Nontransfected tsA201 cells were exposed to the same voltage protocol to check for endogenous currents. The purpose of this control study was to identify currents other than pKir2.1 and to determine if their activation ranges overlapped pKir2.1. After several experiments using different cell generations, transfections, and incubation times (24 hrs, 48 hrs, and 72 hrs), the only obvious endogenous current found in the nontransfected tsA201 cells was an outward current that activated around -20 mV and increased in amplitude as the voltage became more depolarized (Figure 11A). Figure 11C shows current traces of a tsA201 cell transfected with pKir2.1 incubated for 72 hrs. The endogenous outward current traces in a transfected tsA201 cell over the voltage range from -20 mV to +40 mV is shown in Figure 11D.

A typical I-V plot of a nontransfected tsA201 cell and a tsA201 cell transfected with pKir2.1 is shown in Figure 12A. As seen in this Figure, very little endogenous

inward current was found in the nontransfected tsA201 cells. The outward currents of both traces overlaid each other at voltage levels more positive than -20 mV. The tsA201 cell transfected with pKir2.1 had an outward current in the voltage range between the reversal potential (in this case -90 mV) and -30 mV. When the voltage was moved more negative than the reversal potential, the inward current increased correspondingly.

To test the endogenous mAChR expression on nontransfected tsA201 cells, immunocytochemical stainings (same procedures as Chapter 1) of M3 (M5) mAChRs on tsA201 cells were performed. There was no immunocytochemical staining of nontransfected tsA201 cells with anti-M3 antibody. However, there was positive staining on the tsA201 cells transfected with the plasmids containing M3 mAChR. The pre-adsorption control blocked M3 staining of the transfected tsA201 cells (data not shown). Preliminary experiments with immunocytochemical staining of M5 on the nontransfected tsA201 cells showed some reaction; that was not blocked by the pre-adsorption control. This led us to believe that the staining was likely to be artifactual.

The pharmacological study of endogenous mAChR expression in nontransfected tsA201 cells is shown in Figure 12B. 100  $\mu$ M CCh and 10  $\mu$ M TC application to the cell transfected with pKir2.1 decreased the pKir2.1 currents slightly (<10%). This response could not be blocked by pre-treatment with the mAChR antagonist, atropine. Moreover, application of NE produced the same suppression on the pKir2.1 current, which indicated that the suppression of the pKir2.1 current was not induced by the mAChR activation.

We compared the outward currents at +40 mV and the inward currents at -120 mV between all treatment types: nontransfected tsA201 cells, cells transfected with EGFP, with pKir2.1, with M3&pKir2.1, and with M5&pKir2.1. The comparisons are shown in Figure 12C as mean  $\pm$  S.D. The average value of the peak outward currents at

+40 mV was  $247.7 \pm 111.3$  pA (n=26, nontransfected tsA201 cells),  $97.0 \pm 28.6$  pA (n=5, EGFP),  $267.7 \pm 152.8$  pA (n=22, pKir2.1),  $248.7 \pm 179.5$  pA (n=53, M3&pKir2.1), and  $251.0 \pm 153.2$  pA (n=21, M5&pKir2.1), respectively. There was no significant difference between the mean outward currents between these groups. The average inward currents at -120 mV in the nontransfected nontransfected tsA201 cells and cells transfected with EGFP were  $-55.0 \pm 41.9$  pA (n=26) and  $-27.0 \pm 20.8$  pA (n=5) respectively, and they were not significant different. However, the mean inward currents were significantly larger in cells transfected with pKir2.1 ( $-2247.5 \pm 1088.0$  pA, n=22), M3&pKir2.1 ( $-1781.3 \pm 773.6$  pA, n=53), and M5&pKir2.1 ( $-1483.3 \pm 843.6$  pA, n=21). In addition, the mean inward currents of cells transfected with pKir2.1 were significantly different than other two types of transfected cells.

The resting membrane potential (RMP) of the nontransfected tsA201 cells and cells transfected with different plasmids were recorded and compared under the current clamp mode. As shown in Figure 12D, the nontransfected tsA201 cells had RMP =  $-19.8 \pm 9.6$  mV (n=23). The tsA201 cells transfected with the EGFP had RMP =  $-15.0 \pm 8.8$  (n=8). After the cells were transfected with pKir2.1, the RMP was  $-90.4 \pm 7.2$  (n=22). When the cells were transfected with either M3&pKir2.1 or M5&pKir2.1, the RMPs were  $-91.7 \pm 4.9$  (n=42) and  $-90.9 \pm 4.5$  (n=13) respectively. There were significant differences between groups of cells transfected with pKir2.1 containing plasmids (pKir2.1, M3&pKir2.1, and M5&pKir2.1) and groups of cells without pKir2.1 (nontransfected tsA201 cells & EGFP cells). Thus the expression of Kir2.1 channel shifted the RMP on average about 70 mV in the hyperpolarized or negative direction.

In the experiments to study the kinetics of the pKir2.1 channels, the application of high  $[K^+]$  to the cells transfected with pKir2.1 shifted the cell reversal membrane

potential to a more depolarized value (Figure 13A). Both inward and outward currents were increased. The slope conductance of the pKir2.1 was decreased once the holding voltage was more negative ( $\sim -120$  mV) than the membrane reversal potential ( $\sim -25$  mV) (Figure 13A).

$\text{Ba}^{2+}$  application to the transfected tsA201 cells decreased the pKir2.1 conductance (Figure 13B). After 5 sec of  $\text{Ba}^{2+}$  application, the inward and outward currents were partially reduced which transiently changed the reversal potential to a more hyperpolarized value. Fifteen seconds of  $\text{Ba}^{2+}$  application completely blocked pKir2.1 outward and inward currents, leaving only the small endogenous inward current and setting back the reversal membrane potential close to the RMP of nontransfected tsA201 cells. The complete blockage of pKir2.1 channels changed the reversal potential to a more positive level, which was consistent with earlier studies.

### **Effects of CCh application to the transfected tsA201 cells**

#### **Cells transfected with M3&pKir2.1**

Mammalian tsA201 cells transfected with M3&pKir2.1 demonstrated a time-dependent response to the application of CCh and TC. During voltage clamp, the amplitude of the peak pKir2.1 current ( $I_{\text{pKir2.1}}$ ) at  $-120$  mV changed as a function of the time of application.  $I_{\text{pKir2.1}}$  increased from  $-730.6$  pA to  $-965.6$  pA during the initial second of drug application, then decreased to  $-692.5$  pA at 5 sec of CCh application,  $-518$  pA at 15 sec, and finally  $-465$  pA at 30 sec of drug application. NE was then applied and after 30 sec the pKir2.1 current at  $-120$  mV recovered to the control level (Figure 14).



I-V plots based on current responses from the same cell are shown in Figure 15A. The reversal membrane potential in the control was  $\sim -95$  mV. The pKir2.1 current during 1 sec of CCh and TC application depolarized membrane potential to  $\sim -88$  mV. Continued drug application for 30 sec moved the membrane potential to  $\sim -100$  mV. Pretreatment of the cell with the mAChR antagonist atropine ( $100 \mu\text{M}$ ) for 30 sec completely blocked the IpKir2.1 response to CCh and TC application (Figure 15B).

In current clamp mode, the membrane potential showed similar responses as the reversal membrane potential changes in the I-V plot (Figure 15A). As shown in Figure 16, during the first few seconds ( $< 3$  sec) following application of CCh and TC, the cell's RMP ( $-93\text{mV}$ ) depolarized  $5\text{-}6$  mV ( $-87$  mV). For the remaining 8 sec application, the cell's membrane potential was repolarized to  $-100.4$  mV, and remained at that value. Washing with NE completely restored the membrane potential level to the control value in 20-30 sec. Four replications of the mAChR agonist to the cell produced similar responses. However, the depolarization of the RMP became smaller when the time interval between each drug application was shortened from 30 sec (depolarized to  $-88$  mV) to 5 sec (depolarized to  $-93.7$  mV).

#### **Cells transfected with M5&pKir2.1**

During application of a mixture of  $50 \mu\text{M}$  CCh and  $10 \mu\text{M}$  TC to cells transfected with M5&pKir2.1, the IpKir2.1 increased in a time-dependent fashion (Figure 17A). The amplitude of IpKir2.1 ( $-947.5$  pA) after 30 sec drug mixture application was 3.7 times greater than that of control ( $-254.4$  pA) currents. Washout of the drug mixture with NE almost completely restored the IpKir2.1 to the control value within 30 ~ 60 sec. When the cell was pre-incubated with atropine and TC for 20 sec, application of CCh and TC to the

cell did not change IpKir2.1 during the first 15 sec. It took 30 ~ 40 sec for the mAChR agonist solution to slowly enhance the IpKir2.1 from -190 pA to -285 pA, an increment of only 1.5 (Figure 17B).

During current clamp, the membrane potential of the cell transfected with M5&pKir2.1 was depolarized by CCh and TC application. Superfusion of CCh and TC over the cell moved its membrane potential from -99.8 mV to -86.9 mV within 22 sec (Figure 18). Subsequent superfusion of NE for 30 sec resulted in the cell's membrane potential recovering to the control level. Increased CCh (100  $\mu$ M) and TC treatment depolarized the membrane potential to -87.1 mV in 2 sec, followed by rapid repolarization to the RMP in 7 sec. The membrane potential continued to hyperpolarize to -100 mV for 10 sec. NE superfusion caused the membrane potential to recover to the control level. The third drug application, doubling the concentration of CCh (200  $\mu$ M) and TC caused a membrane potential shift to -87.6 mV in 1.3 sec that repolarized to the RMP in 5 sec, and continued to hyperpolarize to -102 mV. The membrane potential partially recovered to the control level following superfusion with NE. In contrast, atropine and TC application didn't change the membrane potential. The minimal response (Figure 18) during atropine and TC application was the artifact caused by dead space in the pipette tip prior to the drug application system.

### **Membrane potential changes in transfected tsA201 cells at voltages other than the RMP**

In addition to current clamp studies of transfected tsA201 cells at the RMP, negative and positive currents, to hyperpolarize and depolarize the cell membrane potential respectively, were injected into transfected cells while CCh was applied. These

experiments were carried out because the sensitivity of the M2 mAChR subtype was reported to be the voltage-dependent (Ben Chaim et al., 2003). In the present experiments, the voltage levels were driven from  $E_K = -98 \text{ mV} \pm 30 \text{ mV}$  ( $T = 23^\circ\text{C}$ ,  $[\text{K}^+]_{\text{in}} = 140 \text{ mM}$ ,  $[\text{K}^+]_{\text{out}} = 3 \text{ mM}$ ) since this produced the largest pKir2.1 outward and inward currents (Figure 12A). When the current protocol shown in Figure 19B was used to drive the membrane potentials of a nontransfected tsA201 cell about its RMP ( $-11 \text{ mV}$ ), the response was primarily ohmic. However, when pKir2.1 was expressed and the membrane potential was driven from the RMP to  $-50 \text{ mV}$  a large depolarization was seen (Figure 19C). The depolarization had a pulsatile waveform corresponding to the current injection waveform. When, however, current was injected into a cell expressing pKir2.1 and M3 (or M5), the same large depolarization occurred at a threshold voltage but the depolarization was followed by a partial repolarization (Figure 19D). The mean thresholds for the large overshoot in cells expressing pKir2.1 was  $-67.8 \pm 9.4 \text{ mV}$  ( $n=7$ );  $-73 \pm 10.6 \text{ mV}$  ( $n=11$ ) for cells expressing M3&pKir2.1: and  $-73.2 \pm 7.5 \text{ mV}$  ( $n=3$ ) for cells expressing M5&pKir2.1. There were no significant differences between the mean peak voltage in each of these groups ( $P<0.05$ ) (Figure 20).

To find out which ion was responsible for the overshoot current, three separate experiments were performed on cells transfected with either pKir2.1 or M3&pKir2.1. In one set of experiments,  $\text{Na}^+$  in the normal external solution was replaced by N-Methyl-D-Glucamine (NMDG). In a second set of experiments, Niflumic acid (NFA,  $100 \mu\text{M}$ ), a chloride channel blocker, was included in both the normal external solution and the internal KCl solution. And finally,  $\text{BaCl}_2$  ( $100 \mu\text{M}$ ), a  $\text{K}^+$  channel blocker, was added to the external solution. The traces shown in Figure 21F show that only the  $\text{K}^+$  channel

blocker BaCl<sub>2</sub> prevented the large depolarization from happening during the current injections.

## **DISCUSSION**

Our present studies provided important information about the functional roles of M3 and M5 mAChR subtype modulation on pKir2.1 channels. These results can be used to understand the roles of mAChRs in native vestibular hair cells.

Mammalian tsA201 cells were chosen since previous studies have used these cells as vehicles for expressing the M1 muscarinic receptor subtype and inward rectifier channels (Jones, 1996; Firth and Jones, 2001). We chose a heterologous expression system because there are not specific agonists and antagonists for mAChR subtypes and we wished to control the precise mAChR subtypes that were in the cell. We chose two receptor subtypes (M3 and M5) that had not been previously studied. Since there was not a previous literature on the modulation of pKir2.1 by the M3 and M5 receptor subtypes in HES, we had to develop and test expression of these subtypes in tsA201 cells.

Confocal images of transfected tsA201 cells (Figure 10) demonstrate that plasmid vectors were successfully expressed in tsA201 cells. The vector (Figure 9) containing the DNA sequences for pKir2.1 and mRFP1 used the same promoter, CMV. In contrast, the vector pCMS M3/EGFP had two different promoters. The promoter for M3 was CMV; EGFP's promoter was SV40. It has been shown that the promoter activity of CMV is about 12 times more effective than that of SV40 in HEK293 cells (Kronman et al., 1992; Liu et al., 1997). If this is true in tsA201 cells, the expression of mAChR subtype (CMV promoter) would be stronger than the expression of EGFP (SV40 promoter). Theoretically, the expression and location of EGFP within the cells is not correlated with

the exact expression level and location of mAChR M3 (M5) since the ORFs of M3 (M5) and EGFP, unlike pKir2.1-mRFP1, are expressed from separate promoters. In addition, the expressed EGFP within the cell had no relation with the total amount of plasmids used for the transfection. Even when tsA201 cells were transfected with a small amount of pCMS M3/EGFP plasmids, such as 0.2  $\mu$ g, EGFP still was expressed throughout the cell. This result is nearly identical to that found in earlier studies of the EGFP transfected to HEK293 cells (Thomas and Smart, 2005).

Regardless, the voltage clamp and current clamp electrophysiological results strongly suggest that M3 and M5 receptors were present in the cell membrane and activate the G-protein transduction pathway that ultimately resulted in the modulation of pKir2.1.

In control studies, we examined the endogenous outward and inward currents in tsA201 cells to make sure that they did not confound the inward currents in the activation range of pKir2.1. To our knowledge, the endogenous ionic channels in tsA201 cells have not been carefully studied. In the HEK293 cell line, several native ionic currents have been reported to be expressed endogenously, including the tetrodotoxin (TTX) sensitive Na<sup>+</sup> currents (Berjukow et al., 1996), Kv currents (Yu and Kerchner, 1998; Petersen and Nerbonne, 1999; Jiang et al., 2002), Ca<sup>2+</sup> currents (Berjukow et al., 1996), and Cl<sup>-</sup> currents (Zhu et al., 1998). In the present study, no attempt was made to distinguish those ion channels that might be located in tsA201 cells, but control studies were performed to ensure that mAChR induced responses were mediated through transfected pKir2.1 channels. We found that the only non pKir2.1 current within the voltage range -120 mV to +40 mV was a small outward current that activated at -20 mV. The amplitude of this current was small in comparison to the large inward currents induced through pKir2.1

(Figure 11). It has been reported that the outward currents are  $K_v$  (probably delayed rectifier type) currents in HEK293 cells (Jiang et al., 2002) and they are TEA-sensitive (Jones, 1996). Previous data showed that tsA201 cells transfected with human M1 mAChR produced a reduction of the endogenous outward current after CCh application (Jones, 1996). In the present work, when the tsA201 cells were transfected with pigeon M3 and M5 mAChR subtypes, the endogenous outward current of nontransfected tsA201 cells was not changed during CCh application. This might be due to the different mAChR subtypes (M1 vs. M3 & M5) or difference in animal models (human vs. pigeon).

We carried out studies to determine the effects of transfection of pKir2.1, M3&pKir2.1, and M5&pKir2.1 on tsA201 cells. Cells transfected with pKir2.1 showed significantly more hyperpolarized RMPs and significantly larger inward currents at -120 mV than nontransfected tsA201 cells (Figure 12). An additional control study was tsA201 cells transfected with only EGFP to detect whether the vector itself had any effects on the tsA201 cells. The mean outward and inward currents and the RMP of the nontransfected tsA201 cells and the cells transfected with EGFP were not significantly different, which indicated that the vector itself had no effects on the currents and RMP in nontransfected tsA201 cells (Figure 12).

Next, we asked if endogenous mACh receptors were expressed in nontransfected tsA201 cells. HEK293 cells are the transformed HEK cells with adenovirus 5 DNA; while mammalian tsA201 cells are the modified HEK293 cell line containing the SV40 large T antigen. Those genetic modifications on the cell line might have some unknown effects on endogenous receptor expression, such as mAChRs. For example, the HEK cell line was used for the transfection of the cloned human mAChR subtypes more than 20 years ago (Peralta et al., 1987a). Later, it was found that the application of the mAChR

agonist CCh didn't significantly alter the formation of phosphatidylethanol (PEt) and inositol phosphates (IP) in the nontransfected HEK cells, but caused great increases of PEt and IP production in the cells expressing M1 or M3 mAChR subtypes (Sandmann et al., 1991). This indicated that few or no mAChRs were expressed in the HEK cell line. However, when Dr. Conkline's group studied the  $G\alpha_q$  protein subunit that stimulates phosphoinositide-specific phospholipase C (PI-PLC) in HEK293 cells, they found that CCh stimulated PI-PLC in the intact HEK293 cells which suggested the existence of endogenous mAChRs (Conklin et al., 1992). Furthermore, using RNA interference and DNA microassay methods, M3 was the only mAChR family member present in the HEK293 cells (Hakak et al., 2003; Luo et al., 2008). In the present work, immunocytochemical and pharmacological control studies didn't find the presence of any endogenous mAChRs on or in nontransfected tsA201 cells.

The Kir2.1 channels possess properties of mechano-receptors. It has been reported that the stretch or the hyposmotic challenge either inhibits IKir2.1 in the cerebral arterial smooth muscle cells or facilitates IKir2.1 in the CHO (Chinese hamster ovary) cells transfected with cloned human Kir2.1 (He et al., 2006; Wu et al., 2007). Consistent with this idea, we found that CCh as well as NE applications induced the same inhibitory IpKir2.1 responses in the cells transfected with pKir2.1. The most plausible explanation for these results is that the drug application system might produce a wave, thus stretching the cell, and changing pKir2.1 current due to the mechano-sensitive properties.

One of the functional roles of pKir2.1 is to keep the cell membrane potential close to  $E_K$  (Hille, 2001). Expression of pKir2.1 in the transfected tsA201 cells drove the nontransfected tsA201 cells' mean membrane potential from  $-19.8 \pm 1.9$  mV to  $\sim -90$  mV which was close to the theoretical  $E_K$  ( $-98$  mV ( $3$  mM  $[K^+]_{out}$ ,  $140$  mM  $[K^+]_{in}$ , at  $23^\circ\text{C}$ ).

The mean RMPs of the cells expressing pKir2.1, M3&pKir2.1, and M5&pKir2.1 were not significantly different, but the amplitude of the inward currents in the cells transfected with pKir2.1 only was significantly bigger than those transfected with M3&pKir2.1 and M5&pKir2.1 (Figure 12). The explanation for this could be that the cells transfected with pKir2.1 had more pKir2.1 channels expressed on the cell membrane than those transfected with both mAChR subtypes and pKir2.1. Due to the limitation of the synthetic materials used for protein biosynthesis within the cell, the cells transfected with a single type of plasmids could yield more pKir2.1 expression on the cell membrane than the cells transfected with two plasmids. And, the more pKir2.1 channels expressed; the bigger inward pKir2.1 currents.

The typical pKir2.1 current in the voltage range between -40 mV and the reversal potential was an outward current. In the native pigeon vestibular hair cells, the pKir2.1 channel had little outward current (c.f. Figure 1B and 12A) over the same voltage range. This observation suggests that in transfected cells, the pKir2.1 channels are overexpressed and this overexpression results in a much larger current compared to a negligible outward current in nontransfected cells (de Jeu et al., 2002; Miake et al., 2003). Suppression of the Kir2.1 channel, such as the site-directed mutation of the pore-forming motif, significantly decreased the inward and outward current density of the IKir2.1 (Miake et al., 2003). The exact molecular mechanism for the IpKir2.1 reduction upon hyperpolarization is not clear. The possible reasons could be attributed to decreased K<sup>+</sup> permeability (Kurachi, 1985; Shieh, 2000), blockage by the external cations, such as Na<sup>+</sup>, Rb<sup>+</sup>, Mg<sup>2+</sup>, Ca<sup>2+</sup>, and NH<sub>4</sub><sup>+</sup> (Ohmori, 1978; Standen and Stanfield, 1980; Reuveny et al., 1996; Shieh and Lee, 2001), depletion of K<sup>+</sup> near the channels (Adrian and Freygang,



1962; Adrian et al., 1970; Almers, 1972; Maughan, 1976; Standen and Stanfield, 1979), or conformation changes of K<sup>+</sup> channel (Chang and Shieh, 2003).

To make sure that pKir2.1 transfected into tsA201 cell showed similar kinetics and responses to those previously described for potassium channels in general and this channel in particular, high [K<sup>+</sup>] (in one set of experiment) and Ba<sup>2+</sup> (in another set of experiments) were applied to the cells. When the high concentration of KCl was applied externally, both pKir2.1 outward and inward currents increased and the reversal potential shifted to a positive potential which was close to the theoretical value of  $E_K$ : -17 mV ([K<sup>+</sup>]<sub>o</sub> = 72 mM and [K<sup>+</sup>]<sub>i</sub> = 140 mM at 23°C). On the other hand, application of Ba<sup>2+</sup>, a K<sup>+</sup> channel blocker, to the tsA201 cells reduced both the inward and outward current components of Kir2.1 and depolarized the cell membrane potential (Figure 13). This result was consistent with earlier reports of Ba<sup>2+</sup> blockage of Kir2.1 channels in cells from interstitial muscle, corneal endothelium, and vestibular hair cells (Flynn et al., 1999; Yang et al., 2003; Correia et al., 2004). However, the overexpressed pKir2.1 channels in tsA201 cells showed two kinetic states during the blockage: initially an increased conductance and finally a decreased conductance. The reason was not explored.

Activation of M3 and M5 mAChR caused time- and concentration-dependent modulation of IpKir2.1. Both current amplitude and reversal membrane potentials were modified (Figure 15). The molecular pathways for this modulation were not dissected.

Previous experiments, however, have shown that mAChR stimulation can modulate, for example, intracellular ionic concentration, ion channel currents, ligand receptor expression, transmitter release, post synaptic potentials and secondary intracellular messengers in a time- and concentration-dependent manner. For example, concentration-dependent mAChR agonist application has been shown to increase the

intracellular  $\text{Na}^+$  concentration (Korth and Kuhlkamp, 1985) and modify  $\text{K}^+$  (Nabekura et al., 1993; Nishikawa et al., 1994; Hsu et al., 1996; Wang et al., 1999; Zhang et al., 2002a),  $\text{Ca}^{2+}$  (Jeong and Wurster, 1997; Liu et al., 2002; Bett et al., 2002; Endoh, 2007), and  $\text{Cl}^-$  (Kuwahara et al., 1987; Du et al., 2006) current amplitude.

Receptors and neurotransmitters that have been shown to be modulated by a mAChR agonist in a dose-dependent manner include  $\beta$ -adrenergic receptor (Limas and Limas, 1985), glutamic acid receptor (Marchi et al., 1989) and GABA receptor (Hashimoto et al., 1986). An example of mAChR activation of neurotransmitter release includes potassium-evoked release of aspartate (Raiteri et al., 1990).

In addition, many intracellular processes exhibited a concentration-dependent response to mAChR agonists, such as  $\text{G}\alpha$  protein subunits (Murthy and Makhoulf, 2000), cyclic AMP (Jumblatt et al., 1990; Kubalak et al., 1991; Esqueda et al., 1996), cyclic GMP (Castoldi et al., 1993), intracellular  $[\text{Ca}^{2+}]$  (Ikeda et al., 1995; Fukuta et al., 1999; Catlin et al., 2000), inositol phospholipid hydrolysis products (IP1, IP2, and IP3) (Moroi-Fetters et al., 1988; He et al., 1989; Prestwich and Bolton, 1995), phospholipase D (PLD) (Gustavsson et al., 1993; Pochet et al., 2003), endothelial nitric oxide synthase (Murthy and Makhoulf, 2000), protein kinase c zeta (Guizzetti and Costa, 2000), mitogen-activated protein kinase (MAPK) (Wotta et al., 1998; Kanno et al., 2003), and c-fos mRNA (Cohen et al., 1996).

Other processes that have been shown to be modulated in a dose dependent manner by mAChR activation include: LMM3 cell proliferation (Rimmaudo et al., 2005), fast excitatory post-synaptic potentials (EPSPs) of guinea-pig myenteric and submucous plexus neurons (North et al., 1985), EPSPs from CA1 pyramidal neurons (Sheridan and

Sutor, 1990), and the contractions in the smooth muscles (Adami et al., 1985; Konno and Takayanagi, 1985; Lograno and Reibaldi, 1986; O'Rourke and Vanhoutte, 1987).

While most of the effects listed in the preceding paragraphs were dose dependent, some of the effects mentioned above were also time-dependent following mAChR agonist application, such as the  $G\alpha$  protein subunits, intracellular  $[Ca^{2+}]$ , PLD, PKC, and MAPK. So, most likely, the M3 and M5 mAChRs induced time- and concentration-dependent responses of pKir2.1 channel could be considered as downstream effects of the intracellular signal pathways.

Several time dependent features of the membrane potential response of tsA201 cells transfected with M3 or M5 and pKir2.1 are worth noting. For example, the current clamp membrane potential response to each CCh application showed a rapid repolarization following the transient depolarization (Figures 16, 18). It is likely that this response reflected mAChR desensitization like that shown in the frog atrial muscle (Tokimasa et al., 1981). The molecular mechanisms for desensitization in tsA201 cells expressing the M3 (M5) mAChR probably is not due to a loss of cell surface receptors or PLD activation by GTP-binding proteins, but possibly by the uncoupling of receptors from GTP-binding proteins and a loss of the undefined essential intracellular signaling messengers (Schmidt et al., 1995).

The transient depolarization of the membrane potential and part of the repolarization that we saw following mAChR activation (Figures 16, 18) is likely caused by altered kinetics of pKir2.1. It seems that overexpression of pKir2.1 changes the I-V response in tsA201 transfected cells from a strong inward rectifier to a weak inward rectifier. As such, a positive and negative slope conductance is observed at potentials positive to the resting membrane potential rather than no conductance as in a strong

inward rectifier and native pigeon vestibular hair cells. It is also possible that the properties of the pKir2.1 channel itself are changed. It has been shown that Kir2.1 channels are subject to phosphorylation by PKC, a downstream product of mAChR activation (Fakler et al., 1994; Jones, 1996; Jones, 1997). No matter how the pKir2.1 channel is expressed or modified the membrane potential, results are attributable to passage of K<sup>+</sup> ions and not an interacting sodium, chloride or calcium currents (Figure 21).

Regardless of the molecular mechanisms, pretreatment of transfected cells with a muscarinic antagonist (atropine) greatly attenuated the transient membrane response (Figure 18 - last application) and we conclude that this response is specific and not artifactual.

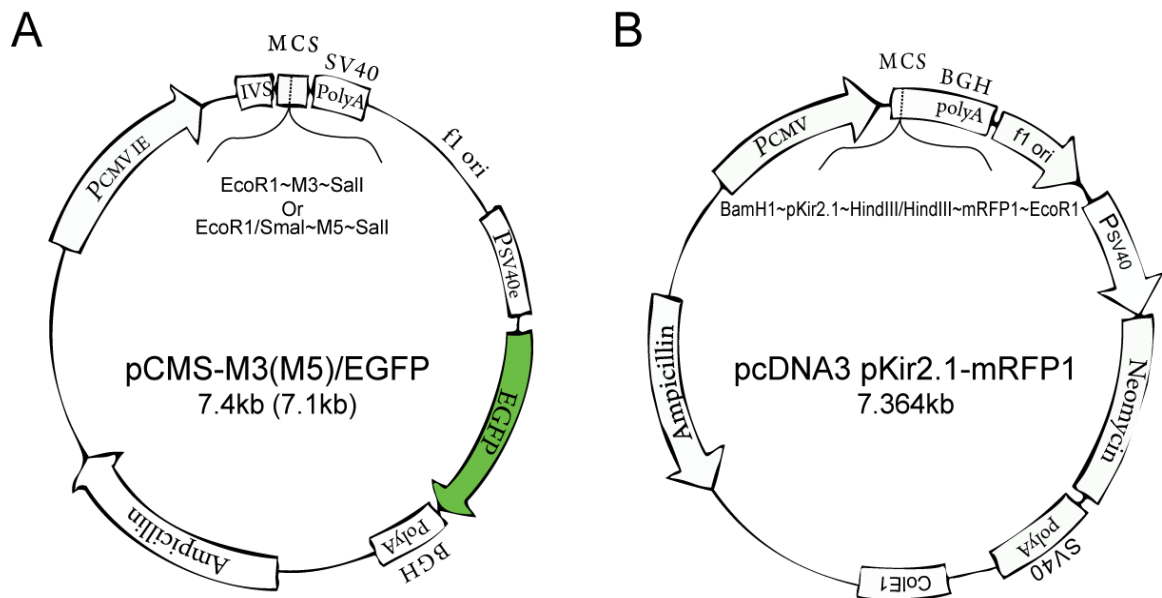


Figure 9. Cartoons of DNA vectors used for the transfection of tsA201 cells. (A) pCMS/EGFP vector was used for the expression of mAChR subtype M3 and M5 ORFs. The M3 DNA fragment was inserted into the EcoR1 and Sall restriction sites, while the M5 DNA fragment was inserted into the EcoR1 site (treated with T4 DNA polymerase I to create a blunt end) and the Sall restriction site. The promoter for M3 and M5 ORFs was CMV. (B) The pKir2.1 ORF BamH1-HindIII fragment and the mRFP1 ORF HindIII-EcoR1 fragment are inserted at the BamH1 and EcoR1 sites of pcDNA3. The promoter for the pKir2.1-mRFP1 fusion was CMV.

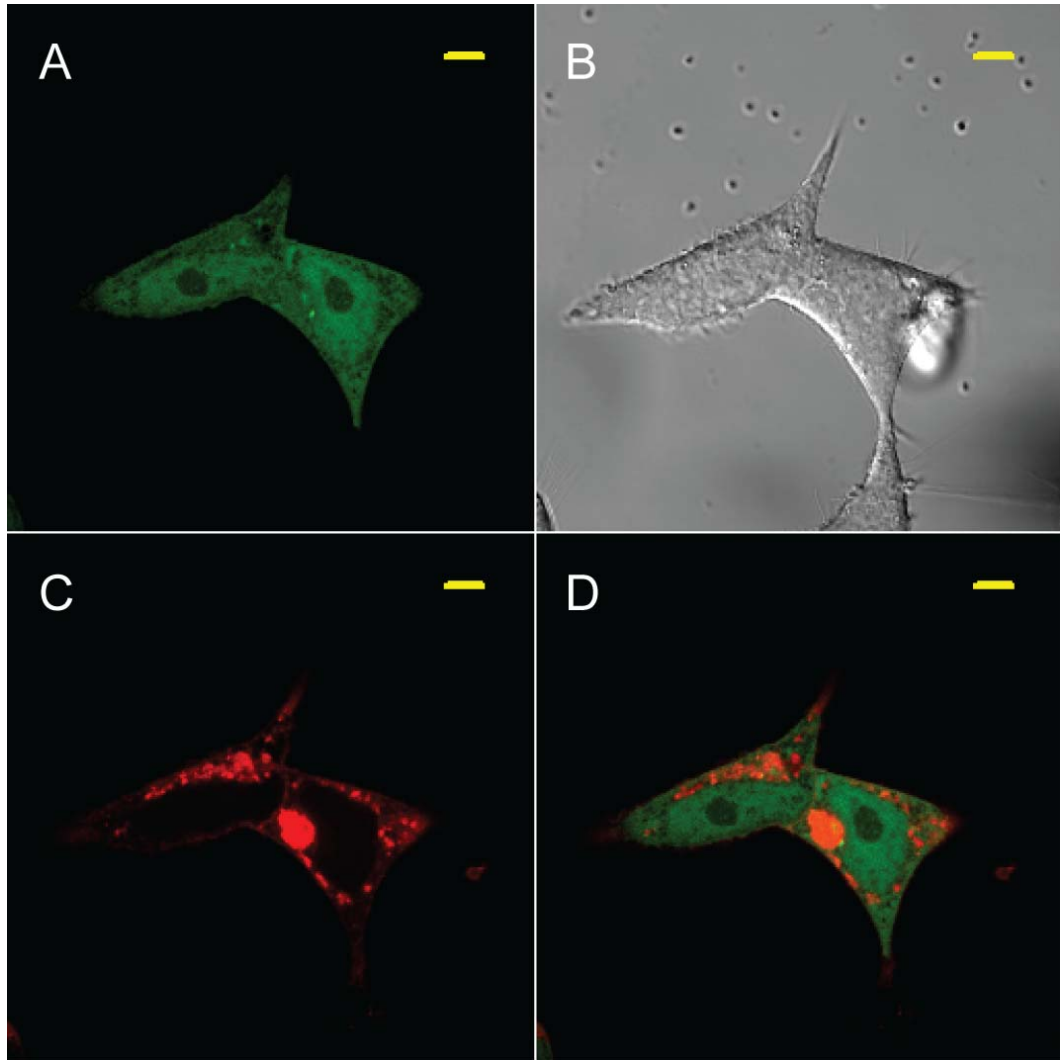


Figure 10. Confocal image of the tsA201 cell transfected with pCMS M3&EGFP and pcDNA3 pKir2.1-mRFP1 at the excitation wavelengths of 488nm (A), 543nm (C) and both (D). The corresponding DIC image is shown in (B). Cell was incubated for 24 hrs post transfection. Scale bars = 5 $\mu$ M.

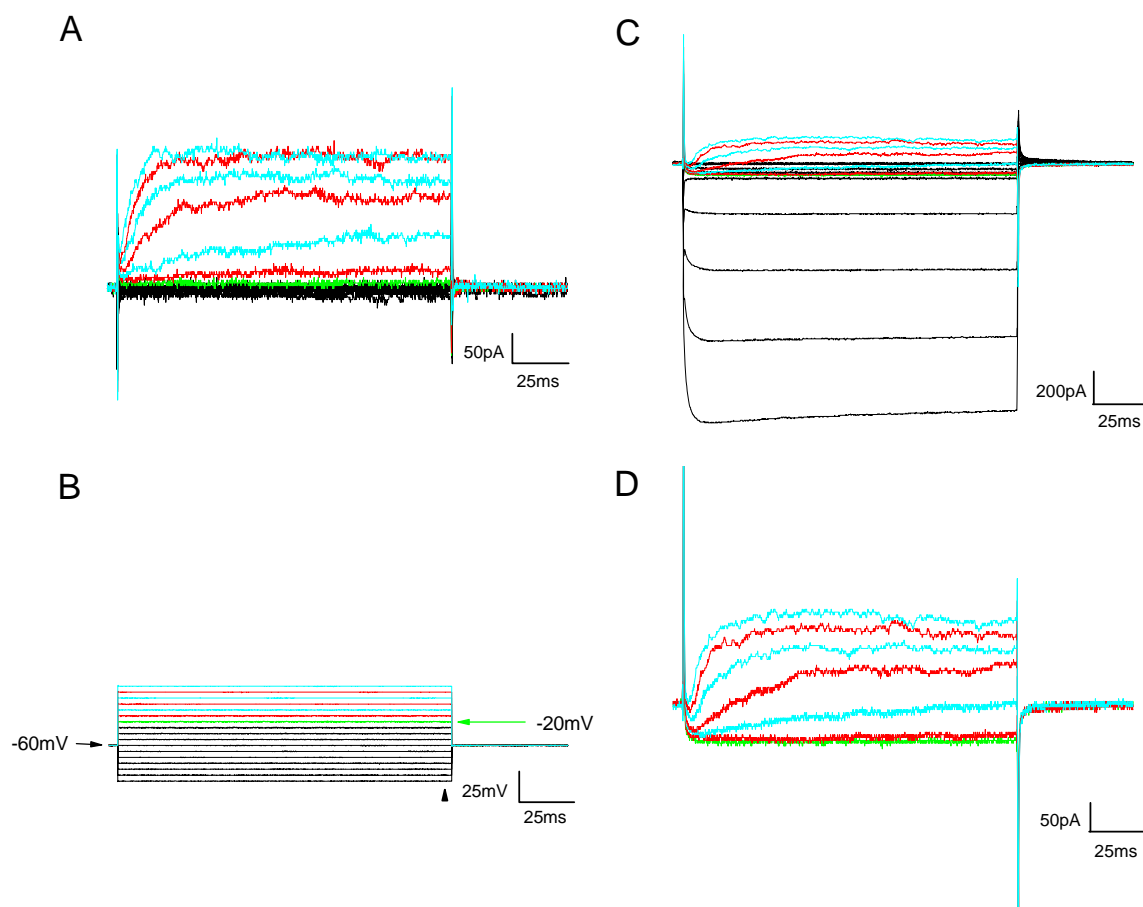


Figure 11. Raw traces of the endogenous currents present in nontransfected tsA201 cells (A) and currents in cells transfected with pKir2.1-mRFP1 (C). As seen in the voltage protocol (B), the cell was held at -60 mV and the voltage was varied from -120 mV to +40 mV in 10 mV increments. For clarity, voltages and currents are colored green at -20 mV and alternately red and cyan at more positive voltages. The endogenous outward currents in (C) occurred over the range -20 mV ~ +40 mV are enlarged and they are enlarged and shown in (D). The black arrow head shown in (B) indicates the time point where voltages and corresponding currents were measured to make the subsequent the I-V plots presented in the following figures.

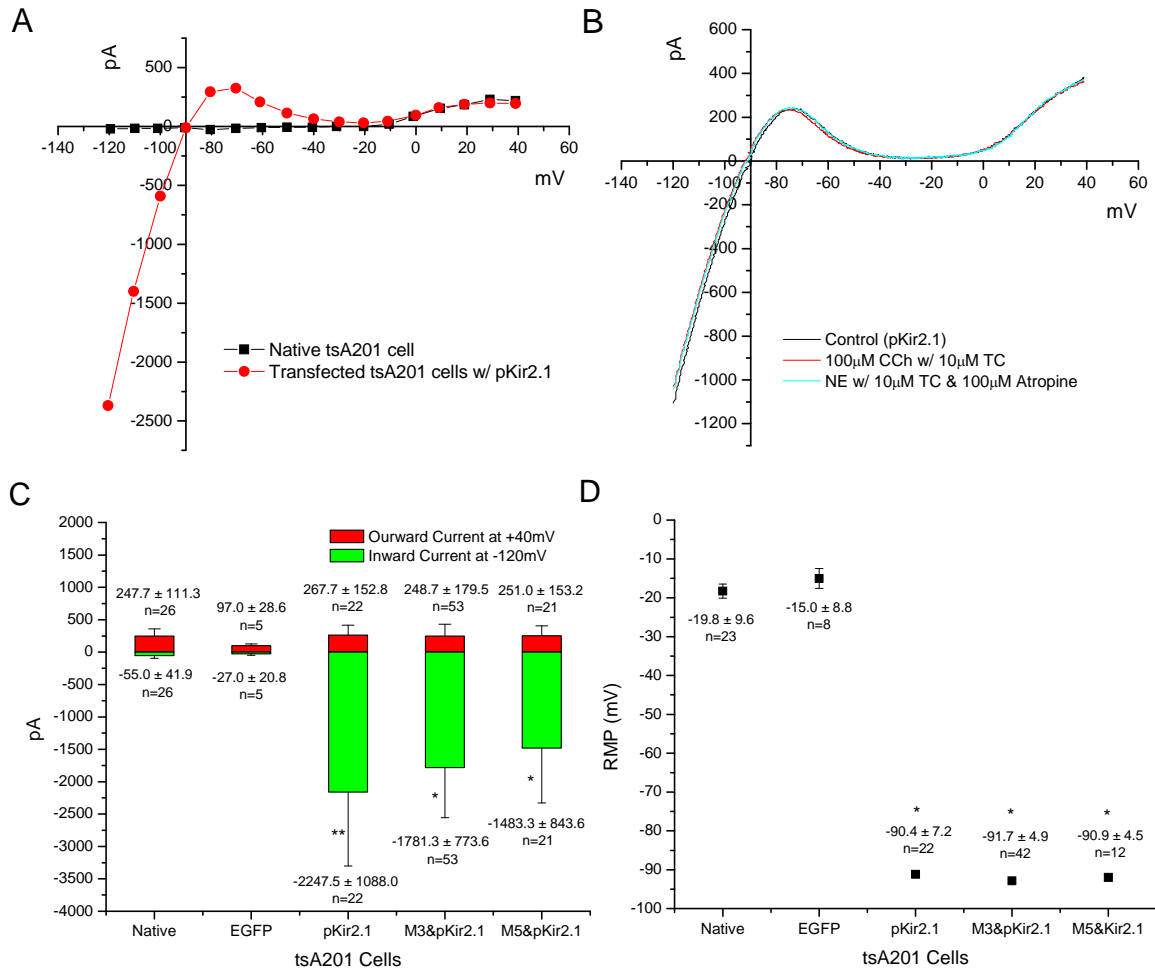


Figure 12. A typical I-V plot for a nontransfected tsA201 cell and the cell transfected with pKir2.1 only (A). A typical I-V plot for a tsA201 cell transfected with pKir2.1 only during CCh and NE application (B). Note no difference in overlaid plots. Bar histograms of average value (Mean ± S.D.) of the outward and inward currents at voltages of +40 mV and -120 mV (C) and the RMPs (D) of nontransfected tsA201 cells and cells transfected with plasmids containing ORFs for different molecules. In panel (C), the inward currents of cells transfected with M3&pKir2.1 and M5&pKir2.1 are not significantly different ( $P>0.05$ ), but they are significantly different from the inward currents of nontransfected tsA201 cells and cells transfected with EGFP and pKir2.1 (\*). Cells transfected with pKir2.1 show inward currents whose mean value is significantly different from the mean current of nontransfected tsA201 cells and cells transfected with EGFP (\*\*). The mean outward currents of nontransfected tsA201 cells and cells transfected with EGFP, pKir2.1, M3&pKir2.1, and M5&pKir2.1 were not significantly different ( $P>0.05$ ). In panel (D), the RMP of nontransfected and EGFP cells are not significantly different, but their mean RMPs were significantly different from those of pKir2.1, M3&pKir2.1, and M5&pKir2.1 (\*) transfected cells. A Newman-Keuls multiple comparison procedure was performed at the  $\alpha=0.05$  significance level to determine specific pairwise differences.



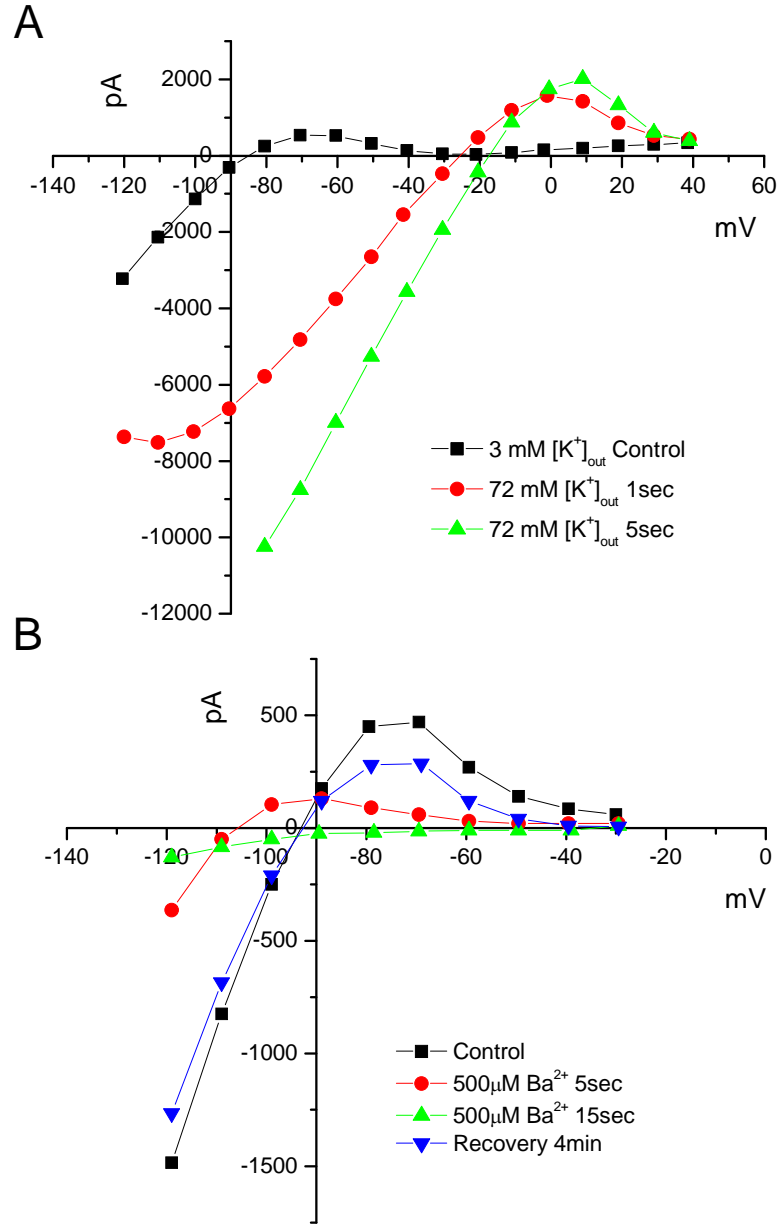


Figure 13. I-V plots of the tsA201 cells transfected with M3&pKir2.1 exposed to different concentrations and different duration of  $[K^+]$  (A) and  $[Ba^{2+}]$  (B). Note that in panel A when the voltage is well beyond the reversal potential the slope conductance changes slope (c.f. current at -120 mV and current at -110 mV in plot denoted by red circles).

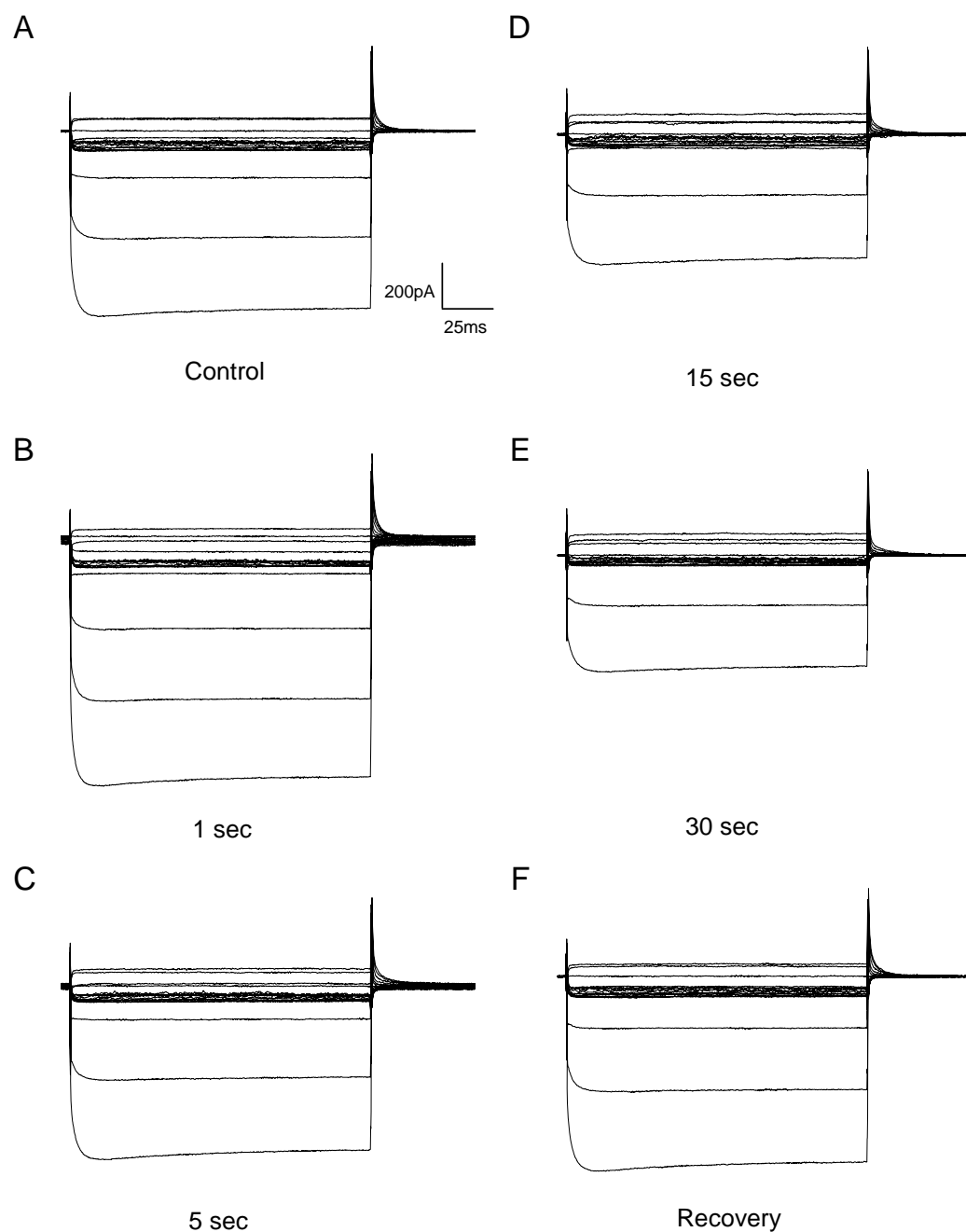


Figure 14. Raw current traces from tsA201 cells transfected with M3&pKir2.1 during application of 100 $\mu$ M CCh and 10  $\mu$ M TC. The voltage protocol was the same as that shown in Figure 11B. Traces are shown for the control condition (A) and superfusion of 100  $\mu$ M CCh + 10  $\mu$ M TC for 1 sec (B), 5 sec (C), 15 sec (D), and 30 sec (E), and the recovery (F) following 30 sec NE rinse.

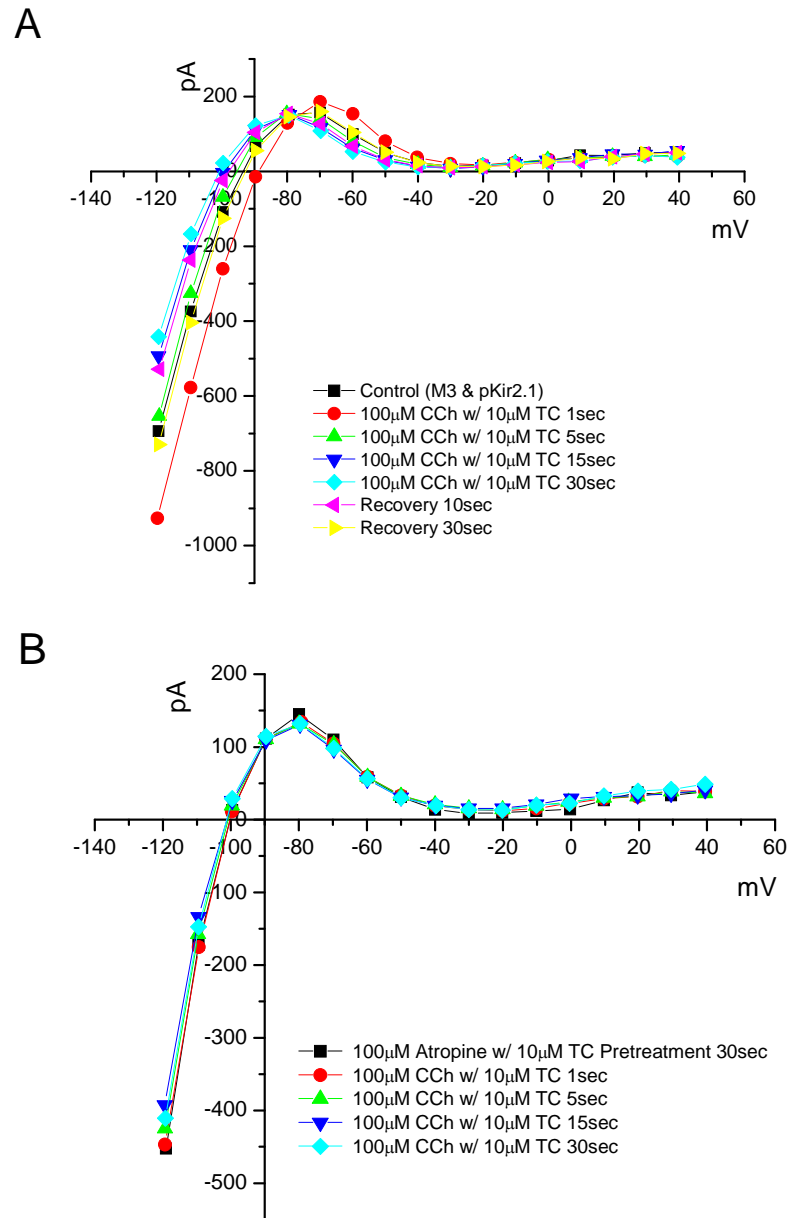


Figure 15. Overlaid I-V plots showing the effects of varying the duration of superfusion of 100  $\mu$ M CCh and 10  $\mu$ M TC onto tsA201 cells transfected with M3&pKir2.1. In (A) the drugs were continually applied to the cell for 30 sec and recordings were made at different times (1 sec, 5 sec, 15 sec, and 30 sec). In (B) the same measurements were made as in panel A, but the cell was pre-treated with 100  $\mu$ M atropine and 10  $\mu$ M TC.

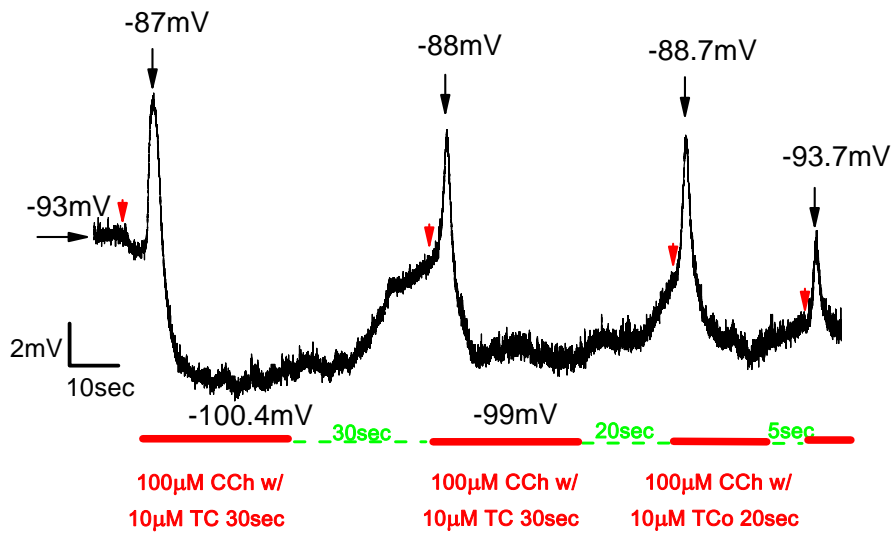


Figure 16. A continuous trace of the membrane potential of a tsA201 cell (transfected with M3&pKir2.1) during 4 applications of 100 μM CCh and 10 μM TC. The durations of the applications are denoted by red solid lines and the times between application are denoted by green dashed lines. Application of the drug mixture leads to a transient depolarization of the cell's membrane potential within a first few seconds. This is followed by a repolarization of the membrane potential to more hyperpolarized values (overshoot) but the membrane slowly returns toward the RMP (denoted by black arrow) in 20-30 sec. The red arrows are the times when the drugs were applied. Note that when the time between application is shortened from 30 to 5 sec, the membrane potential is depolarized less.

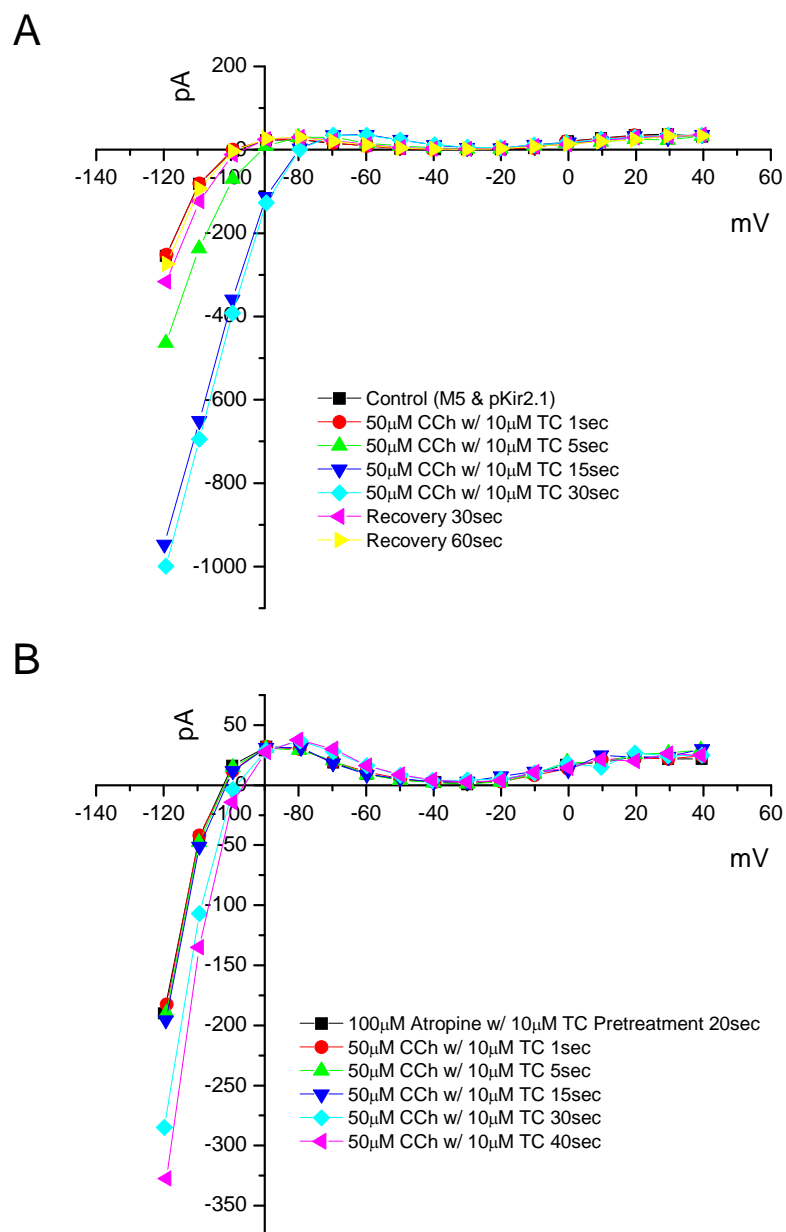


Figure 17. Overlaid I-V plots showing the effects of varying the duration of superfusion of 50  $\mu\text{M}$  CCh and 10  $\mu\text{M}$  TC onto tsA201 cells transfected with M5&pKir2.1. In (A) the drugs were continually applied to the cell for 30 sec and recordings were made at different times (1 sec, 5 sec, 15 sec, and 30 sec). In (B) the cells were pre-treated with 100  $\mu\text{M}$  atropine and 10  $\mu\text{M}$  TC.

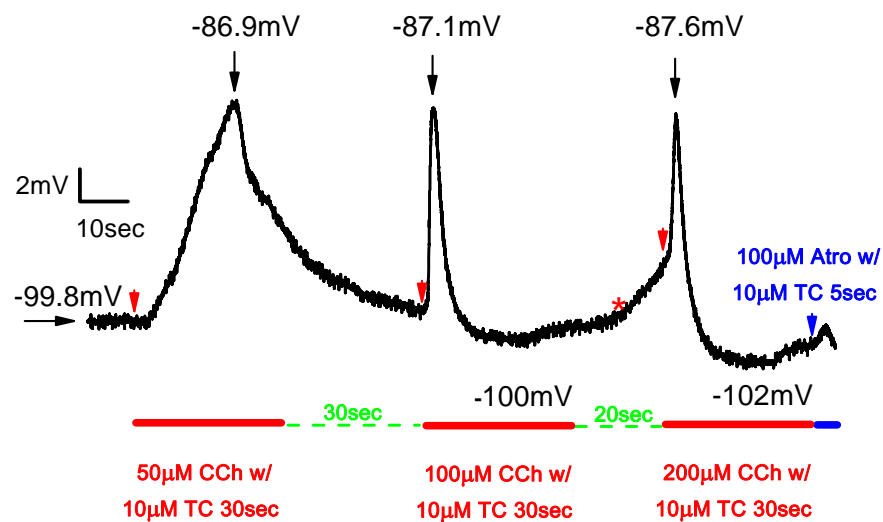


Figure 18. Current clamp traces of the effects of application (red solid lines) of different concentrations of CCh plus 10  $\mu$ M TC on the membrane potential of a tsA201 cell transfected with M5&pKir2.1. The time following termination of drug application and beginning of the next application varied (green dash lines). Note that a 50  $\mu$ M concentration depolarizes the cell membrane potential followed by a repolarization to the RMP. Application of the drug mixture with concentrations of 100  $\mu$ M and 200  $\mu$ M CCh produce both a depolarization and an repolarization overshoot. The red arrows indicate the time points when the drugs were applied using constant air pressure maintained under computer control. The \* shows time point when the drug application system was manually switched and the drug mixture delivered by the action of gravity. The blue arrow points at the time when 100 $\mu$ M atropine/10 $\mu$ M TC was applied for 5 seconds (blue bar). Note the absence of a large depolarization and repolarization.

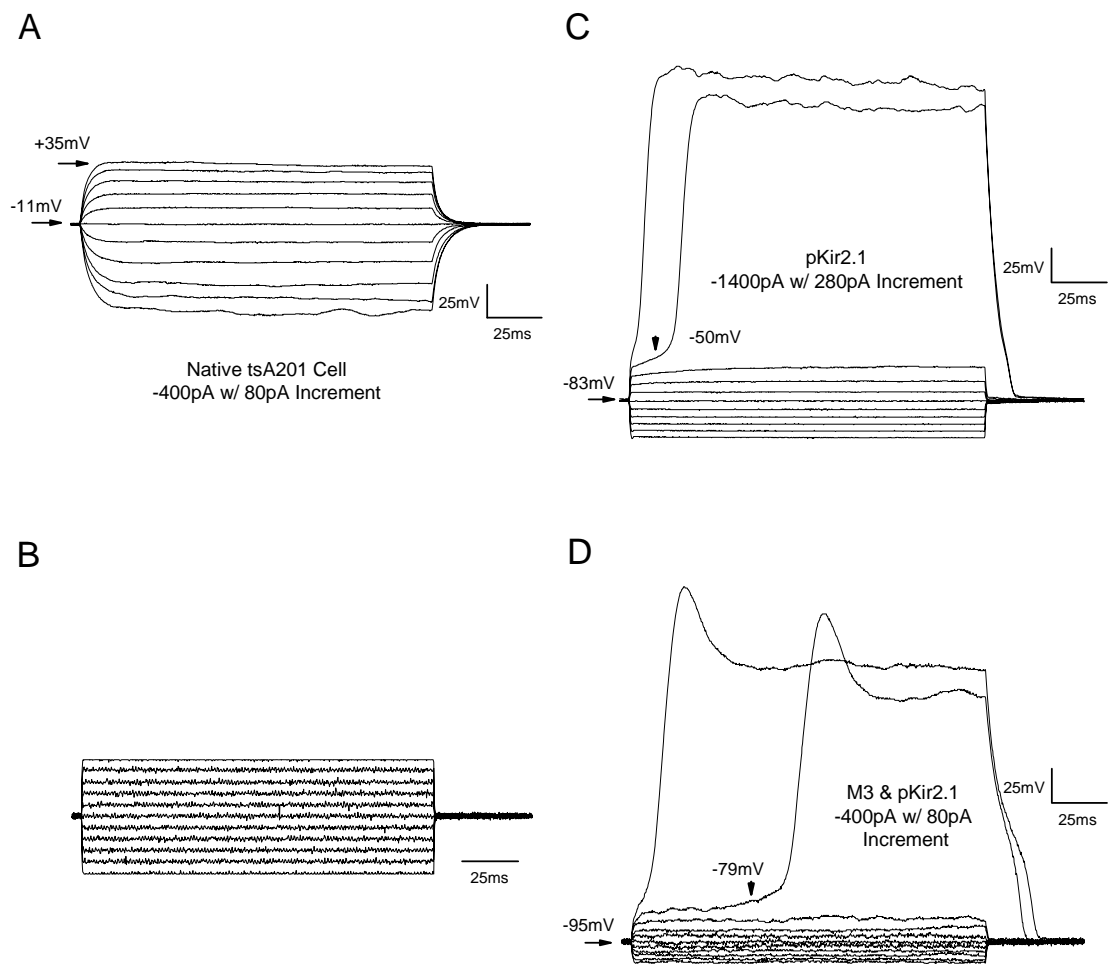


Figure 19. Current clamp recordings of membrane potentials of a nontransfected tsA201 cell (A) and cells transfected with either pKir2.1 (C) or M3&pKir2.1 (D). As seen from the current protocol (B), positive and negative currents were injected to the cells to drive the cells membrane potential over the range from -30 mV to +30 mV relative to the RMP. The scale for current injection in (B) is not marked because each cell required a different amount of current injection. Basically, however, the currents that were initially injected varied from -100 pA to +100 pA with a 20 pA increment. If the membrane potential was not optimally hyperpolarized or depolarized 30mV, the amount of injected current was adjusted but the ratio between the largest current injection and step increment was maintained at 5:1. Note that in transfected cells, a large depolarization of the membrane potential occurs once a threshold value is exceeded.

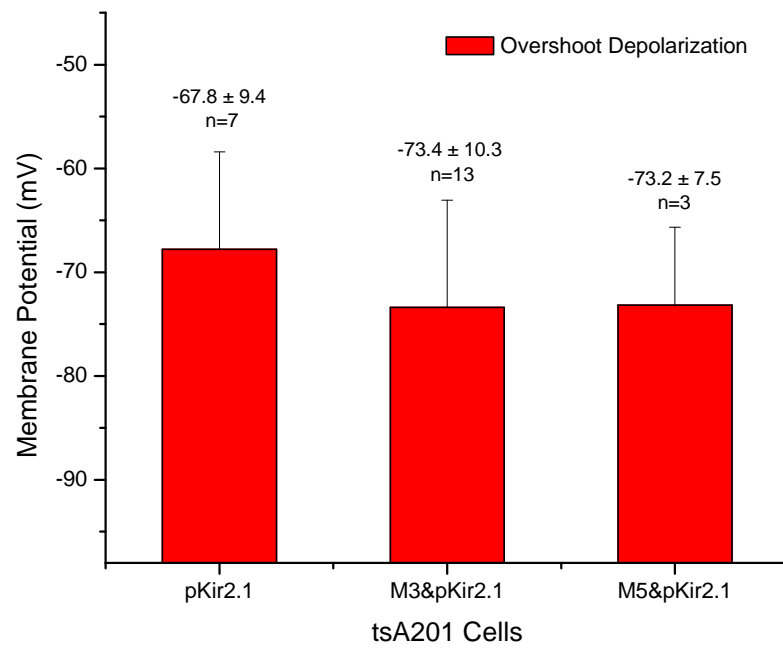


Figure 20. The average values of the voltage levels to induce the overshoot depolarization in the tsA201 cells transfected with pKir2.1, M3&pKir2.1, and M5&pKir2.1. There are no significant differences between the group.



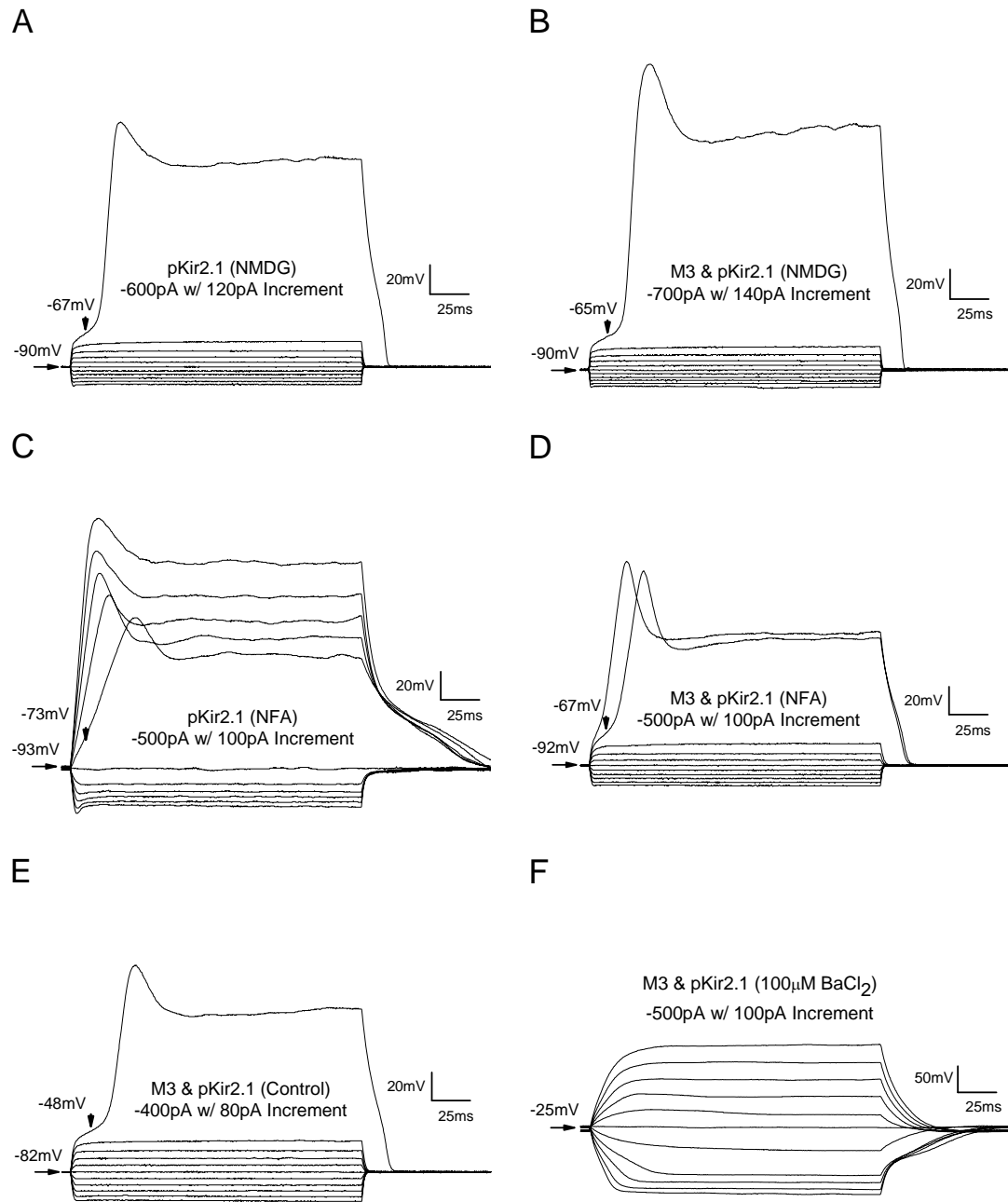


Figure 21. NMDG (145 mM), NFA (100  $\mu$ M), and BaCl<sub>2</sub> (100  $\mu$ M) were applied to tsA201 cells. The membrane voltage responses are shown when a current protocol (Figure 19B) was applied to cells transfected with pKir2.1 (A, C) or M3&pKir2.1(B, D, E, F). In the pre- Ba<sup>2+</sup> control (E), the overshoot depolarization occurs at -48 mV. After BaCl<sub>2</sub><sup>+</sup> application, the overshoot depolarization is completely abolished (F).

## **Chapter 3: The Responses of Isolated Pigeon Vestibular Hair Cells to Acetylcholine Receptor Agonist and Antagonist Application**

### **INTRODUCTION**

Fish and frogs have only one type of hair cells, type II hair cells (Lysakowski, 1996). Bird, mammals, and reptiles (amniotes) have an additional type: type I hair cells. Type I and type II hair cells can be distinguished by their morphology, neural innervation and their ionic currents. Afferent boutons innervate type II hair cells; nerve calyces surround type I hair cells. The membranes of type II hair cells have a cadre of ion channels including potassium, sodium and calcium channels; type I hair cells display a unique, dominant potassium channel (Correia and Lang, 1990) probably a member of the KCNQ family. Afferent fibers course from the neuroepithelium to the brainstem with their cell bodies in the vestibular or Scarpa's ganglion. In pigeon, vestibular efferent fibers originate in the reticular formation and brainstem and course peripherally to innervate hair cells (Eden and Correia, 1982). The efferent nerve terminals innervate type I vestibular hair cells, type II vestibular hair cells, afferent calyces of type I vestibular hair cells, and bouton afferents of type II hair cells. Considering that peripheral efferent terminals innervate both type II and type I hair cells, afferent responses are presumably mediated by a modulation of transmitter released from hair cells to afferent terminals by efferent signals. In different animal models, including fish, frogs, birds, and mammals, it has been shown that efferent stimulation can modify the afferent firing rates as many as three ways in the vestibular organ: inhibitory, excitatory and inhibitory plus excitatory (Rossi et al., 1980; Dechesne and Sans, 1980; Goldberg and Fernandez, 1980; Hartmann and Klinke, 1980; Furukawa, 1981; Dickman and Correia, 1993). One possible

explanation for these contrasting responses may be due to the release of different neurotransmitters from the efferent terminals. Alternatively, these diverse changes may be induced by the dominant efferent transmitter, ACh, acting on different AChRs.

Consistent with the idea that different AChRs participate in the efferent responses, the application of ACh to the isolated semicircular canals (SCCs) mimics efferent stimulation by producing facilitatory and inhibitory changes in afferent discharge (Bernard et al., 1985; Guth et al., 1986; Norris et al., 1988). Bernard et al. 1985 found that the individual afferent discharge frequency was increased by muscarinic agonists while nicotinic agonists produced both increases (most cases) and decreases. The afferent firing rate of semicircular canal afferents was facilitated during ACh application, but was inhibited in the saccule (Guth et al., 1994). In addition, vestibular hair cells isolated from the toadfish saccule (Steinacker and Rojas, 1988), frog saccule (Sugai et al., 1992), and frog semicircular canal (Housley et al., 1990; Holt et al., 2001; Holt et al., 2003; Derbenev et al., 2005) all respond to the application of ACh, suggesting the presence of AChRs on the vestibular hair cells.

All the data obtained from electrophysiological and pharmacological studies of vestibular hair cells indicate that at least three distinguishable AChRs are present on the hair cells. Two of these AChRs belong to nAChRs (Holt et al., 2003) and the third one is a mAChR. Most of time, the activation of  $\alpha 9/\alpha 10$  nAChRs (Elgoyhen et al., 1994; Elgoyhen et al., 2001) produces an inhibitory response of afferent firing due to the downstream activation of calcium-dependent potassium channels (Sugai et al., 1992; Holt et al., 2001). However the activation of DMPP-sensitive nAChR produces rapid depolarization of SCC hair cells (Holt et al., 2003), probably through a classical nicotinic action.

Other evidence also supports the expression of mAChRs on the vestibular hair cells. “Atropine-preferring” (Norris et al., 1988) or ‘muscarinic-like’ (Guth and Norris, 1996) receptors were found on the isolated vestibular hair cell membrane. The ion channels responsible for the ‘muscarinic-like’ AChR-induced changes in outward current were potassium selective and calcium-dependent (Housley et al., 1990; Yoshida et al., 1994). While  $\alpha 9/\alpha 10$  nAChRs functionally coupled activation of calcium-dependent potassium channels, the application of mAChR agonists caused an increase in open time and opening rate of a  $K^+$  channel. This supports the involvement of an intracellular mediator when the cell-attached patch clamp mode of recording was used and the drugs were applied extracellularly (Steinacker and Rojas, 1988). In addition to the physiological and pharmacological results, the presence of both mRNA of mAChR subtypes and the protein expression of mAChR subtypes have been reported in the vestibular periphery (Wackym et al., 1996; Ishiyama et al., 1997; Li et al., 2007). The activation of mAChRs on vestibular hair cells produces either hyperpolarization or depolarization of the membrane potential. The mechanism of ACh-induced hyperpolarization of the vestibular hair cell membrane potential is better understood than ACh-induced depolarization (Guth and Norris, 1996). It is suggested that the pathway of muscarinic receptor induced hyperpolarization uses the following cascade: a muscarinic receptor, a G protein, activation of PLC, increased level of IP<sub>3</sub>, increased intracellular  $Ca^{2+}$  concentration and  $Ca^{2+}$  activated  $K^+$  channel as the effector (Shigemoto and Ohmori, 1991; Yoshida et al., 1994; Guth and Norris, 1996). However, the molecular mechanisms of hair cell depolarization by muscarinic receptor activation are still unknown. Housley et al. found that ACh-induced reduction of potassium selective outward current was abolished by removal of  $Ca^{2+}$  from the external solution and was associated with a

depolarization. The amplitude of the membrane potential was depolarized approximately +2 mV at the reversal membrane potential (Housley et al., 1990). Since then, no ion channels modulated by mAChRs that participate in the hair cell depolarization have been clearly identified. This is possibly due to the lack of electrical responses of isolated vestibular hair cells to mAChR agonist application. It has been proposed that mAChR induced transmitter release from vestibular hair cells is not voltage dependent, but nonelectrogenic (Derbenev et al., 2005), which means the exocytosis happened directly from  $\text{Ca}^{2+}$ , PKA, or PKC stimulation (Koh et al., 2000).

In our previous studies, the inhibitory effect on one of the inwardly rectifying potassium channels Kir2.1 (IRK1) currents during mAChR agonist application was found in pigeon vestibular hair cells (Li and Correia, 2005; Li et al., 2007). Given the functional roles of Kir2.1 channels, it indicates that the vestibular hair cell membrane potential can be modulated by the suppression of IRK1 mediated through mAChR activation. In this study, pharmacological and electrophysiological protocols were used to study membrane potential responses and hair cell current responses initiated by activation of nAChRs or mAChRs and determine if Kir2.1 might act as an effector for the G-protein cascade..

## **EXPERIMENTAL PROCEDURES**

### **Animals**

Adult (6-40 wk old) white king pigeons (*Columba livia*) (Double T Farms, Glenwood, IA) of either sex were used for the present studies. During and prior to surgery, pigeons were anesthetized using an isoflurane tabletop system (VWR International, Cat. # 100229-042, West Chester, PA). Thirty minutes prior to anesthesia,

pigeons were given 0.01-0.02 mg/kg atropine (IV) to decrease bronchial and salivary secretions. Liquid isoflurane and O<sub>2</sub> were mixed in an isoflurane VIP 3000 vaporizer (Midmark, Cat. # 91305430, Versailles, OH). Flow of O<sub>2</sub> was set at 100-200 cc/min and the concentration of isoflurane was held at 4-5%. The output of the vaporizer was connected to either (switch selectable) a small feline mask or to a T-shaped “flow by” tube that could be connected to a tracheotomy tube. Excess isoflurane/O<sub>2</sub> was vented to a self contained “trap”. Initially, the pigeon’s head was put into the feline mask and once anesthesia was achieved, a 9 cm tracheal tube was inserted into pigeon’s trachea and the pigeon was placed in a stereotaxic apparatus (David Kopf Instruments, Tujunga, CA). Next the T-shaped flow by tube was connected to the tracheotomy tube, flow was directed through the tube and the pigeon was observed. After the pigeon was completely unresponsive to foot pinch, the concentration of isoflurane was decreased to 2-3% for maintenance.

Under deep anesthesia, the labyrinths containing the vestibular end organs (including semicircular canals, utricle, and saccule) were taken out from the bony labyrinths (Correia et al., 1989) and put in ice-chilled low Ca<sup>2+</sup> dissociation solution to perform the isolation of single vestibular hair cells. The experimental procedures used in this study were approved by the Institutional Animal Care and Use Committee at UTMB.

### **Isolation of vestibular hair cells**

The end organs were dissected apart using fine iris scissors in 4°C low Ca<sup>2+</sup> saline (containing in mM: 0.1 CaCl<sub>2</sub>, 110 NaCl, 2 KCl, 2 MgCl<sub>2</sub>, 3 D-Glucose and 10 HEPES at pH 7.25) (Hirono et al., 2004). Next, the end organs were incubated with 0.05% trypsin/EDTA (Cellgro, Cat. # MT25-052-CI, Manassas, VA) at RT for 6 min. To

increase the efficiency of enzymatic activity on hair cells, the roof of the semicircular canals and the otolithic membranes of the utricle and saccule were removed prior to putting them into the enzyme solution. After the enzyme treatment, vestibular end organs were kept in 10% fetal bovine serum (FBS, Sigma, Cat. # F2442-500ML, St. Louis, MO) for 30 sec followed by 500  $\mu\text{g}/\mu\text{l}$  bovine serum albumin (BSA, Fisher, Cat. # 03-600-501, Pittsburgh, PA) for 10 min (both FBS and BSA were dissolved in the low  $\text{Ca}^{2+}$  solution that was freshly prepared on the day of the experiment). Next, a glass wisp was used to dissociate hair cells by gently stroking the vestibular neuroepithelium in 200  $\mu\text{l}$  low  $\text{Ca}^{2+}$  solution. To separate the hair cells that were still attached to supporting cells, the hair cell/low  $\text{Ca}^{2+}$  solution was triturated in and out of a pipette having a fire polished 100  $\mu\text{l}$  tip. Finally, the dissociated hair cells were put into a recording chamber whose cover slide bottom was coated with 0.5 mg/ml concanavalin A (Sigma, Cat. # 7275, St. Louis, MO). The cells were allowed to settle for 15 min before the NE superfusion was started. Concanavalin A helped isolated hair cells attach to the chamber bottom without damage and prevented them from floating away during patch clamp and drug application.

To determine the optimal yield of isolated vestibular hair cells while keeping them in good condition, the hair cells treated with 0.05% trypsin/EDTA were compared with two other dissociation methods. The first was physical dissociation without enzyme treatment. All the steps described above were operated within the low  $\text{Ca}^{2+}$  solution. It turned out that most of the hair cells were clustered or died. Low  $\text{Ca}^{2+}$  saline treatment (at least 10 min incubation) didn't successfully break the tight junctions between hair cells and adjacent supporting cells. The yield of isolated single hair cells was poor. Furthermore, patch clamp on the few available isolated hair cells was difficult. It was hard to form a tight seal and cells died within a few seconds. The 2<sup>nd</sup> method of hair cell

dissociation was the same as that described in Chapter 1: Isolated single cell preparation. The vestibular end organs were treated with 65  $\mu\text{g/ml}$  protease XXIV. The yield of isolated hair cells after protease XXIV treatment was as good as that with trypsin/EGTA. The condition of the isolated hair cell membrane was smooth and easily formed a tight seal with the electrode. However, very few hair cells had a response to ACh application (3/50). Protease XXIV enzymatic treatment of hair cells seemingly altered the AChRs or disrupted the intracellular signaling cascade and resulted in nonresponsive cells (Holt et al., 2001). Given the results of the above described trials on dissociation methods, hair cells treated with 0.05% trypsin/EDTA were used routinely.

### **Electrophysiology**

The equipment for the electrophysiological studies described in this chapter, including the amplification, acquisition, perfusion and voltage protocol delivery systems were the same as those described in Chapters 1 & 2. Both perforated patch (Weng and Correia, 1999) and ruptured patch (Masetto and Correia, 1997a) recordings were made. As described in Chapter 2, both voltage clamp and current clamp variants of the patch clamp technique were used. There were however some important differences in the procedures leading to the data in this chapter and those procedures described previously. Those differences involved the use of two particular specific voltage protocols and application of a variety of pharmacological agents (agonists and antagonists) and the use of a unique pipette solution.

In order to study mAChRs induced modulation on the outward and inward currents in isolated vestibular hair cells, two voltage clamp protocols were applied. The first one was negative to positive step voltage protocol. The voltage was held at -60 mV



for 30 ms, then stepped to -120 mV for 230 ms, then stepped to +40 mV for 230 ms, and finally stepped back to -60 mV. The second protocol was a negative to positive ramp voltage protocol. The membrane potential was held at -60 mV for 25 ms, then -120 mV for 25 ms, then ramped to +40 mV within 445 ms, and finally held at -60 mV for 5 ms. Each sweep in both protocols lasted 500 ms and there were 30 sweeps per run with 2 s delay between each sweep (Figure 22). The protocol for type I HCs was different. The type I HCs were initially held at a voltage of -80 mV. The remainder of the protocol for type I HCs was the same as that for type II HCs. A third protocol was also used for current clamp studies. In that protocol no current was injected into the cell but recordings were made of the membrane potential for 60 sec per sweep/run. During the duration of the recording, agonists and antagonists were applied to the cell either by pressure driven or gravity driven force.

The agonists and antagonists used included: the general AChR agonists acetylcholine (100  $\mu$ M) and CCh (2, 100, and 200  $\mu$ M); the selective nicotinic antagonist TC (10  $\mu$ M), and the general AChR antagonist atropine (100  $\mu$ M). In voltage clamp mode, drugs were applied for several sweeps (5-10) during the voltage protocol. Multiples of the several sweeps were used during control, drug application and wash out phases of the data acquisition. Data that are presented in the figures in this chapter are the average value of those sweeps during the control, drug application, and recovery phases.

Since internal  $\text{Ca}^{2+}$  is involved as a second messenger in pathways mediated by mAChR activation, EGTA and  $\text{CaCl}_2$  were removed from the internal KCl pipette solution in some of the ruptured patch experiments. However, no qualitative differences were observed for the agonist/antagonists effects whether EGTA or  $\text{CaCl}_2$  was in the pipette or not. Moreover, no qualitative differences were observed for the

agonist/antagonist effects between ruptured patch and perforated patch experiments. During perforated patch experiments  $\text{Ca}^{2+}$  should not cross in or out of the cell.

Additionally,  $\text{Na}_2\text{ATP}$  (3 mM; Table 4) (Sigma, Cat. # A7699-1G, St. Louis, MO) was added to the pipette solution to: increase ATP-dependent enzyme activities and protein phosphorylation (Collins et al., 1987); phosphorylate GDP to maintain the requirement for GTP (Heidbuchel et al., 1990; Heidbuchel et al., 1993), and prevent run-down of Kir2.1 (Kamouchi et al., 1997).

Finally, instead of using  $\text{MgSO}_4$  in the NE solution,  $\text{MgCl}_2$  was used to maintain a balance of  $\text{Cl}^-$  in the internal and external solution. However, no differences were noticed between external solutions containing either  $\text{MgSO}_4$  or  $\text{MgCl}_2$  (Table 4).

Type II hair cells were grouped depending on their current traces measured at +40 mV. The cells were catalogued by fitting a Boltzmann function, using the Marquardt-Levenberg optimization algorithm, to the activation and inactivation regions of their current trace as shown in Figure 25 and described in Figure 25's legend.

The exponential equation that was fitted to the activation and inactivation regions was of the form:

$$I(t) = A / (1 + e^{-t/\tau}) + C \quad (1)$$

Where:  $I$  is the current at time  $t$ ;  $A$  is the value of the final asymptote;  $C$  is the value of the initial asymptote, and  $\tau$  is the time constant of the change in slope.

## **RESULTS**

### **Type I and type II vestibular hair cells (VHCs)**

Because a different method of enzymatic dissociation was used to obtain type I and type II hair cells for this study (to preserve AChRs), it was important to compare the activation and inactivation kinetics of type I and type II hair cells using this method with recordings made from hair cells in slice preparations where no enzyme was used (Masetto and Correia, 1997a; Weng and Correia, 1999) and recordings from hair cells where different enzymes (such as papain) were used (Lang and Correia, 1989; Rennie and Correia, 1994). Moreover in this study most of the pharmacological experiments used ruptured patch techniques. It was important to verify that control recordings using ruptured patch techniques were the same qualitatively as those obtained using perforated patch techniques (Rennie and Correia, 1994; Weng and Correia, 1999). As detailed below the current responses obtained in the present experiments were the same as those found in previous studies in the lab.

In the present study, type I and type II hair cells were identified based on both the morphology and the characteristic ionic current traces obtained from voltage clamp measurements. Based on the ratio of the minimum neck width to the cuticular plate width and the ratio of the neck width to the body width, vestibular hair cells were identified as type I and type II hair cells (Correia et al., 1989; Ricci et al., 1997). Consistent with earlier studies (Correia and Lang, 1990), voltage clamp of type I and type II hair cells produced different currents (Figure 23). During step voltages (voltage clamp mode), the membrane potential of type I HCs was initially held at -80 mV instead of -60 mV as in type II HCs. In Type I HCs outward current is already present at -60 mV. Negative to that

level a large inward current appears which represents deactivation (Rennie and Correia, 1994) of the current present at -60 mV. When the holding potentials were stepped more positive than -80 mV, the outward currents activated rapidly and showed little or no inactivation (Figure 23A). Type II HCs often showed an inward current which in the past has been shown to be either of two inward rectifiers a slow inward rectifier  $I_h$  or Kir2.1 (Masetto and Correia, 1997a). In the case of the traces shown in Figure 23B, the current is likely Kir2.1 since a blocker of  $I_h$  (ZD7288) was included in the pipette. With more positive voltages the currents activated rapidly and showed either inactivation or little inactivation. It has previously been shown that the activation and inactivation kinetics vary from otolith type II hair cell to type II hair cell depending upon the cadre of potassium currents in the cell (Weng and Correia, 1999). The I-V plot in Figure 23C indicates that the type I HC activated more negatively than the type II hair cell. As such, the type I hair cell showed large outward currents between -50 mV and -70 mV while the type II HC was not yet activated.

The biggest outward currents for type I HCs (at +20 mV) and type II HCs (at +40 mV) and the largest inward currents for type I HCs (at -140 mV) and type II HCs (at -120 mV) collected from both SCCs and otolith end organs were analyzed. The mean value of the current amplitude with S.D. is shown in Figure 23D. No significant differences ( $p < 0.01$ ) were found between the mean inward or outward currents of type I HCs from SCCs ( $n=11$ ) and otoliths ( $n=14$ ). In type II HCs of SCCs ( $n=85$ ) and otoliths ( $n=111$ ), no significant difference was found in the inward currents; but the outward currents were significantly different ( $P < 0.01$ ).

The resting membrane potential (RMP) of both types of HCs from either SCCs or otoliths was measured under current clamp mode. As shown in Figure 24, the RMP of

type I HCs is  $-79.3 \pm 7.0$  mV (SCCs, n=14) and  $-73.1 \pm 4.8$  mV (otoliths, n=11). Type II HCs have RMPs of  $-66.6 \pm 10.0$  mV (SCCs, n=92) and  $-64.8 \pm 9.8$  mV (otoliths, n=112). The RMPs of HCs from SCCs were close to that reported previously:  $-70 \pm 3$  mV (type I, n=14) and  $-57 \pm 3$  mV (type II, n=15) (Correia and Lang, 1990). There are no significant differences of the RMPs in either type I or type II HCs between SCCs and otoliths. However, the RMPs for the two different types of HCs (type I and type II) from the same vestibular end organ are significantly different ( $P < 0.01$ ). Type I HCs have a more negative RMP than that of type II HCs.

To quantitatively categorize the variety of traces seen for type II hair cells, Boltzmann functions were fitted to activation and inactivation regions of the currents at a potential of +40 mV. Best fitted parameters were obtained including the time constant ( $\tau$ ) of the slope. We also measured the time between the start of outward current initiation and the peak of outward current (activation state) and the time between the peak outward current and the steady state of the outward current (inactivation state) as illustrated in Figure 25. Based on the two statistics time and  $\tau$ , type II HCs were divided into four groups. The number of type II hair cells in each group was variable and is presented in Table 6. These groups were fast activation with inactivation (FI), fast activation without inactivation (FN), slow activation with inactivation (SI), and slow activation without inactivation (SN). As shown in Table 5, during outward current activation, FI and FN HCs in both SCCs and otoliths have  $\tau$  values less than 0.08 ms and take 3~4 ms to reach the peak outward current. In contrast, SI and SN take more than 10 ms to attain the peak outward current and their  $\tau$  values are approximately 2 ms. Once the outward current reaches the peak amplitude, it either inactivates or shows a almost constant activation (Figure 25 B, D). The  $\tau$  values of the HCs with inactivation were negative, whereas the

values were positive in HCs without inactivation. We are confident of the  $\tau$  values for each group since as shown in Table 5, the goodness of fit estimate, the correlation ranged from 0.97 to 0.98. Two other parameters (A and C) derived from the Boltzmann function fits are shown in Table 5, but they do not seem to correlate with the different type II HC groups.

Table 6 summarizes the steady state outward currents (measured at +40 mV) and inward currents (measured at -120 mV) and RMPs of the four groups of type II HCs from the SCCs and otoliths. The majority HCs recorded from otoliths (n=111) are SN (36.94%) and SI (34.23%). However, in the semicircular canals (n=87) most HCs are FI (33.33%) and SI (25.29%). The outward currents of SI type II HCs in the otolithic maculae are significantly different from those in the cristae ( $P < 0.01$ ). Also, the inward currents of FI type II HCs in cristae were significantly different than those in the maculae. No significant differences were found in RMPs between any of the type II HC groups or between HCs from SCCs or otoliths. In addition, the  $I_{out}$  of FI, FN, and SN and the  $I_{in}$  of FN, SI, and SN were not significantly different between any HCs of SCCs and/or otoliths.

While there were statistically significant differences between the amplitudes of inward and outward currents for SSCs and otoliths in the four groups of type II hair cells (Table 6, Figure 23), no effort was made to analyze them differently in the pharmacological studies described below. Similarly, no attempt was made to separate the pharmacological responses of type I hair cells from the otoliths and SSCs.

## Pharmacological studies of type II VHCs

### *Voltage clamp at constant holding membrane potential of -60 mV*

The mean RMPs of type II HCs from both SCCs and otolith was  $-65.6 \pm 9.9$  (n=204). In order to study the current changes at RMPs during AChR activation, the membrane potential was held at -60 mV while the drugs were applied. Figure 26 is a typical current trace of a SN type II HC responding to ACh application. At -60 mV, there is a small outward current with the amplitude of 10 pA. 100  $\mu$ M ACh application increased the outward current from 10 pA to 205 pA (Figure 26A). After NE rinse, the current returned to near control values (Figure 26B). Application of a mixture 100  $\mu$ M ACh and 10  $\mu$ M TC produced inward current (Figure 26B, C). The second application of ACh also facilitated the outward current (Figure 26C). Since TC is a blocker for nAChRs, this indicates that at voltages close to RMP, the activation of nAChRs increases the outward current, while the activation of mAChRs facilitates the inward current.

### *The negative-positive step voltage clamp*

Figure 27 shows the current traces when the negative-positive step protocol during voltage clamp is performed. The application of 100  $\mu$ M ACh increases outward currents (at voltage potentials -60 mV and +40 mV) and inward current (at -120 mV) (Figure 27A). Conversely, application of a mixture of TC with ACh prevents the increase in both inward and outward currents (Figure 27B). Both outward and inward currents return towards control values after washout (Figure 27C). The current traces marked by the color cyan in Figure 27A & B are currents obtained by subtracting the trace during drug application from the control trace. Since TC selectively blocked nAChR induced

effects, the difference current in Figure 27B is actually the response produced by the activation of mAChRs. However, in Figure 27A, the difference current is a combination of the activation of both nAChRs and mAChRs. Considering that the activation of mAChRs produce an inhibitory response; while the activation of the combination of mAChR/nAChR is excitatory, the pure nAChR induced response (olive line) is the sum of difference currents (cyan traces) in Figure 27A and Figure 27B. The above analysis assumes that both nAChRs and mAChRs are simultaneously expressed on the same HC.

Not all the HCs had the same response to ACh application. Among 23 type II HCs that responded to ACh applications, 16 (69.6%) showed an increase of outward current at +40 mV potential and 13 (56.5%) showed an increase of the inward current at the -120 mV potential. Other HCs demonstrated a decrease of the outward current (n=7, 30.4%) and a decrease of the inward current (n=8, 34.8%). Of the 10 HCs that were treated with the mixture of ACh and TC (mAChR activation), the outward current was either decreased (5/10 cells, 50%) or increased (5/10 cells, 50%) at +40 mV. The inward current was either decreased (4/10 cells, 40%) or increased (2/10 cells, 20%) when the voltage was held at -120 mV (data not shown). The reason for these opposing different responses of HCs to the same drug application paradigm is unknown. It could be due to the expression of different AChR subtypes on the hair cells and/or the possibility that ionic channels different from Kir2.1 were modulated.

### ***The negative-positive ramp voltage clamp***

Using the ramp protocol in voltage clamp, the current modification by drug application over the range of voltage potentials from -120 mV to +40 mV was more obvious than that observed using the step protocol in voltage clamp. The reversal



potential of HCs before, during, and after drug application can be estimated from the I-V plot.

The application of 100  $\mu$ M ACh increased the inward current when the membrane potential was held more negative than the reversal potential and increased the outward current when the voltage potential was more positive than the reversal potential (Figure 28A). Rinsing the HC with NE restored the current to control levels. However, administration of a mixture of ACh and TC treatment to the same cell inhibited both the inward and outward currents (Figure 28B). A second application of ACh application again facilitated the inward and outward currents on either side of the reversal potential (Figure 28C). I-V plots of the ramp voltage clamp are shown in Figure 28D. The effects induced by ACh application also resulted in a shift of the reversal membrane potential from -50 mV to -80 mV (1<sup>st</sup> time) and -73 mV (2<sup>nd</sup> time). The mixture of TC with ACh resulted in inhibition of the inward and outward currents. It could be assumed that the current change due to nAChRs would be larger than that of ACh application shown in Figure 28. The second application of ACh produced a smaller response than that of the first trial which could be due to either the degenerative condition of the HC or incomplete recovery from previous treatment.

A total of 11 HCs had responses to ACh during ramp clamp. Ten out of 11 (91%) HCs showed an increase of inward and outward current after ACh application (as in Figure 28A). Of these 10 HCs the increase was constant over the entire voltage range for 6 (60%) cells. However, in 4/10 (40%) the amplitude of outward current was decreased when the membrane potential was more positive than  $6.4 \pm 4.6$  mV (data not shown). This might be due to run down of some outward current above this potential. In addition, 1/11 (9%) of the HCs had inhibition of inward and outward current following ACh

application. However, all 7 (100%) of the type II HCs responding to a mixture of ACh and TC had decreased amplitude of inward and outward currents.

***The current clamp at the resting membrane potential (RMP)***

The voltage clamp results indicated that the responses of type II HCs to ACh and ACh with TC application did not differ in either step or ramp voltage clamp protocols. Generally, cells treated with ACh were most likely to have an increase of inward (67.6%, 23/34) and outward (76.5%, 26/34) current; whereas cells treated with ACh and TC had a decrease of inward (64.7%, 11/17) and outward (70.6%, 12/17) current.

In current clamp mode, application of ACh to type II HCs hyperpolarized the cell membrane potential (Figure 29B, C). Atropine pre-treatment and mixture of TC with ACh completely blocked this ACh induced hyperpolarization (Figure 29C). This result indicated that the induced responses were through the nAChRs. The average ( $\pm$  S.D.) value of membrane potential changes during ACh application was  $-15 \pm 7.9$  mV ( $n=7$ ). No depolarization response of type II hair cells to ACh treatment was observed.

Application of a mixture of ACh with TC produced either depolarization (Figure 29A) or hyperpolarization (Figure 29D). Similar responses were observed when a mixture of CCh and TC was applied (Figure 29E and F). These results indicated that the responses were through the mAChRs. The number of HCs that were depolarized with ACh and TC was 1 and CCh and TC was 1. The number of HCs that were hyperpolarized following application of ACh and TC was 3 and CCh and TC was 1.

### **Pharmacological studies of type I VHCs**

Type I HCs have large outward currents (Figure 23A). The application of CCh to type I HCs produced a strong effect on the outward current when the step voltage protocol was performed (Figure 11B). Rinsing partially restored the amplitude of the current. The I-V plots of type I HCs responding to application of CCh is shown in Figure 30. At +20 mV, the amplitude of the outward current is decreased 87%; while at -140 mV it decreases the inward current 35%. In addition, the reversal membrane potential after 2  $\mu$ M CCh application shifts from -68 mV to -55 mV and partially recovers after NE washout.

In the negative-positive step voltage clamp mode (protocol shown as an insert in Figure 30B), the application of ACh with TC to type I HCs resulted in a further inhibition of the outward current (67%) than that following 100  $\mu$ M ACh application (26%). Since ACh application to the cell activated both mAChRs and nAChRs, the increased inhibition of the outward current by mAChRs (ACh & TC) indicated that nAChR response on the outward current was excitatory. Otherwise, the inhibitory responses of the outward current produced by mAChRs should be less than when both mAChRs and nAChRs were activated. In current clamp mode, the depolarization induced by ACh application was blocked by the addition of TC (Figure 30C). In addition, TC application prevented the hyperpolarization produced by application of CCh. The current clamp data indicated that both depolarization and hyperpolarization were induced by the activation of nAChRs, but not mAChRs. A total of 18 type I HCs had been recorded and 2 out of 18 HCs responded to ACh application.

## DISCUSSION

Type I and type II HCs are different on the basis of their morphological and ionic current properties. Type I HCs are flask-shaped, while type II HCs are columnar (Wersall, 1956). Both the ratio of the neck width to the cuticular plate width (NPR) and the neck width to cell body width (NBR) have been used to differentiate type I and type II HCs (Correia et al., 1989; Kevetter et al., 1994; Ricci et al., 1996b). Type I HCs have NPR values less than 0.72 and NBR values less than 0.64 whereas the average values of NPR and NBR in type II HCs are larger than those of type I HCs. The whole cell patch clamp can also differentiate the type of HCs. Type I HCs have big outward currents at voltage potentials above -80 mV, but type II HCs do not activate until -60 mV (see Figure 23C). Type I hair cells have stereotypical activation kinetics; rapid activation followed by little or no inactivation (Figure 23A) whereas type II hair cells show a variety of activation and inactivation kinetics (Figure 25, Table 5). Additionally type I currents are larger than type II currents. For example, we measured the outward current of type I HCs at +20 mV to be  $3390 \pm 104.27$  pA, which is more than three times larger than that in type II HCs at +40 mV. Another difference between type I and type II HCs is their RMPs. Type I HCs have more negative RMP than type II HCs at least 10 to 20 mV.

Several ion channels have been identified in the avian's vestibular type II HCs, including the delayed rectifier outward  $K^+$  current,  $I_K$ , which has a slow activation conductance and is sensitive to tetraethylammonium (TEA); the A type outward potassium current,  $I_A$ , which has rapid activation conductance and is sensitive to 4-aminopyridine (4-AP); the  $Ca^{2+}$ -dependent outward  $K^+$  current,  $I_{K(Ca)}$ ; the inward  $Ca^{2+}$  current; and two inward rectifier  $K^+$  currents,  $IRK1$  and  $I_h$  (Ohmori, 1984; Lang and Correia, 1989; Correia, 1999). Based on the previous pharmacological studies that have

each outward current (Lang and Correia, 1989; Masetto et al., 1996), it can be proposed that fast outward current activation is due to  $I_A$  and  $I_{K(Ca)}$  on the type II HCs; while the slow outward current activation is because of the high expression of  $I_K$  on the HCs. In pigeon inactivation is caused by  $I_A$  (Lang and Correia, 1989) or more precisely the association of Kv $\alpha$ 1.4 with Kv $\beta$ 1.1 (Correia et al., 2008). In pigeon, the lack of inactivation of outward current is considered to be the absence of expression of  $I_A$  and the combined expression of both  $I_K$  and  $I_{K(Ca)}$  (Weng and Correia, 1999). In the frog semicircular canal HCs, two types of  $I_A$  exist: fast inactivation and slow inactivation (Norris et al., 1992). In addition, the ion channels are reported to be expressed differently according to regions of the vestibular neuroepithelium. For example, in frog crista ampullares,  $I_K$  and  $I_A$  were located in the peripheral region;  $I_A$  showed little presence in the central region; and  $I_{K(Ca)}$  was seen in both regions (Masetto et al., 1994). Our experimental procedure (dissociated hair cells as opposed to a neuroepithelium slice) didn't allow us to determine which region the HCs came from, but the results indicated that in our sample of SSC HCs, 56% had an outward current with a rapid rise to peak; while the remaining HCs (44%) had slowly activated outward currents. Almost half of the SSC HCs (41%) had outward current w/o inactivation. The corresponding ratios of outward current in otolithic HCs are 29%, 71%, and 37%.

The effects of activation of nAChRs and mAChRs are summarized in Table 7. We isolated the components of the response due to mAChR and that due to nAChR activation by treatment with TC. TC is a classical nAChR antagonist. At the concentration of 10  $\mu$ M, it blocked both types of nAChRs,  $\alpha$ 9/ $\alpha$ 10 and DMPP, found in hair cells (Holt et al., 2003). In general, our data indicate that ACh application to type II HCs facilitated the outward current under different voltage protocols. The facilitatory effects induced by

ACh application are mediated through nAChRs. To verify this conclusion, further experiments, using selective or general mAChR antagonists, should be applied with ACh.

Since all four categories of type II HCs (FI, FD, SI and SD) responded similarly to drug application, it was difficult to differentiate which type were more likely to be modulated by AChR activation. The outward current that was facilitated by nAChRs in type II HCs has been proposed to be  $I_{K(Ca)}$  (Guth and Norris, 1996). In the present study, the kinetics of the outward current modulated by nAChRs is very close to  $I_{K(Ca)}$  (Masetto et al., 1996), but with slow inactivation, which means that other types of currents are also present. In fact, in 7 type II HCs that responded to ACh application in the negative-positive step voltage clamp mode, 3 clearly showed a brief activation ( $I_{K(Ca)}$ ) followed by a slow activation with or without any inactivation. We proposed that another ion channel,  $I_K$ , was also modulated by nAChR. To identify which ion channel was involved in the modulation by nAChR activation, two sets of experiments could be performed. We could apply TEA to block the  $I_K$  current; or we could do the experiments in a  $Ca^{2+}$  free solution or add a  $Ca^{2+}$  chelator, such as BAPTA, to identify  $I_{K(Ca)}$ .

Activation of mAChRs inhibited the outward current. The modulated outward current trace was more likely to be due to a mixture of ion channels, the dominant  $I_K$  with small amount of  $I_{K(Ca)}$ . It might also involve  $I_A$ . In guinea-pig inner hair cells, the fast activating current  $I_{K,f}$  ( $I_A?$ ) was modulated by PKA (Jagger and Ashmore, 1999). Application of the PKA inhibitor, H-89, to auditory HCs decreased the amplitude of outward current,  $I_{K,f}$ . Previous studies have shown that the even numbered mAChRs (M2 and M4) worked through  $G_{ai/o}$  to inhibit the activity of adenylate cyclase which consequently decreased the level of cAMP-dependent PKA (Jones, 1993). So, mAChR

activation could modulate the outward current by changing intracellular signaling pathways by the activation of M2 and M4 mAChR subtypes.

The most likely candidate for the inward current modulated by both nAChR and mAChRs is Kir2.1 because the recording electrode was filled with ZD7288, which completely blocked the other inward rectifier potassium channel,  $I_h$ . Also the current could not be an inward  $Ca^{2+}$  current since  $Ca^{2+}$  currents are activated at around -50 mV, far from what we recorded at -120 mV (Ohmori, 1984; Art and Fettiplace, 1987; Lang and Correia, 1989; Fuchs et al., 1990; Fettiplace and Fuchs, 1999). The mechanism of AChR induced inward current responses was not clear, especially for nAChRs. It is hypothesized that the inhibitory response induced by mAChR acts via Kir2.1. The odd number mAChRs (M1, M3, and M5) work through  $G_{\alpha q/11}$  to activate PLC, which consequently activates PKC; phosphorylation of Kir2.1 channel decreases the ion channel conductance (Jones, 1993).

To understand how current modification during voltage clamp would change the HC membrane potential, current clamp experiments were performed. ACh induced hyperpolarization was either blocked by TC or atropine pre-treatment of the cell when the cell was held at RMP. This meant that nAChRs played a role in hyperpolarization. Activation of mAChR produced either depolarization or hyperpolarization of type II HCs' membrane potentials. This hyperpolarization was consistent with the shift of reversal membrane potential in I-V plots analyzed from negative-positive ramp voltage clamp recording. The time line for nAChR responses was faster than that from mAChR activation. This was consistent with the properties of the ionotropic receptor (nAChR) compared with the metabotropic receptor (mAChR).

The functional roles of  $I_A$ ,  $I_K$ , and  $I_{K(Ca)}$  are to suppress excitability during large depolarizing currents and contribute to action potential repolarization (Sah and McLachlan, 1992) and afterhyperpolarization (AHP) (Viana et al., 1993). Blockage of  $I_A$  in neonatal spiral ganglion neurons lowered the threshold of action potentials; decreased the rate of repolarization, decreased the amplitude of the AHP; and increased the firing rate of action potentials (Jagger and Housley, 2002). Blockage of  $I_K$  broadened the duration of the action potential (Jurkiewicz and Sanguinetti, 1993; Varro et al., 2000; Cheng and Kodama, 2004). Two types of  $I_{K(Ca)}$  have been identified in the hair cells. They are the small conductance  $I_{K(Ca)}$  (SK) (Doi and Ohmori, 1993; Nenov et al., 1996; Guth et al., 1998; Fuchs, 2002) and the large conductance  $I_{K(Ca)}$  (BK) (Fuchs and Evans, 1990; Sugihara, 1994; Roberts, 1994; Ramanathan et al., 1999). SK contributes to midrange AHP (Schwindt et al., 1988); while BK participates in repolarization following the action potential (Skinner et al., 2003). Blockage of the bicuculline-sensitive  $I_{K(Ca)}$ , an apamin-sensitive SK, depolarized the resting membrane potential about 5 mV and increased the spontaneous firing frequency in the rat medial preoptic nucleus (Johansson et al., 2001). The role of BK channels in HCs is not known; however, they are believed to produce the oscillatory voltage responses (Lewis and Hudspeth, 1983; Hudspeth and Lewis, 1988a; Hudspeth and Lewis, 1988b; Fettiplace and Fuchs, 1999), to regulate neurotransmitter release (Pattillo et al., 2001) and to be involved in HC maintenance (Nemzou et al., 2006). Even though the present data could not separate and identify which ionic current had been modulated by the AChR activation, our results confirmed the functional roles of the outward currents. Facilitation of the outward currents inhibited the HCs' activity by hyperpolarizing the membrane potential.



Inward current, IRK1 (Kir2.1), is also important. Activation of nAChRs increases while mAChRs decreases IRK1. The functional role of Kir2.1 is to keep the cell membrane potential close to  $E_K$  (Hille, 2001). Blockage of Kir2.1 depolarized the membrane potential in native vestibular HCs (Correia et al., 2004). In the present studies, even though nAChR activation facilitated IRK1 in type II HCs, the membrane potential was hyperpolarized. Activation of mAChR inhibited IRK1 in type II HCs, resulting in the membrane potential being either hyperpolarized or depolarized. This emphasizes the need to consider both inward and outward currents when studying membrane potential changes in native hair cells.

Voltage clamp studies on Type I HCs indicated that the activation of mAChRs inhibited outward currents by 60%. In type I hair cells, outward currents include  $I_{K(Ca)}$  and the M-type current (Ricci et al., 1996b; Rennie et al., 2001; Hurley et al., 2006). As reported in previous studies, the M-type current was modulated by the activation of mAChR M1 expressed in CHO cells (Selyanko et al., 2000). The M-type current was also modulated with other intracellular secondary messengers, such as PIP2 (Zhang et al., 2003; Suh and Hille, 2007), DAG (Suh and Hille, 2006), PLC (Horowitz et al., 2005), and PKC (Nakajo and Kubo, 2005), all signaling pathway that are mediated via odd numbered mAChRs. Even though mAChR activation inhibited type I HC outward current, there was no effect on membrane potential.

Most HCs do not respond to application of ACh. Fewer type I HCs respond to ACh application (11.1%) than type II HCs (27.6%). This is similar to previous results that reported that 7.5% of type I HCs were sensitive to ACh application (Zhu et al., 2008). A maximum of 21% of type I HCs have the M-like current (Eatock and Hutzler, 1992). So, the reason that we saw few type I HCs that responded to ACh might be

because the majority do not respond to ACh. The question remains what the physiological role of AChR might be when so few HCs respond to ACh. The answer might be in the recent proposal that the mAChR induced response in vestibular hair cells is not voltage dependent, but nonelectrogenic (Derbenev et al., 2005).

In summary, responses induced by AChR activation in both type I and type II HCs is shown in Table 7. We believe that nicotinic AChR activation increases the outward currents (type I & type II) and inward currents (type II) resulting in hyperpolarization (type I & type II) or depolarization (type II) of the membrane potential. Muscarinic AChR activation decreases both inward and outward currents (type I & type II) which consequently produces hyperpolarization (type II) and depolarization (type II). Since many ion channels are located on the HCs and each HC expresses the five mAChR subtypes, it is hard to identify specific receptor responses on a single ionic channel. The mechanism of each receptor induced response requires further study.

Table 4.

## Concentration of solutions (mM)

	External		Internal	
	Previous	Modified	Previous	Modified
NaCl	145	145	-	-
KCl	3	3	140	150
CaCl <sub>2</sub>	2	2	1	-
MgSO <sub>4</sub>	1	-		
MgCl <sub>2</sub>	-	1	2	2
HEPES	15	15	10	10
D-Glucose	10	10	-	-
Na <sub>2</sub> ATP	-	-	-	3
EGTA	-	-	11	-
Vitamin C	0.283	0.283	-	-
Na Pyruvate	2	2	-	-

Table 5.

Best fitted parameters for Boltzmann function fits of current traces for the four groups of dissociated type II HCs from the semicircular canal and otolith organs

HCs		Semicircular Canal					Otolith				
		A (pA)	$\tau$ (ms)	C (pA)	Correlation	Time (ms)	A (pA)	$\tau$ (ms)	C (pA)	Correlation	Time (ms)
Activation	F I	1318.3 $\pm$ 745.7	0.634 $\pm$ 0.266	-257.2 $\pm$ 358.5	0.983 $\pm$ 0.008	3.4 $\pm$ 1.3	1398.2 $\pm$ 1170.8	0.644 $\pm$ 0.406	-412.3 $\pm$ 577.4	0.977 $\pm$ 0.012	3.3 $\pm$ 1.7
	F N	874.5 $\pm$ 643.6	0.673 $\pm$ 0.2	-72.1 $\pm$ 379.7	0.987 $\pm$ 0.009	3.4 $\pm$ 1.1	1009.2 $\pm$ 352.1	0.667 $\pm$ 0.218	-70.9 $\pm$ 398.3	0.986 $\pm$ 0.006	3.7 $\pm$ 9.2
	S I	1598.5 $\pm$ 990.3	1.813 $\pm$ 0.85	-351.7 $\pm$ 467.7	0.98 $\pm$ 0.007	10.9 $\pm$ 3.7	2546.1 $\pm$ 1075.3	2.37 $\pm$ 0.854	-811.3 $\pm$ 575	0.977 $\pm$ 0.009	16.9 $\pm$ 5.6
	S N	1031.3 $\pm$ 521.7	2.181 $\pm$ 1.16	-19.9 $\pm$ 266.1	0.969 $\pm$ 0.01	15.4 $\pm$ 6.1	2085.2 $\pm$ 1123	2.551 $\pm$ 1	-625.7 $\pm$ 495	0.976 $\pm$ 0.007	19.4 $\pm$ 7.3
Inactivation	F I	351.2 $\pm$ 272.6	-28.3 $\pm$ 21.1	866.4 $\pm$ 338	0.979 $\pm$ 0.007	141.7 $\pm$ 1.4	18223.8 $\pm$ 53363.6	-4587.4 $\pm$ 13692.2	-8150 $\pm$ 26644.1	0.956 $\pm$ 0.062	142 $\pm$ 1.7
	F N	100.4 $\pm$ 171	6.5 $\pm$ 19	744.4 $\pm$ 323.6	0.981 $\pm$ 0.009	141.6 $\pm$ 9.6	128.4 $\pm$ 265.8	9.85 $\pm$ 17.7	862.1 $\pm$ 310.4	0.981 $\pm$ 0.013	141.3 $\pm$ 0.9
	S I	56463.6 $\pm$ 179361.7	-9254.9 $\pm$ 0.9	-27042 $\pm$ 89494	0.985 $\pm$ 0.006	134.6 $\pm$ 3.2	25393.8 $\pm$ 131714.6	-5899.8 $\pm$ 30086.4	-10900.4 $\pm$ 65710.6	0.989 $\pm$ 0.005	128.3 $\pm$ 5.6
	S N	0.5 $\pm$ 85.3	1.438 $\pm$ 8.171	365.1	0.976 $\pm$ 0.008	130.7 $\pm$ 5.7	81.1 $\pm$ 53.1	8.125 $\pm$ 9.27	1549.3 $\pm$ 674.9	0.990 $\pm$ 0.004	124.3 $\pm$ 3.8

Table 6.

Summary of inward and outward current amplitudes and RMPs of the four groups of dissociated type II HCs from the semicircular canal and otolith organs

Current Traces	Semicircular Canal (n=87)			Otolith (n=111)		
	$I_{out}$ (pA)	$I_{in}$ (pA)	RMP (mV)	$I_{out}$ (pA)	$I_{in}$ (pA)	RMP (mV)
FI	n=29 (33.33%)			n=21 (18.91%)		
	890.86±354.24	-158.45±96.34*	-65.60±10.17	813.10±595.47	-83.10±70.98	-60.17±7.62
FN	n=20 (22.99%)			n=11 (9.91%)		
	827.05±385.51	-113.25±77.75	-66.42±10.99	999.55±387.61	-133.18±109.25	-63.67±9.28
SI	n=22 (25.29%)			n=38 (34.23%)		
	1148.86±547.60	-152.73±84.55	-67.33±9.28	1657.76±584.91*	-124.34±91.22	-66.11±9.51
SN	n=16 (18.39%)			n=41 (36.94%)		
	1064.06±338.51	-123.44±96.88	-66.42±10.99	1537.32±704.58	-120.98±79.45	-66.61±10.60

\* Significant different between semicircular canal and otolith at  $p < 0.01$ .

Table 7.

A summary of the AChR activation induced responses in type I and type II dissociated vestibular HCs

HCs		Voltage Clamp Mode			Current Clamp Mode	
		Inward current	Current at holding potential	Outward current	Hyperpolarized RMP	Depolarized RMP
Type I	nAChR	n/a	n/a	↑ Outward Current	Y	Y
	mAChR	↓ Inward Current	n/a	↓ Outward Current	n/a	Y
Type II	nAChR	↑ Inward Current	↑ Outward Current	↑ Outward Current	Y	n/a
	mAChR	↓ Inward Current	n/a	↓ Outward Current	Y	Y

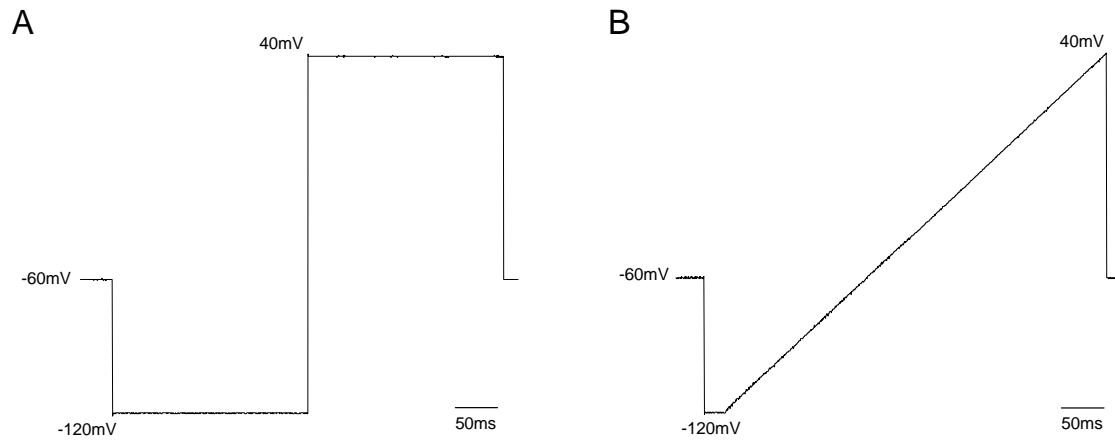


Figure 22. Traces representing most frequently used voltage protocols to test currents in dissociated hair cells as drugs were applied. A negative-positive step voltage protocol (A) and a negative-positive ramp voltage protocol (B) were used to study the complex current (primarily Kir2.1) modulation in the isolated vestibular hair cells during drug application. Both protocols were initiated at a membrane potential holding voltage of -60 mV, then stepped to -120 mV and then changed to +40 mV using a step (A) or a ramp (B) waveform. Finally, the membrane was set back to -60 mV. Each protocol was run multiple times with 30 sweeps/run and there were 2 sec delay between each sweep. Within run responses were averaged and runs usually consisted of groups of control, drug application and recovery responses.

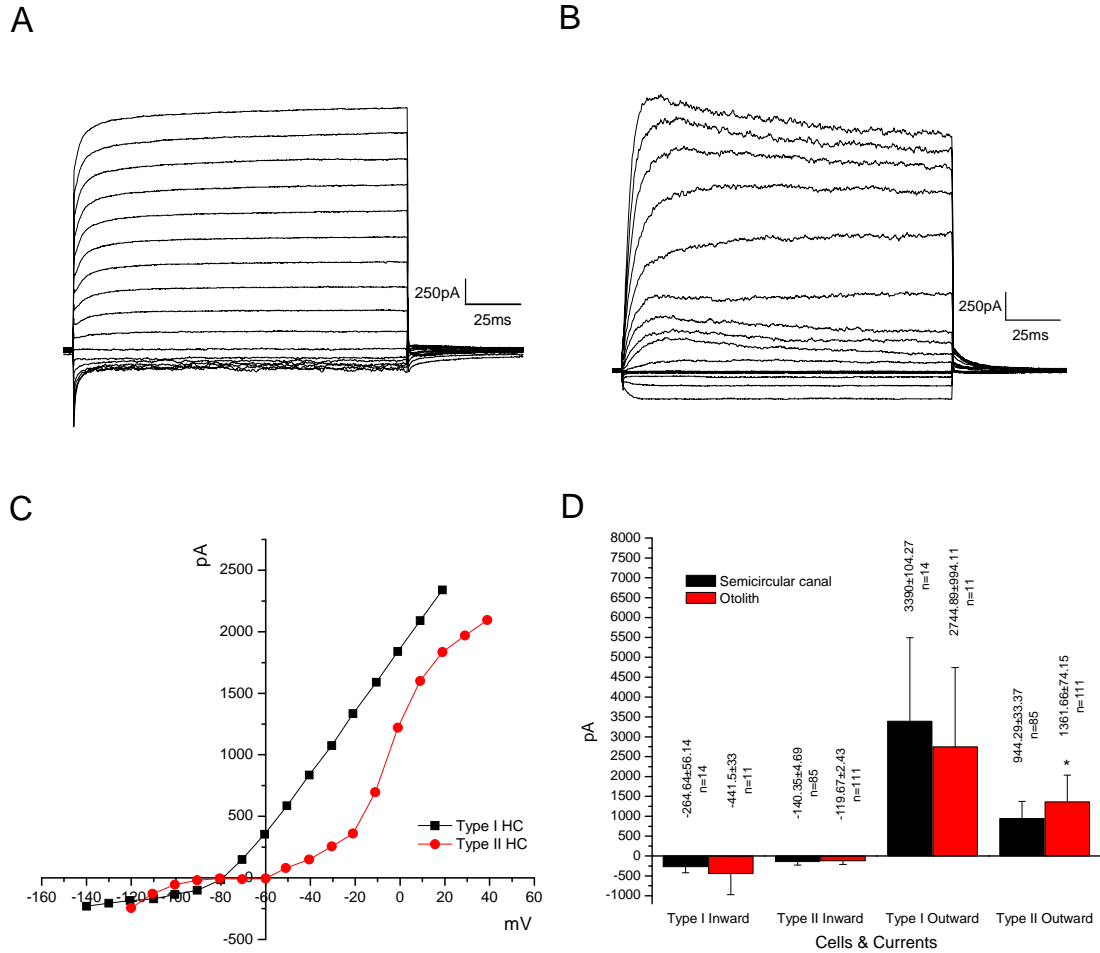


Figure 23. Typical current traces of dissociated type I (A) and type II (B) vestibular hair cells. The voltage protocol used is shown in Figure 11B. Type II hair cells (B) were initially held at -60mV and type I hair cells (A) were initially clamped at -80 mV. The I-V plots, presented in panel C, were based on steady state currents (shown in panels A, B) measured at the end of the voltage steps. Note that zero current for type II and type I hair cells is at -60mV and -80mV, respectively. Also note the inward currents in (B) which were probably Kir2.1 since the other inward rectifier  $I_h$  was blocked using ZD7288. The average (+ 1 S.D.) amplitude of inward and outward currents for otolith and semicircular canal type I and type II hair cells are shown in (D). The currents for type II HCs were recorded at -120 mV and +40 mV; the currents for type I HCs were recorded at -140 mV and +20 mV. The mean inward and outward currents from the two end organs were statistically compared. Comparing mean otolith and semicircular canal currents, there was no significant difference ( $P>0.05$ ,  $t$ -test) between type I inward current amplitude, type II inward current amplitude and type I outward current amplitude. The mean outward current of type II HCs from semicircular canals and otoliths were, however, significantly different ( $P<0.01$ ,  $t$ -test). The reason for this difference is unknown.

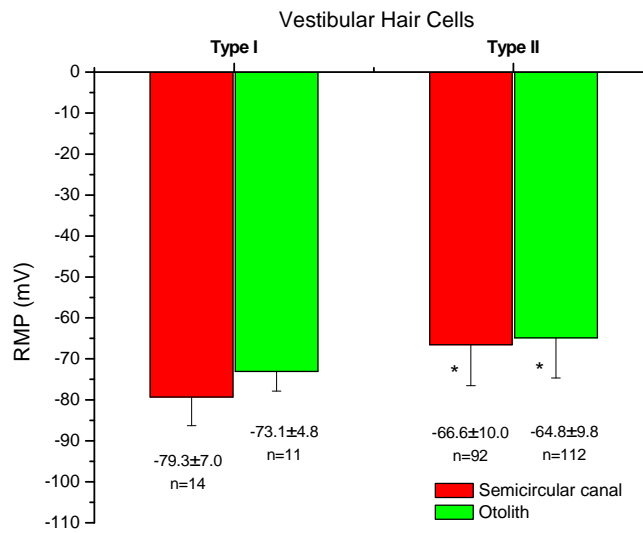


Figure 24. A bar histogram showing the mean (+1 S.D.) RMPs (measured in current clamp) for dissociated type I and type II HCs from semicircular canals and otoliths. While there was no statistical difference between the average RMPs for the end organs, there was a significant difference ( $P < 0.01$ ,  $t$ -test) between the mean RMPs for type I and type II hair cells for each receptor.



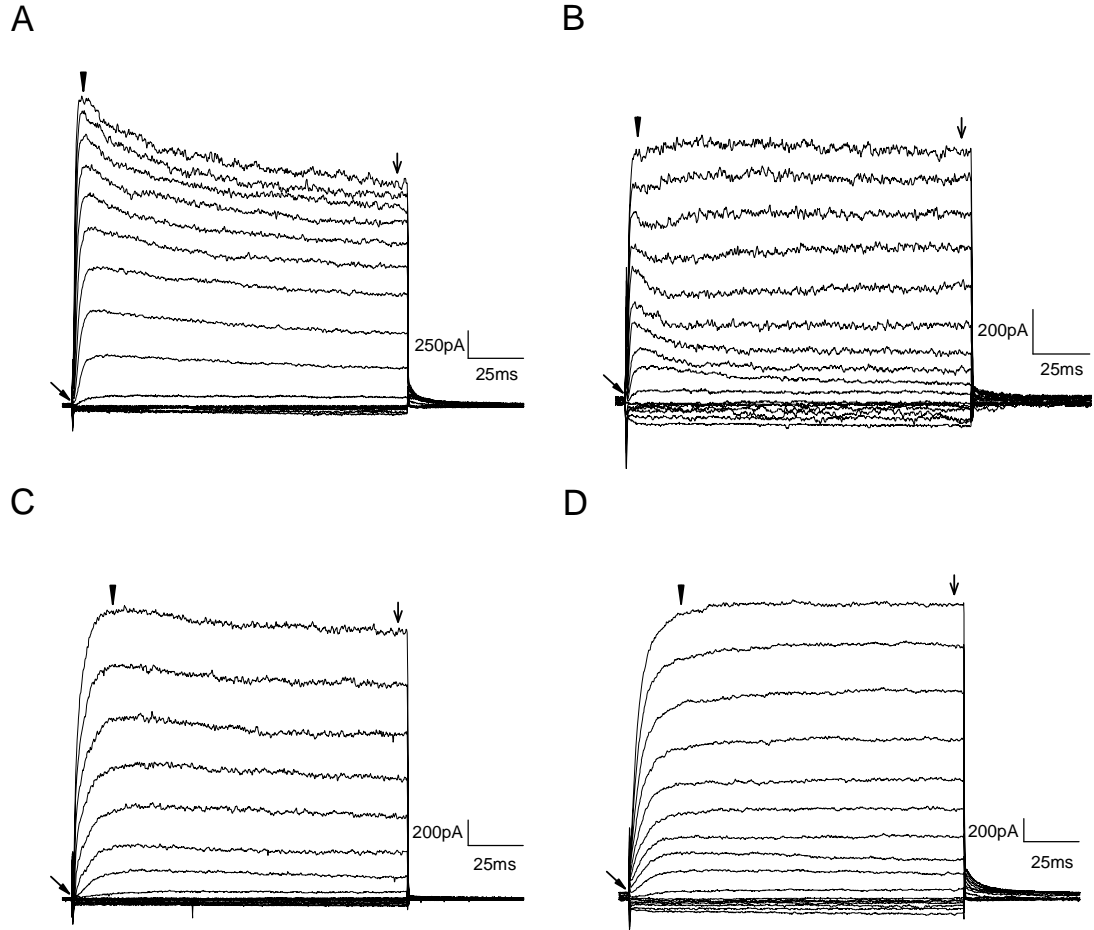


Figure 25. Four types of current traces observed from dissociated type II vestibular HCs. Based on the outward current trace recorded at +40 mV, type II HCs are divided into four groups: fast outward current w/ inactivation (FI, A); fast outward current w/ no inactivation (FN, B); slow outward current w/ inactivation (SI, C) and slow outward current w/ no inactivation (SN, D). Boltzmann functions (see equation in the methods section) were fitted to the current data values over two regions of the traces; the activation region (denoted by initial arrow and arrowhead) and the inactivation region (denoted by the part of the trace from the arrowhead to the second arrow). A comparison of the best fitted parameters of the Boltzmann function for the four groups are shown in Table 5 and mean inward and outward current amplitudes and RMPs for the four groups from each receptor is presented in Table 6.

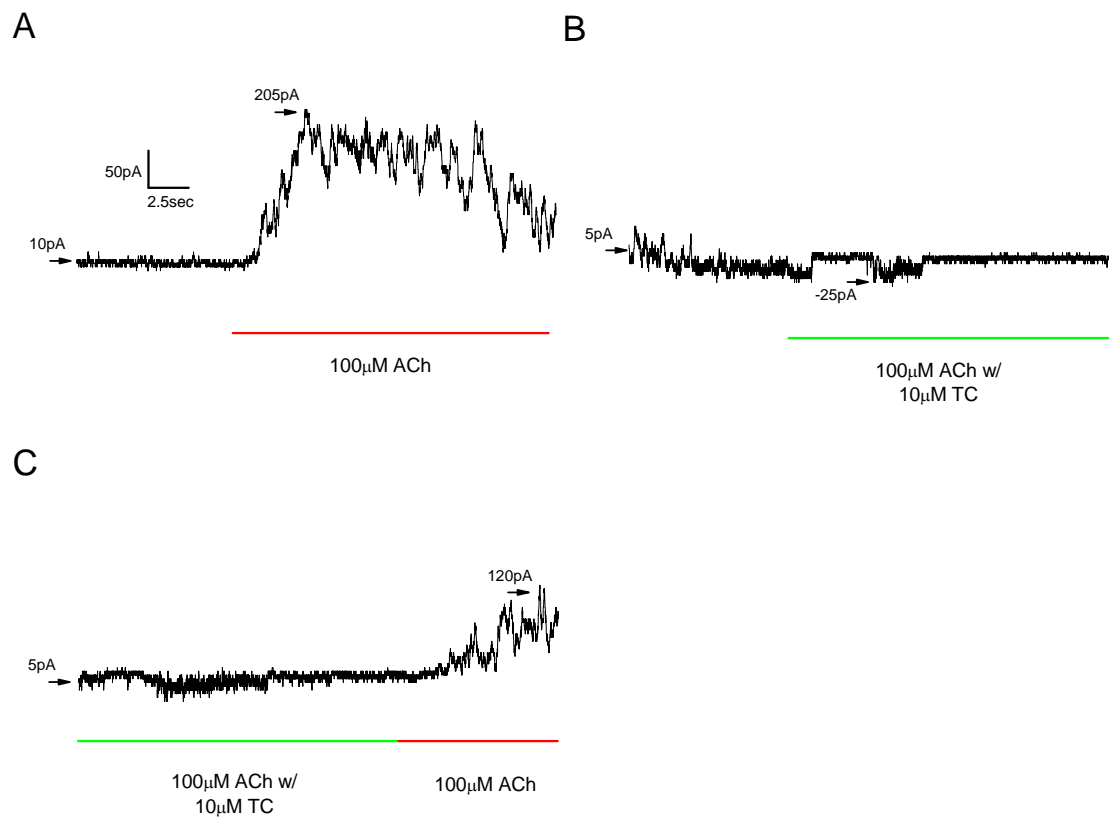


Figure 26. Current traces from a dissociated type II HC with its membrane potential held at -60 mV. The application of 100  $\mu$ M ACh increased the outward current (A) and (C), while 100  $\mu$ M ACh w/ 10  $\mu$ M TC produces an inward current (B) and (C). The red and green bars indicate the duration of the application of 100  $\mu$ M ACh and 100  $\mu$ M ACh w/ 10  $\mu$ M TC, respectively.

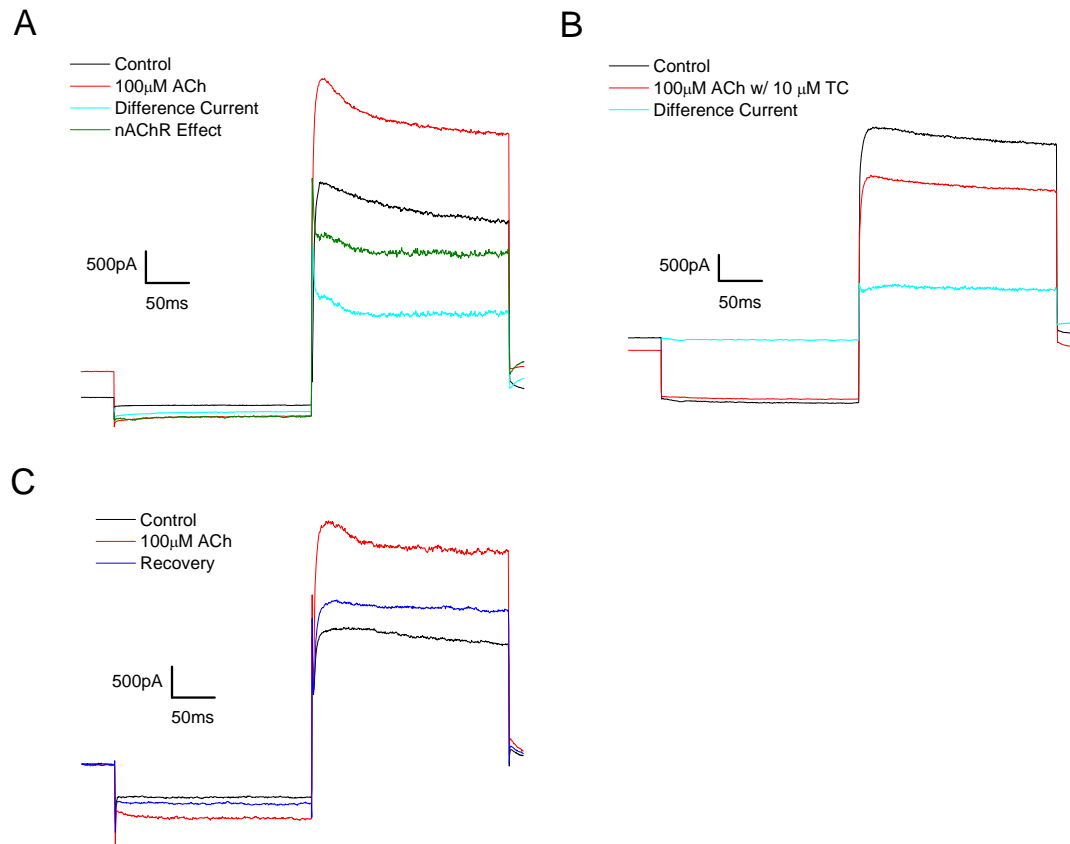


Figure 27. Current traces from different type II HCs using the negative-positive step voltage protocol (Figure 22 A) while drugs were applied to the HCs. These traces indicate that depending on which AChR (mAChR or nAChR) is activated the current can be increased or decreased. As shown by the red trace in panel (A), 100  $\mu$ M ACh transiently increases the inward current (at -120 mV) and increases the outward current (at -60 mV and +40 mV). The control trace is the black trace in all panels. The cyan trace in panels A and B represents the difference current between the control current and the current during drug application. The red trace in panel B demonstrates that the mixture of 100  $\mu$ M ACh and 10  $\mu$ M TC produces an inhibitory effect on the current when the voltage is at -60 mV, -120 mV, and +40 mV. The pure nAChR induced response (olive) is calculated from the difference current in (A) and (B). To make the trace more resolute, the initial holding membrane current traces of the difference currents in (A) and (B) are ignored. Facilitatory effects induced by ACh application are partially recovered after NE rinse for 10 sec. This is indicated by the blue trace in panel C.

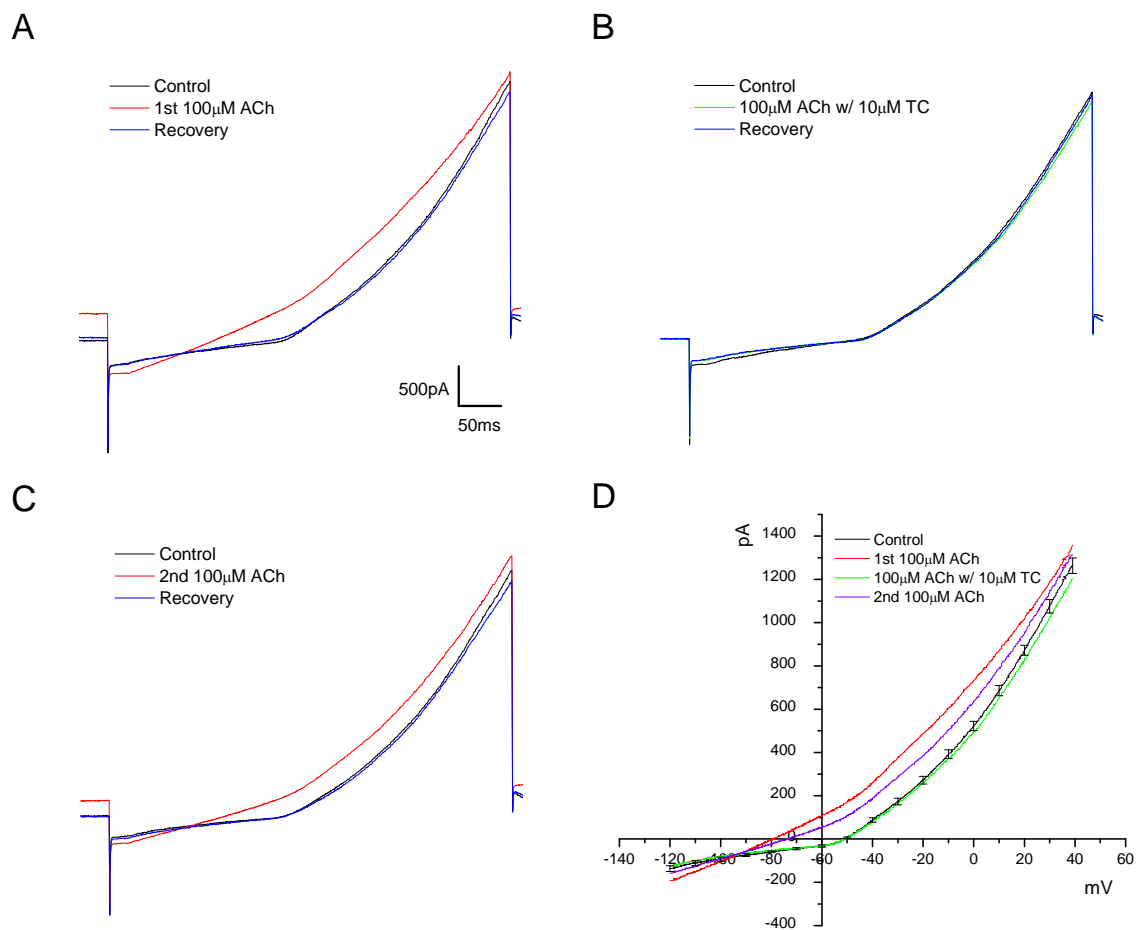


Figure 28. Current traces from a dissociated type II HC using the negative-positive ramp voltage protocol (Figure 22 B) during drug application. The first application of 100  $\mu$ M ACh facilitates both the inward current and outward current (A). Application of 100  $\mu$ M ACh and 10  $\mu$ M TC inhibits this response (B). A second application of 100  $\mu$ M ACh to the same HC produces a response similar to the first application but one which is decreased in amplitude. Panel D presents I-V plots for each ramp current response. The control values in (D) are average values for controls from A-C. Error bars represent  $\pm 1$  S.D. As shown in panel D the increased outward current at the RMP hyperpolarizes the reversal membrane potential from -50 mV to -80 mV.

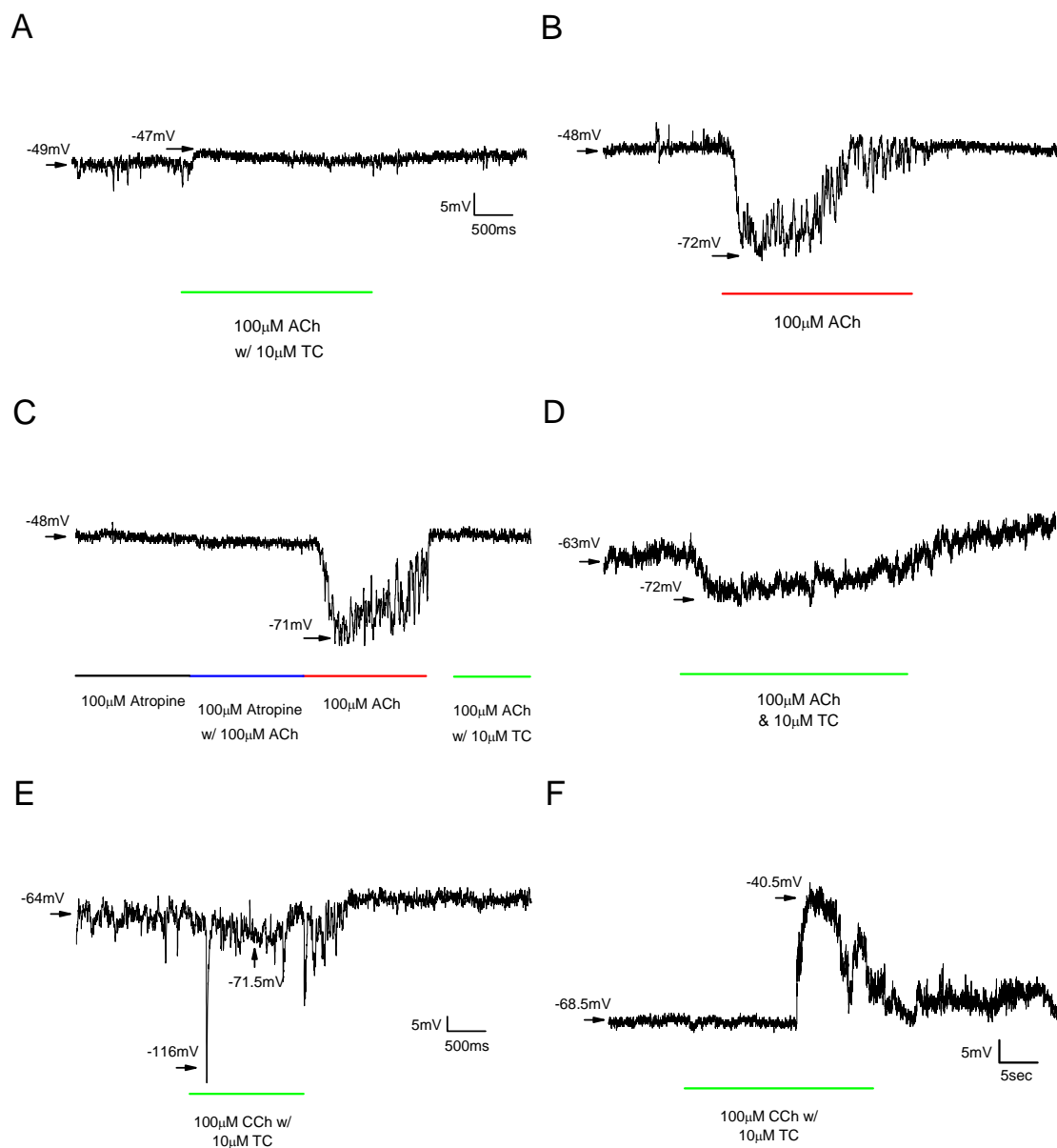


Figure 29. Membrane potential recordings from dissociated type II HCs (obtained in current clamp mode) during various AChR agonist and antagonist application are illustrated in panels A-F. The duration of drug application is denoted by color coded bars. Application of 100  $\mu$ M ACh and 10  $\mu$ M TC (green bar) produced either depolarization (A) or hyperpolarization (D) of the RMP. 100  $\mu$ M ACh application (red bar) induced hyperpolarization (B). The hyperpolarization was blocked by atropine pretreatment (C; black bar). In addition, application of mixtures of 100  $\mu$ M CCh with 10  $\mu$ M TC resulted in either hyperpolarization (E) or depolarization (F). All the effects induced by drug application recovered to control levels after NE wash.

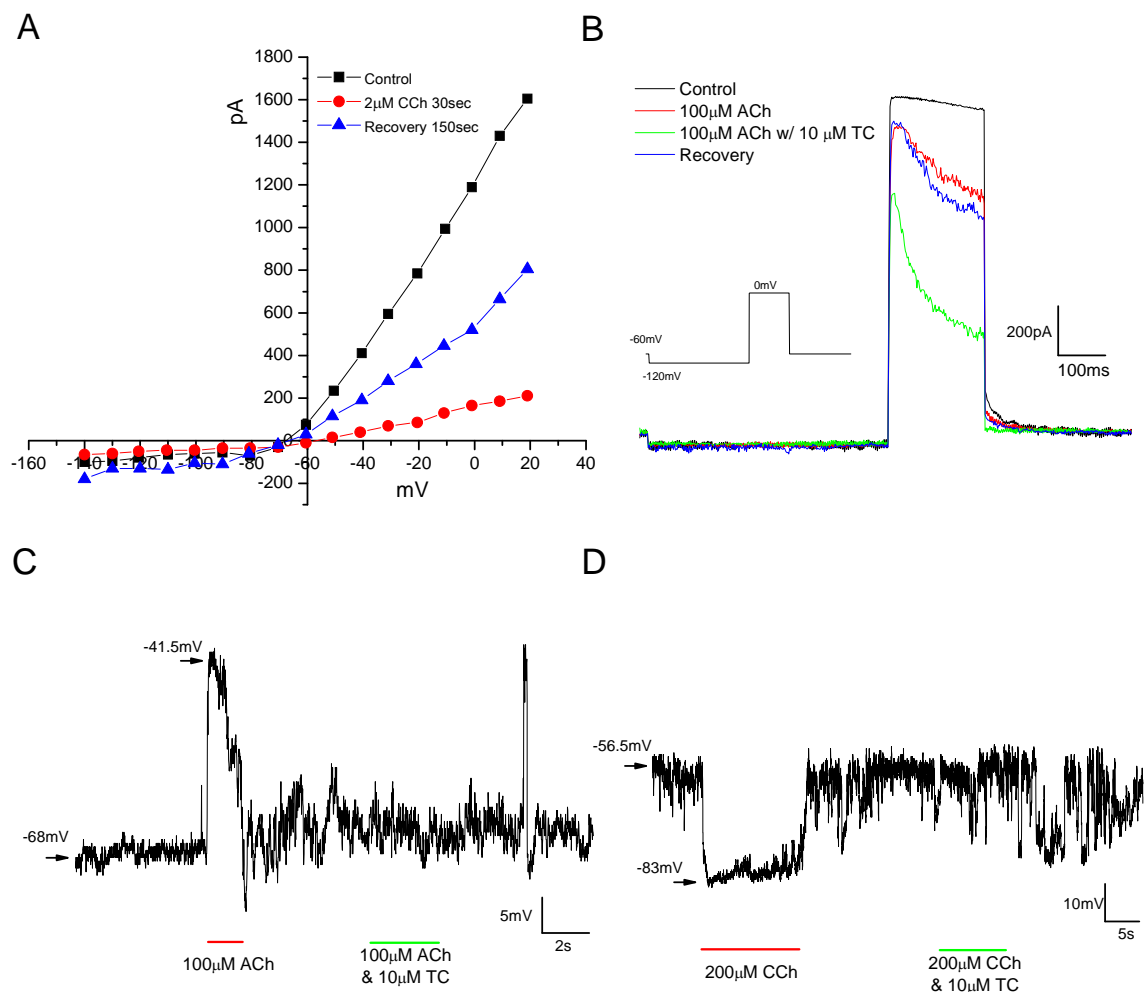


Figure 30. Voltage clamp and current clamp recordings from dissociated Type I HCs that illustrate responses induced by AChR activation. Panel A shows an I-V plot for a type I HC recorded using the step voltage protocol shown in Figure 11B. 2  $\mu$ M CCh application inhibits the outward current (red circles) 87% (at +20 mV) and inward current 35% (at -140 mV). This change in current amplitude consequently depolarizes the reversal membrane potential shown in panel A from -68 mV to -55 mV. Following washout of the CCh with NE, the current (blue triangles) partially recovers to the control level. Panel B shows type I hair cell current responses (red trace) to 100  $\mu$ M ACh. The voltage protocol used is inset in the figure. The control outward current (black trace) is reduced during application of the ACh. The current (green trace) is further reduced by the application of 100  $\mu$ M ACh and 10  $\mu$ M TC. Following 150 sec of NE wash; the outward current (blue trace) partially recovered. Panel C illustrates depolarization of the RMP using a recording obtained in current clamp mode. Application of 100  $\mu$ M ACh (red bar) depolarizes the membrane 26 mV. Subsequent application of 100  $\mu$ M ACh and 10  $\mu$ M TC (green bar) blocks the effect. Panel D illustrates the hyperpolarizing effect of application of an mAChR agonist on type I hair cells. Application of 200  $\mu$ M CCh hyperpolarizes the RMP by 26 mV. Subsequent superfusion of 200  $\mu$ M CCh and 10  $\mu$ M TC (green bar) blocks the effect.

## References

1. Adami M, Bertaccini G, Coruzzi G, Poli E (1985) Characterization of cholinoreceptors in the rat urinary bladder by the use of agonists and antagonists of the cholinergic system. *J Auton Pharmacol* 5: 197-205.
2. Adrian RH, Chandler WK, Hodgkin AL (1970) Slow changes in potassium permeability in skeletal muscle. *J Physiol* 208: 645-668.
3. Adrian RH, Freygang WH (1962) The potassium and chloride conductance of frog muscle membrane. *J Physiol* 163: 61-103.
4. Aiello E, Kennedy J, Hernandez C (1991) Stimulation of frog ciliated cells in culture by acetylcholine and substance P. *Comp Biochem Physiol C* 99: 497-506.
5. Almers W (1972) The decline of potassium permeability during extreme hyperpolarization in frog skeletal muscle. *J Physiol* 225: 57-83.
6. Anderson AD, Troyanovskaya M, Wackym PA (1997) Differential expression of alpha2-7, alpha9 and beta2-4 nicotinic acetylcholine receptor subunit mRNA in the vestibular end-organs and Scarpa's ganglia of the rat. *Brain Res* 778: 409-413.
7. Arenal A, Pimentel R, Garcia C, Pimentel E, Alestrom P (2004) The SV40 T antigen nuclear localization sequence enhances nuclear import of vector DNA in embryos of a crustacean (*Litopenaeus schmitti*). *Gene* 337: 71-77.
8. Art JJ, Fettiplace R (1987) Variation of membrane properties in hair cells isolated from the turtle cochlea. *J Physiol (Lond)* 385: 207-242.
9. Bard J, Kunkel MT, Peralta EG (2000) Single channel studies of inward rectifier potassium channel regulation by muscarinic acetylcholine receptors. *J Gen Physiol* 116: 645-652.
10. Basile AS, Fedorova I, Zapata A, Liu X, Shippenberg T, Duttaroy A, Yamada M, Wess J (2002) Deletion of the M5 muscarinic acetylcholine receptor attenuates morphine reinforcement and withdrawal but not morphine analgesia. *Proc Natl Acad Sci U S A* 99: 11452-11457.
11. Ben Chaim Y, Tour O, Dascal N, Parnas I, Parnas H (2003) The M2 muscarinic G-protein-coupled receptor is voltage-sensitive. *J Biol Chem* 278: 22482-22491.

12. Berjukow S, Doring F, Froschmayr M, Grabner M, Glossmann H, Hering S (1996) Endogenous calcium channels in human embryonic kidney (HEK293) cells. *Br J Pharmacol* 118: 748-754.
13. Berkeley JL, Levey AI (2000) Muscarinic activation of mitogen-activated protein kinase in PC12 cells. *J Neurochem* 75: 487-493.
14. Bernard C, Cochran SL, Precht W (1985) Presynaptic actions of cholinergic agents upon the hair cell-afferent fiber synapse in the vestibular labyrinth of the frog. *Brain Res* 338: 225-236.
15. Bett GC, Dai S, Campbell DL (2002) Cholinergic modulation of the basal L-type calcium current in ferret right ventricular myocytes. *J Physiol* 542: 107-117.
16. Bonner TI, Buckley NJ, Young AC, Brann MR (1987) Identification of a family of muscarinic acetylcholine receptor genes. *Science* 237: 527-532.
17. Bonner TI, Young AC, Brann MR, Buckley NJ (1988) Cloning and expression of the human and rat m5 muscarinic acetylcholine receptor genes. *Neuron* 1: 403-410.
18. Borowiec JA, Dean FB, Bullock PA, Hurwitz J (1990) Binding and unwinding--how T antigen engages the SV40 origin of DNA replication. *Cell* 60: 181-184.
19. BoSmith RE, Briggs I, Sturgess NC (1993) Inhibitory actions of ZENECA ZD7288 on whole-cell hyperpolarization activated inward current (I<sub>h</sub>) in guinea-pig dissociated sinoatrial node cells. *Br J Pharmacol* 110: 343-349.
20. Braun T, Schofield PR, Shivers BD, Pritchett DB, Seeburg PH (1987) A novel subtype of muscarinic receptor identified by homology screening. *Biochem Biophys Res Commun* 149: 125-132.
21. Bruce LL, Christensen MA, Warr WB (2000) Postnatal development of efferent synapses in the rat cochlea. *J Comp Neurol* 423: 532-548.
22. Bruce LL, Kingsley J, Nichols DH, Fritzsche B (1997) The development of vestibulocochlear efferents and cochlear afferents in mice. *Int J Dev Neurosci* 15: 671-692.
23. Burgess DR, Broschat KO, Hayden JM (1987) Tropomyosin distinguishes between the two actin-binding sites of villin and affects actin-binding properties of other brush border proteins. *J Cell Biol* 104: 29-40.



24. Castoldi AF, Manzo L, Costa LG (1993) Cyclic GMP formation induced by muscarinic receptors is mediated by nitric oxide synthesis in rat cortical primary cultures. *Brain Res* 610: 57-61.
25. Catlin MC, Kavanagh TJ, Costa LG (2000) Muscarinic receptor-induced calcium responses in astroglia. *Cytometry* 41: 123-132.
26. Caulfield MP (1993) Muscarinic receptors--characterization, coupling and function. *Pharmacol Ther* 58: 319-379.
27. Chang HK, Shieh RC (2003) Conformational changes in Kir2.1 channels during NH<sub>4</sub><sup>+</sup>-induced inactivation. *J Biol Chem* 278: 908-918.
28. Chawla N, Johri MB, Saxena PN, Singhal KC (1975) Cholinergic mechanisms in central thermoregulation in pigeons. *Br J Pharmacol* 53: 317-322.
29. Chen K, Waller HJ, Godfrey DA (1995) Muscarinic receptor subtypes in rat dorsal cochlear nucleus. *Hear Res* 89: 137-145.
30. Cheng JH, Kodama I (2004) Two components of delayed rectifier K<sup>+</sup> current in heart: molecular basis, functional diversity, and contribution to repolarization. *Acta Pharmacol Sin* 25: 137-145.
31. Chi SM, Li CX, Liu YL, Zhu YL, Gu JW, Du L, Wang FZ (2002) [The effect of acetylcholine on the proliferation and apoptosis of three kinds of cultured human pituitary adenoma cells]. *Sheng Li Xue Bao* 54: 251-257.
32. Chomczynski P, Sacchi N (1987) Single-step method of RNA isolation by acid guanidinium thiocyanate-phenol-chloroform extraction. *Anal Biochem* 162: 156-159.
33. Citi S, Kendrick-Jones J (1991) Localization of myosin in the cytoskeleton of brush border cells using monoclonal antibodies and confocal laser-beam scanning microscopy. *Tissue Cell* 23: 789-799.
34. Cohen GM (1987) Acetylcholinesterase activity in the embryonic chick's inner ear. *Hear Res* 28: 57-63.
35. Cohen RI, Molina-Holgado E, Almazan G (1996) Carbachol stimulates c-fos expression and proliferation in oligodendrocyte progenitors. 43: 193-201.

36. Collins SA, Pon DJ, Sen AK (1987) Phosphorylation of the alpha-subunit of (Na<sup>+</sup> + K<sup>+</sup>)-ATPase by carbachol in tissue slices and the role of phosphoproteins in stimulus-secretion coupling. *Biochim Biophys Acta* 927: 392-401.
37. Conklin BR, Chabre O, Wong YH, Federman AD, Bourne HR (1992) Recombinant Gq alpha. Mutational activation and coupling to receptors and phospholipase C. *J Biol Chem* 267: 31-34.
38. Contrera JG, Mcleskey SW, Holopainen I, Xu J, Wojcik WJ (1993) Muscarinic m2 receptors in cerebellar granule cell cultures from rat: mechanism of short-term desensitization. *J Pharmacol Exp Ther* 265: 433-440.
39. Correia MJ (1999) Hair Cells. In: *Encyclopedia of Life Sciences Nature Publishing Group*, New York, NY.
40. Correia MJ, Christensen BN, Moore LE, Lang DG (1989) Studies of solitary semicircular canal hair cells in the adult pigeon. I. Frequency- and time-domain analysis of active and passive membrane properties. *J Neurophysiol* 62: 924-934.
41. Correia MJ, Lang DG (1990) An electrophysiological comparison of solitary type I and type II vestibular hair cells. *Neurosci Lett* 116: 106-111.
42. Correia MJ, Lang DG, Eden AR (1985) A light and transmission electron microscope study of the neural processes within the pigeon anterior semicircular canal neuroepithelium. *Prog Clin Biol Res* 176: 247-262.
43. Correia MJ, Weng T, Prusak D, Wood TG (2008) Kvbeta1.1 associates with Kvalpha1.4 in Chinese hamster ovary cells and pigeon type II vestibular hair cells and enhances the amplitude, inactivation and negatively shifts the steady-state inactivation range. *Neuroscience* 152: 809-820.
44. Correia MJ, Wood TG, Prusak D, Weng T, Rennie KJ, Wang HQ (2004) Molecular characterization of an inward rectifier channel (IKir) found in avian vestibular hair cells: cloning and expression of pKir2.1. *Physiol Genomics* 19: 155-169.
45. de Azevedo LC, Zizemer JR, Hackl LP, Marino-Neto J, Paschoalini MA (2002) Muscarinic cholinergic receptor blockade impairs free fatty acid mobilization during fasting in pigeons (*Columba livia*). *J Comp Physiol [B]* 172: 115-123.
46. de Chasseval R, de Villartay JP (1992) High level transient gene expression in human lymphoid cells by SV40 large T antigen boost. *Nucleic Acids Res* 20: 245-250.

47. de Jeu M, Geurtsen A, Pennartz C (2002) A Ba(2+)-sensitive K(+) current contributes to the resting membrane potential of neurons in rat suprachiasmatic nucleus. *J Neurophysiol* 88: 869-878.
48. Dechesne C, Sans A (1980) Control of the vestibular nerve activity by the efferent system in the cat. *Acta Otolaryngol* 90: 82-85.
49. Del Castillo P, Llorente AR, Stockert JC (1989) Influence of fixation, exciting light and section thickness on the primary fluorescence of samples for microfluorometric analysis. *Basic Appl Histochem* 33: 251-257.
50. Derbenev AV, Linn CL, Guth PS (2005) Muscarinic ACh receptor activation causes transmitter release from isolated frog vestibular hair cells. *J Neurophysiol* 94: 3134-3142.
51. Dickman JD, Correia MJ (1993) Bilateral communication between vestibular labyrinths in pigeons. *Neuroscience* 57: 1097-1108.
52. Dietl MM, Cortes R, Palacios JM (1988) Neurotransmitter receptors in the avian brain. II. Muscarinic cholinergic receptors. *Brain Res* 439: 360-365.
53. Doi T, Ohmori H (1993) Acetylcholine increases intracellular Ca<sup>2+</sup> concentration and hyperpolarizes the guinea-pig outer hair cell. *Hear Res* 67: 179-188.
54. Dorje F, Levey AI, Brann MR (1991) Immunological detection of muscarinic receptor subtype proteins (m1-m5) in rabbit peripheral tissues. *Mol Pharmacol* 40: 459-462.
55. Dousmanis AG, Pennefather PS (1992) Inwardly rectifying potassium conductances in AtT-20 clonal pituitary cells. *Pflugers Arch* 422: 98-104.
56. Drenckhahn D, Engel K, Hofer D, Merte C, Tilney L, Tilney M (1991) Three different actin filament assemblies occur in every hair cell: each contains a specific actin crosslinking protein. *J Cell Biol* 112: 641-651.
57. Drescher DG, Upadhyay S, Wilcox E, Fex J (1992) Analysis of muscarinic receptor subtypes in the mouse cochlea by means of the polymerase chain reaction. *J Neurochem* 59: 765-767.
58. Du JY, Zuo WL, Chen MH, Xiang H, Zhou WL (2006) Involvement of muscarinic acetylcholine receptors in chloride secretion by cultured rat epididymal epithelium. *Cell Biol Int* 30: 741-746.

59. Eatock RA, Hutzler MJ (1992) Ionic currents of mammalian vestibular hair cells. *Ann N Y Acad Sci* 656: 58-74.
60. Eden AR, Correia MJ (1981) Vestibular efferent neurons and catecholamine cell groups in the reticular formation of the pigeon. *Neurosci Lett* 25: 239-242.
61. Eden AR, Correia MJ (1982) Identification of multiple groups of efferent vestibular neurons in the adult pigeon using horseradish peroxidase and DAPI. *Brain Res* 248: 201-208.
62. Eglen RM (2006) Muscarinic receptor subtypes in neuronal and non-neuronal cholinergic function. *Auton Autacoid Pharmacol* 26: 219-233.
63. Eglen RM, Nahorski SR (2000) The muscarinic M(5) receptor: a silent or emerging subtype? *Br J Pharmacol* 130: 13-21.
64. Elgoyhen AB, Johnson DS, Boulter J, Vetter DE, Heinemann S (1994) Alpha 9: an acetylcholine receptor with novel pharmacological properties expressed in rat cochlear hair cells. *Cell* 79: 705-715.
65. Elgoyhen AB, Vetter DE, Katz E, Rothlin CV, Heinemann SF, Boulter J (2001) alpha10: a determinant of nicotinic cholinergic receptor function in mammalian vestibular and cochlear mechanosensory hair cells. *Proc Natl Acad Sci U S A* 98: 3501-3506.
66. Endoh T (2007) Muscarinic M2 receptor inhibition of calcium current in rat nucleus tractus solitarius. *Neuroreport* 18: 1141-1145.
67. Esqueda EE, Gerstin EH, Jr., Griffin MT, Ehlert FJ (1996) Stimulation of cyclic AMP accumulation and phosphoinositide hydrolysis by M3 muscarinic receptors in the rat peripheral lung. *Biochem Pharmacol* 52: 643-658.
68. Evans MG, Lagostena L, Darbon P, Mammano F (2000) Cholinergic control of membrane conductance and intracellular free Ca<sup>2+</sup> in outer hair cells of the guinea pig cochlea. *Cell Calcium* 28: 195-203.
69. Fakler B, Brandle U, Glowatzki E, Zenner HP, Ruppersberg JP (1994) Kir2.1 inward rectifier K<sup>+</sup> channels are regulated independently by protein kinases and ATP hydrolysis. *Neuron* 13: 1413-1420.
70. Fernandez JM, Hoeffler JP (1999) Gene expression systems : using nature for the art of expression. San Diego, CA: Academic Press.

71. Fettiplace R, Fuchs PA (1999) Mechanisms of hair cell tuning. *Annu Rev Physiol* 61: 809-834.
72. Fink-Jensen A, Fedorova I, Wortwein G, Woldbye DP, Rasmussen T, Thomsen M, Bolwig TG, Knitowski KM, McKinzie DL, Yamada M, Wess J, Basile A (2003) Role for M5 muscarinic acetylcholine receptors in cocaine addiction. *J Neurosci Res* 74: 91-96.
73. Firth TA, Jones SV (2001) GTP-binding protein Gq mediates muscarinic-receptor-induced inhibition of the inwardly rectifying potassium channel IRK1 (Kir 2.1). *Neuropharmacology* 40: 358-365.
74. Flock A, Bretscher A, Weber K (1982) Immunohistochemical localization of several cytoskeletal proteins in inner ear sensory and supporting cells. *Hear Res* 7: 75-89.
75. Flock A, Cheung HC (1977) Actin filaments in sensory hairs of inner ear receptor cells. *J Cell Biol* 75: 339-343.
76. Flynn ER, McManus CA, Bradley KK, Koh SD, Hegarty TM, Horowitz B, Sanders KM (1999) Inward rectifier potassium conductance regulates membrane potential of canine colonic smooth muscle. *J Physiol* 518 ( Pt 1): 247-256.
77. Fritz S, Fohr KJ, Boddien S, Berg U, Brucker C, Mayerhofer A (1999) Functional and molecular characterization of a muscarinic receptor type and evidence for expression of choline-acetyltransferase and vesicular acetylcholine transporter in human granulosa-luteal cells. *J Clin Endocrinol Metab* 84: 1744-1750.
78. Fuchs P (2002) The synaptic physiology of cochlear hair cells. *Audiol Neurotol* 7: 40-44.
79. Fuchs PA, Evans MG (1990) Potassium currents in hair cells isolated from the cochlea of the chick. *J Physiol* 429: 529-551.
80. Fuchs PA, Evans MG, Murrow BW (1990) Calcium currents in hair cells isolated from the cochlea of the chick. *J Physiol (Lond)* 429: 553-568.
81. Fujii T, Kawashima K (2001) An independent non-neuronal cholinergic system in lymphocytes. *Jpn J Pharmacol* 85: 11-15.
82. Fukuta H, Hashitani H, Yamamoto Y, Suzuki H (1999) Calcium responses induced by acetylcholine in submucosal arterioles of the guinea-pig small intestine. *J Physiol* 515: 489-499.

83. Furukawa T (1981) Effects of efferent stimulation on the saccule of goldfish. *J Physiol* 315: 203-215.
84. Gacek RR, Nomura Y, Balogh K (1965) Acetylcholinesterase activity in the efferent fibers of the stato-acoustic nerve. *Acta Otolaryngol* 59: 541-553.
85. Gadbut AP, Galper JB (1994) A novel M3 muscarinic acetylcholine receptor is expressed in chick atrium and ventricle. *J Biol Chem* 269: 25823-25829.
86. Garcia N, Santafe MM, Salon I, Lanuza MA, Tomas J (2005) Expression of muscarinic acetylcholine receptors (M1-, M2-, M3- and M4-type) in the neuromuscular junction of the newborn and adult rat. *Histol Histopathol* 20: 733-743.
87. Glenney JR, Jr., Glenney P, Weber K (1982) Erythroid spectrin, brain fodrin, and intestinal brush border proteins (TW-260/240) are related molecules containing a common calmodulin-binding subunit bound to a variant cell type-specific subunit. *Proc Natl Acad Sci U S A* 79: 4002-4005.
88. Glenney JR, Jr., Glenney P, Weber K (1983) The spectrin-related molecule, TW-260/240, cross-links the actin bundles of the microvillus rootlets in the brush borders of intestinal epithelial cells. *J Cell Biol* 96: 1491-1496.
89. Godfrey DA, Park JL, Ross CD (1984) Choline acetyltransferase and acetylcholinesterase in centrifugal labyrinthine bundles of rats. *Hear Res* 14: 93-106.
90. Goldberg JM, Fernandez C (1980) Efferent vestibular system in the squirrel monkey: anatomical location and influence on afferent activity. *J Neurophysiol* 43: 986-1025.
91. Gomeza J, Zhang L, Kostenis E, Felder C, Bymaster F, Brodtkin J, Shannon H, Xia B, Deng C, Wess J (1999) Enhancement of D1 dopamine receptor-mediated locomotor stimulation in M(4) muscarinic acetylcholine receptor knockout mice. *Proc Natl Acad Sci U S A* 96: 10483-10488.
92. Graham FL, Smiley J, Russell WC, Nairn R (1977) Characteristics of a human cell line transformed by DNA from human adenovirus type 5. *J Gen Virol* 36: 59-74.
93. Guiramand J, Mayat E, Bartolami S, Lenoir M, Rumigny JF, Pujol R, Recasens M (1990) A M3 muscarinic receptor coupled to inositol phosphate formation in the rat cochlea? *Biochem Pharmacol* 39: 1913-1919.

94. Guizzetti M, Costa LG (2000) Possible role of protein kinase C zeta in muscarinic receptor-induced proliferation of astrocytoma cells. *Biochem Pharmacol* 60: 1457-1466.
95. Gustavsson L, Lundqvist C, Hansson E (1993) Receptor-mediated phospholipase D activity in primary astroglial cultures. *GLIA* 8: 249-255.
96. Guth PS, Dunn A, Kronomer K, Norris CH (1994) The cholinergic pharmacology of the frog saccule. *Hear Res* 75: 225-232.
97. Guth PS, Norris CH (1996) The hair cell acetylcholine receptors: a synthesis. *Hear Res* 98: 1-8.
98. Guth PS, Norris CH, Guth SL, Quine DB, Williams WH (1986) Cholinomimetics mimic efferent effects on semicircular canal afferent activity in the frog. *Acta Otolaryngol* 102: 194-203.
99. Guth PS, Perin P, Norris CH, Valli P (1998) The vestibular hair cells: post-transductional signal processing. *Prog Neurobiol* 54: 193-247.
100. Hajos N, Papp EC, Acsady L, Levey AI, Freund TF (1998) Distinct interneuron types express m2 muscarinic receptor immunoreactivity on their dendrites or axon terminals in the hippocampus. *Neuroscience* 82: 355-376.
101. Hakak Y, Shrestha D, Goegel MC, Behan DP, Chalmers DT (2003) Global analysis of G-protein-coupled receptor signaling in human tissues. *FEBS Lett* 550: 11-17.
102. Hamilton SE, Nathanson NM (2001) The M1 receptor is required for muscarinic activation of mitogen-activated protein (MAP) kinase in murine cerebral cortical neurons. *J Biol Chem* 276: 15850-15853.
103. Hartmann R, Klinke R (1980) Efferent activity in the goldfish vestibular nerve and its influence on afferent activity. *Pflugers Arch* 388: 123-128.
104. Hashimoto S, Tanaka C, Taniyama K (1986) Presynaptic muscarinic and alpha-adrenoceptor-mediated regulation of GABA release from myenteric neurones of the guinea-pig small intestine. *Br J Pharmacol* 89: 787-792.
105. Hasson T, Gillespie PG, Garcia JA, MacDonald RB, Zhao Y, Yee AG, Mooseker MS, Corey DP (1997) Unconventional myosins in inner-ear sensory epithelia. *J Cell Biol* 137: 1287-1307.

106. Haynes LW (1983) Neuronal and glial localization of acetylcholinesterase and GABA transaminase in organized cultures of developing rat spinal cord. *Experientia* 39: 223-225.
107. He XJ, Wu XZ, Wellner RB, Baum BJ (1989) Muscarinic receptor regulation of Ca<sup>2+</sup> mobilization in a human salivary cell line. *Pflugers Arch* 413: 505-510.
108. He Y, Xiao J, Yang Y, Zhou Q, Zhang Z, Pan Q, Liu Y, Chen Y (2006) Stretch-induced alterations of human Kir2.1 channel currents. *Biochem Biophys Res Commun* 351: 462-467.
109. Heidbuchel H, Callewaert G, Vereecke J, Carmeliet E (1990) ATP-dependent activation of atrial muscarinic K<sup>+</sup> channels in the absence of agonist and G-nucleotides. *Pflugers Arch* 416: 213-215.
110. Heidbuchel H, Callewaert G, Vereecke J, Carmeliet E (1993) Acetylcholine-mediated K<sup>+</sup> channel activity in guinea-pig atrial cells is supported by nucleoside diphosphate kinase. *Pflugers Arch* 422: 316-324.
111. Heinzel SS, Krysan PJ, Calos MP, DuBridge RB (1988) Use of simian virus 40 replication to amplify Epstein-Barr virus shuttle vectors in human cells. *J Virol* 62: 3738-3746.
112. Henry P, Pearson WL, Nichols CG (1996) Protein kinase C inhibition of cloned inward rectifier (HRK1/KIR2.3) K<sup>+</sup> channels expressed in *Xenopus* oocytes. *J Physiol* 495 ( Pt 3): 681-688.
113. Hilding D, Wersall J (1962) Cholinesterase and its relation to the nerve endings in the inner ear. *Acta Otolaryngol* 55: 205-217.
114. Hille B (2001) Potassium Channels and Chloride Channels. In: *Ion Channels of Excitable Membranes* pp 149-154. Sunderland, MA: Sinauer Associates, Inc.
115. Hirono M, Denis CS, Richardson GP, Gillespie PG (2004) Hair cells require phosphatidylinositol 4,5-bisphosphate for mechanical transduction and adaptation. *Neuron* 44: 309-320.
116. Hofer D, Ness W, Drenckhahn D (1997) Sorting of actin isoforms in chicken auditory hair cells. *J Cell Sci* 110: 765-770.
117. Holt JC, Lioudyno M, Athas G, Garcia MM, Perin P, Guth PS (2001) The effect of proteolytic enzymes on the alpha9-nicotinic receptor-mediated response in isolated frog vestibular hair cells. *Hear Res* 152: 25-42.



118. Holt JC, Lioudyno M, Guth PS (2003) A pharmacologically distinct nicotinic ACh receptor is found in a subset of frog semicircular canal hair cells. *J Neurophysiol* 90: 1526-1536.
119. Holt JR, Eatock RA (1995) Inwardly rectifying currents of saccular hair cells from the leopard frog. *J Neurophysiol* 73: 1484-1502.
120. Horowitz LF, Hirdes W, Suh BC, Hilgemann DW, Mackie K, Hille B (2005) Phospholipase C in living cells: activation, inhibition, Ca<sup>2+</sup> requirement, and regulation of M current. *J Gen Physiol* 126: 243-262.
121. Hosey MM, Benovic JL, DeBurman SK, Richardson RM (1995) Multiple mechanisms involving protein phosphorylation are linked to desensitization of muscarinic receptors. *Life Sci* 56: 951-955.
122. Housley GD, Norris CH, Guth PS (1990) Cholinergically-induced changes in outward currents in hair cells isolated from the semicircular canal of the frog. *Hear Res* 43: 121-133.
123. Hsu KS, Yang CH, Huang CC, Gean PW (1996) Carbachol induces inward current in neostriatal neurons through M1-like muscarinic receptors. *Neuroscience* 73: 751-760.
124. Huang CL, Slesinger PA, Casey PJ, Jan YN, Jan LY (1995) Evidence that direct binding of G beta gamma to the GIRK1 G protein-gated inwardly rectifying K<sup>+</sup> channel is important for channel activation. *Neuron* 15: 1133-1143.
125. Hudspeth AJ (1989) How the ear's works work. *Nature* 341: 397-404.
126. Hudspeth AJ, Jacobs R (1979) Stereocilia mediate transduction in vertebrate hair cells (auditory system/cilium/vestibular system). *Proc Natl Acad Sci U S A* 76: 1506-1509.
127. Hudspeth AJ, Lewis RS (1988a) A model for electrical resonance and frequency tuning in saccular hair cells of the bull-frog, *Rana catesbeiana*. *J Physiol* 400: 275-297.
128. Hudspeth AJ, Lewis RS (1988b) Kinetic analysis of voltage- and ion-dependent conductances in saccular hair cells of the bull-frog, *Rana catesbeiana*. *J Physiol (Lond)* 400: 237-274.

129. Hulme EC, Spalding TA, Curtis CA, Birdsall NJ, Corrie JE (1990) Blockade of muscarinic receptors by alkylating agonist analogues. *Biochem Soc Trans* 18: 440-441.
130. Hurley KM, Gaboyard S, Zhong M, Price SD, Woollorton JR, Lysakowski A, Eatock RA (2006) M-like K<sup>+</sup> currents in type I hair cells and calyx afferent endings of the developing rat utricle. *J Neurosci* 26: 10253-10269.
131. Ikeda K, Ishigaki M, Wu D, Sunose H, Suzuki M, Ishitani K, Takasaka T (1995) Intracellular Ca<sup>2+</sup> responses induced by acetylcholine in the submucosal nasal gland acinar cells in guinea pigs. *Am J Physiol* 268: L361-L367.
132. Inanobe A, Morishige KI, Takahashi N, Ito H, Yamada M, Takumi T, Nishina H, Takahashi K, Kanaho Y, Katada T, . (1995) G beta gamma directly binds to the carboxyl terminus of the G protein-gated muscarinic K<sup>+</sup> channel, GIRK1. *Biochem Biophys Res Commun* 212: 1022-1028.
133. Ishiyama A, Lopez I, Wackym PA (1994) Choline acetyltransferase immunoreactivity in the human vestibular end-organs. *Cell Biology International* 18: 979-984.
134. Ishiyama A, Lopez I, Wackym PA (1997) Molecular characterization of muscarinic receptors in the human vestibular periphery. Implications for pharmacotherapy. *Am J Otol* 18: 648-654.
135. Iurato S, Luciano L, Pannese E, Reale E (1971) Acetylcholinesterase activity in the vestibular sensory areas. *Acta Otolaryngol* 71: 147-152.
136. Iurato S, Luciano L, Pannese E, Reale E (1972) Efferent vestibular fibers in mammals: morphological and histochemical aspects. *Prog Brain Res* 37: 429-443.
137. Jagger DJ, Ashmore JF (1999) The fast activating potassium current, I(K,f), in guinea-pig inner hair cells is regulated by protein kinase A. *Neurosci Lett* 263: 145-148.
138. Jagger DJ, Housley GD (2002) A-type potassium currents dominate repolarisation of neonatal rat primary auditory neurones in situ. *Neuroscience* 109: 169-182.
139. Jeong SW, Wurster RD (1997) Muscarinic receptor activation modulates Ca<sup>2+</sup> channels in rat intracardiac neurons via a PTX- and voltage-sensitive pathway. *J Neurophysiol* 78: 1476-1490.

140. Jiang B, Sun X, Cao K, Wang R (2002) Endogenous Kv channels in human embryonic kidney (HEK-293) cells. *Mol Cell Biochem* 238: 69-79.
141. Johansson S, Druzin M, Haage D, Wang MD (2001) The functional role of a bicuculline-sensitive Ca<sup>2+</sup>-activated K<sup>+</sup> current in rat medial preoptic neurons. *J Physiol* 532: 625-635.
142. Jones SV (1992) m4 muscarinic receptor subtype activates an inwardly rectifying potassium conductance in AtT20 cells. *Neurosci Lett* 147: 125-130.
143. Jones SV (1993) Muscarinic receptor subtypes: modulation of ion channels. *Life Sci* 52: 457-464.
144. Jones SV (1996) Modulation of the inwardly rectifying potassium channel IRK1 by the m1 muscarinic receptor. *Mol Pharmacol* 49: 662-667.
145. Jones SV (1997) Dual modulation of an inwardly rectifying potassium conductance. *Neuropharmacology* 36: 209-215.
146. Jones SV (2003) Role of the small GTPase Rho in modulation of the inwardly rectifying potassium channel Kir2.1. *Mol Pharmacol* 64: 987-993.
147. Jones SV, Choi OH, Beaven MA (1991a) Carbachol induces secretion in a mast cell line (RBL-2H3) transfected with the m1 muscarinic receptor gene. *FEBS Lett* 289: 47-50.
148. Jones SV, Heilman CJ, Brann MR (1991b) Functional responses of cloned muscarinic receptors expressed in CHO-K1 cells. *Mol Pharmacol* 40: 242-247.
149. Jorgensen JM, Anderson T (1973) On the structure of the avian macula. *Acta Zool* 54: 121-134.
150. Jumblatt JE, North GT, Hackmiller RC (1990) Muscarinic cholinergic inhibition of adenylate cyclase in the rabbit iris-ciliary body and ciliary epithelium. *Invest Ophthalmol Vis Sci* 31: 1103-1108.
151. Jurkiewicz NK, Sanguinetti MC (1993) Rate-dependent prolongation of cardiac action potentials by a methanesulfonanilide class III antiarrhythmic agent. Specific block of rapidly activating delayed rectifier K<sup>+</sup> current by dofetilide. *Circ Res* 72: 75-83.

152. Kamouchi M, Van Den BK, Eggermont J, Droogmans G, Nilius B (1997) Modulation of inwardly rectifying potassium channels in cultured bovine pulmonary artery endothelial cells. *J Physiol* 504 ( Pt 3): 545-556.
153. Kanno H, Horikawa Y, Hodges RR, Zoukhri D, Shatos MA, Rios JD, Dartt DA (2003) Cholinergic agonists transactivate EGFR and stimulate MAPK to induce goblet cell secretion. *Am J Physiol Cell Physiol* 284: C988-C998.
154. Kashihara K, Varga EV, Waite SL, Roeske WR, Yamamura HI (1992) Cloning of the rat M3, M4 and M5 muscarinic acetylcholine receptor genes by the polymerase chain reaction (PCR) and the pharmacological characterization of the expressed genes. *Life Sci* 51: 955-971.
155. Kawakami T, Takenaka T, Hori H, Hashimoto Y, Kusakabe T (1995) Effects of acetylcholine and adrenaline on axoplasmic transport at different regions of mouse superior cervical ganglion cells in culture. *Brain Res* 683: 88-92.
156. Kawashima K, Fujii T (2004) Expression of non-neuronal acetylcholine in lymphocytes and its contribution to the regulation of immune function. *Front Biosci* 9: 2063-2085.
157. Kevetter GA, Blumberg KR, Correia MJ (2000) Cellular density and distribution in the normal and regenerating crista ampullaris of the pigeon. *Int J Dev Neurosci* 18: 855-867.
158. Kevetter GA, Correia MJ, Martinez PR (1994) Morphometric studies of type I and type II hair cells in the gerbil's posterior semicircular canal crista. *Journal of Vestibular Research* 4: 429-436.
159. Khan KM, Drescher MJ, Hatfield JS, Drescher DG (1993) Acetylcholinesterase activity is associated with efferent endings in the sensory epithelia of the utricle and semicircular canals of the rainbow trout inner ear. *Anat Rec* 237: 141-147.
160. Khan KM, Drescher MJ, Hatfield JS, Khan AM, Drescher DG (2002) Muscarinic receptor subtypes are differentially distributed in the rat cochlea. *Neuroscience* 111: 291-302.
161. Khan KM, Hatfield JS, Drescher MJ, Drescher DG (1991) The histochemical localization of acetylcholinesterase in the rainbow trout saccular macula by electron microscopy. *Neurosci Lett* 131: 109-112.

162. Kido T, Sekitani T (1994) High-resolution scanning electron microscopic study of cell organelles of the chick's vestibular ganglion. *Eur Arch Otorhinolaryngol* 251: 41-47.
163. Kido T, Sekitani T, Okami K, Endo S, Moriya K (1993) Ultrastructure of the chick vestibular ganglion and vestibular nucleus. A scanning electron microscopic study. *Acta Otolaryngol Suppl* 503: 161-165.
164. Kofuji P, Davidson N, Lester HA (1995) Evidence that neuronal G-protein-gated inwardly rectifying K<sup>+</sup> channels are activated by G beta gamma subunits and function as heteromultimers. *Proc Natl Acad Sci U S A* 92: 6542-6546.
165. Koh DS, Moody MW, Nguyen TD, Hille B (2000) Regulation of exocytosis by protein kinases and Ca(2+) in pancreatic duct epithelial cells. *J Gen Physiol* 116: 507-520.
166. Kohler EC, Messer WS, Jr., Bingman VP (1995) Evidence for muscarinic acetylcholine receptor subtypes in the pigeon telencephalon. *J Comp Neurol* 362: 271-282.
167. Kohler EC, Ritters LV, Chaves L, Bingman VP (1996) The muscarinic acetylcholine antagonist scopolamine impairs short-distance homing pigeon navigation. *Physiol Behav* 60: 1057-1061.
168. Kong WJ, Egg G, Hussl B, Spoendlin H, Schrott-Fischer A (1994) Localization of chat-like immunoreactivity in the vestibular endorgans of the rat. *Hear Res* 75: 191-200.
169. Kong WJ, Guo CK, Zhang S, Hao J, Wang YJ, Li ZW (2005) The properties of ACh-induced BK currents in guinea pig type II vestibular hair cells. *Hear Res* 209: 1-9.
170. Konno F, Takayanagi I (1985) Muscarinic acetylcholine receptors in the rabbit ciliary body smooth muscle: spare receptors and threshold phenomenon. *Jpn J Pharmacol* 38: 91-99.
171. Korth M, Kuhlkamp V (1985) Muscarinic receptor-mediated increase of intracellular Na<sup>+</sup>-ion activity and force of contraction. *Pflügers Arch* 403: 266-272.
172. Krapivinsky G, Krapivinsky L, Wickman K, Clapham DE (1995) G beta gamma binds directly to the G protein-gated K<sup>+</sup> channel, IKACH. *J Biol Chem* 270: 29059-29062.

173. Kronman C, Velan B, Gozes Y, Leitner M, Flashner Y, Lazar A, Marcus D, Sery T, Papier Y, Grosfeld H, . (1992) Production and secretion of high levels of recombinant human acetylcholinesterase in cultured cell lines: microheterogeneity of the catalytic subunit. *Gene* 121: 295-304.
174. Kubalak SW, Newman WH, Webb JG (1991) Differential effect of pertussis toxin on adenosine and muscarinic inhibition of cyclic AMP accumulation in canine ventricular myocytes. *J Mol Cell Cardiol* 23: 199-205.
175. Kubo T, Fukuda K, Mikami A, Maeda A, Takahashi H, Mishina M, Haga T, Haga K, Ichiyama A, Kangawa K, . (1986) Cloning, sequencing and expression of complementary DNA encoding the muscarinic acetylcholine receptor. *Nature* 323: 411-416.
176. Kunkel MT, Peralta EG (1995) Identification of domains conferring G protein regulation on inward rectifier potassium channels. *Cell* 83: 443-449.
177. Kurachi Y (1985) Voltage-dependent activation of the inward-rectifier potassium channel in the ventricular cell membrane of guinea-pig heart. *J Physiol* 366: 365-385.
178. Kuwahara A, Tien XY, Wallace LJ, Cooke HJ (1987) Cholinergic receptors mediating secretion in guinea pig colon. *J Pharmacol Exp Ther* 242: 600-606.
179. Lamah J, Philip M, Sharma YK, Moro O, Ramachandran J, Sadee W (1992) Hm1 muscarinic cholinergic receptor internalization requires a domain in the third cytoplasmic loop. *J Biol Chem* 267: 13406-13412.
180. Lan CT, Shieh JY, Wen CY, Tan CK, Ling EA (1996) Ultrastructural localization of acetylcholinesterase and choline acetyltransferase in oligodendrocytes, glioblasts and vascular endothelial cells in the external cuneate nucleus of the gerbil. *Anat Embryol (Berl)* 194: 177-185.
181. Landolt JP, Correia MJ, Young ER, Cardin RP, Sweet RC (1975) A scanning electron microscopic study of the morphology and geometry of neural surfaces and structures associated with the vestibular apparatus of the pigeon. *J Comp Neurol* 159: 257-287.
182. Landolt JP, Topliff ED, Silverberg JD (1973) Size distribution analysis of myelinated fibers in the vestibular nerve of the pigeon. *Brain Res* 54: 31-42.

183. Lang DG, Correia MJ (1989) Studies of solitary semicircular canal hair cells in the adult pigeon. II. Voltage-dependent ionic conductances. *J Neurophysiol* 62: 935-945.
184. Lassing I, Lindberg U (1988) Evidence that the phosphatidylinositol cycle is linked to cell motility. *Exp Cell Res* 174: 1-15.
185. Levey AI (1993) Immunological localization of m1-m5 muscarinic acetylcholine receptors in peripheral tissues and brain. *Life Sci* 52: 441-448.
186. Levey AI, Edmunds SM, Koliatsos V, Wiley RG, Heilman CJ (1995) Expression of m1-m4 muscarinic acetylcholine receptor proteins in rat hippocampus and regulation by cholinergic innervation. *J Neurosci* 15: 4077-4092.
187. Lewis RS, Hudspeth AJ (1983) Voltage- and ion-dependent conductances in solitary vertebrate hair cells. *Nature* 304: 538-541.
188. Li GQ, Correia MJ (2005) The inhibitory effect of carbachol on pigeon inwardly rectifying potassium channel pKir expressed in transfected tsA-201 cells and native type II vestibular hair cells. *Neurosci Abstrs (On-Line)* 47.7.
189. Li GQ, Kevetter GA, Leonard RB, Prusak DJ, Wood TG, Correia MJ (2007) Muscarinic acetylcholine receptor subtype expression in avian vestibular hair cells, nerve terminals and ganglion cells. *Neuroscience* 146: 384-402.
190. Li GQ, Leonard GK, Leonard RB, Correia MJ (2005) Muscarinic Receptor Subtype Expression in Avian Vestibular Hair Cells and Nerve Terminals. *FASEB J* 19 (5): A1206.
191. Liles WC, Taylor S, Finnell R, Lai H, Nathanson NM (1986) Decreased muscarinic acetylcholine receptor number in the central nervous system of the tottering (tg/tg) mouse. *J Neurochem* 46: 977-982.
192. Limas CJ, Limas C (1985) Carbachol induces desensitization of cardiac beta-adrenergic receptors through muscarinic M1 receptors. *Biochem Biophys Res Commun* 128: 699-704.
193. Liu J, Evans MS, Lee TJ (2002) Presynaptic muscarinic M(2)-receptor-mediated inhibition of N-type Ca(2+) channels in cultured sphenopalatine ganglion: direct evidence for acetylcholine inhibition of cerebral nitric neurogenic vasodilation. *J Pharmacol Exp Ther* 302: 397-405.

194. Liu Y, Liu D, Heath L, Meyers DM, Krafte DS, Wagoner PK, Silvia CP, Yu W, Curran ME (2001) Direct activation of an inwardly rectifying potassium channel by arachidonic acid. *Mol Pharmacol* 59: 1061-1068.
195. Liu Z, Cashion LM, Twu JJ (1997) A systematic comparison of relative promoter/enhancer activities in mammalian cell lines. *Anal Biochem* 246: 150-152.
196. Logothetis DE, Kurachi Y, Galper J, Neer EJ, Clapham DE (1987) The beta gamma subunits of GTP-binding proteins activate the muscarinic K<sup>+</sup> channel in heart. *Nature* 325: 321-326.
197. Lograno MD, Reibaldi A (1986) Receptor-responses in fresh human ciliary muscle. *Br J Pharmacol* 87: 379-385.
198. Lopez I, Meza G (1988) Neurochemical evidence for afferent GABAergic and efferent cholinergic neurotransmission in the frog vestibule. *Neuroscience* 25: 13-18.
199. Luo J, Busillo JM, Benovic JL (2008) M3 muscarinic acetylcholine receptor-mediated signaling is regulated by distinct mechanisms. *Mol Pharmacol* 74: 338-347.
200. Lustig LR, Peng H, Hiel H, Yamamoto T, Fuchs PA (2001) Molecular cloning and mapping of the human nicotinic acetylcholine receptor alpha10 (CHRNA10). *Genomics* 73: 272-283.
201. Lysakowski A (1996) Synaptic organization of the crista ampullaris in vertebrates. *Ann N Y Acad Sci* 781: 164-182.
202. Marchi M, Bocchieri P, Garbarino L, Raiteri M (1989) Muscarinic inhibition of endogenous glutamate release from rat hippocampus synaptosomes. *Neurosci Lett* 96: 229-234.
203. Margolskee RF, McHendry-Rinde B, Horn R (1993) Panning transfected cells for electrophysiological studies. *Biotechniques* 15: 906-911.
204. Martin P, Hudspeth AJ (1999) Active hair-bundle movements can amplify a hair cell's response to oscillatory mechanical stimuli. *Proc Natl Acad Sci U S A* 96: 14306-14311.



205. Masetto S, Correia MJ (1997a) Electrophysiological properties of vestibular sensory and supporting cells in the labyrinth slice: Before and during regeneration. *J Neurophysiol* 78: 1913-1927.
206. Masetto S, Correia MJ (1997b) Ionic currents in regenerating avian vestibular hair cells. *International Journal of Developmental Neuroscience* 15: 387-399.
207. Masetto S, Russo G, Prigioni I (1994) Differential expression of potassium currents by hair cells in thin slices of frog crista ampullaris. *J Neurophysiol* 72: 443-455.
208. Masetto S, Russo G, Prigioni I (1996) Regional distribution of hair cell ionic currents in frog vestibular epithelium. *Annals of the New York Academy of Sciences* 19;781: 663-665.
209. Matsui M, Motomura D, Karasawa H, Fujikawa T, Jiang J, Komiya Y, Takahashi S, Taketo MM (2000) Multiple functional defects in peripheral autonomic organs in mice lacking muscarinic acetylcholine receptor gene for the M3 subtype. *Proc Natl Acad Sci U S A* 97: 9579-9584.
210. Maughan DW (1976) Potassium movement during hyperpolarization of cardiac muscle. *J Membr Biol* 28: 241-262.
211. Miake J, Marban E, Nuss HB (2003) Functional role of inward rectifier current in heart probed by Kir2.1 overexpression and dominant-negative suppression. *J Clin Invest* 111: 1529-1536.
212. Miyakawa T, Yamada M, Duttaroy A, Wess J (2001) Hyperactivity and intact hippocampus-dependent learning in mice lacking the M1 muscarinic acetylcholine receptor. *J Neurosci* 21: 5239-5250.
213. Mooseker MS, Pollard TD, Fujiwara K (1978) Characterization and localization of myosin in the brush border of intestinal epithelial cells. *J Cell Biol* 79: 444-453.
214. Mooseker MS, Tilney LG (1975) Organization of an actin filament-membrane complex. Filament polarity and membrane attachment in the microvilli of intestinal epithelial cells. *J Cell Biol* 67: 725-743.
215. Moro O, Lamah J, Sadee W (1993) Serine- and threonine-rich domain regulates internalization of muscarinic cholinergic receptors. *J Biol Chem* 268: 6862-6865.

216. Moroi-Fetters SE, Neff NH, Hadjiconstantinou M (1988) Muscarinic receptor-mediated phosphoinositide hydrolysis in the rat retina. *J Pharmacol Exp Ther* 246: 553-557.
217. Murthy KS, Makhoul GM (2000) Heterologous desensitization mediated by G protein-specific binding to caveolin. *J Biol Chem* 275: 30211-30219.
218. Nabekura J, Ebihara S, Akaike N (1993) Muscarinic receptor activation of potassium channels in rat dentate gyrus neurons. *J Neurophysiol* 70: 1544-1552.
219. Nakajo K, Kubo Y (2005) Protein kinase C shifts the voltage dependence of KCNQ/M channels expressed in *Xenopus* oocytes. *J Physiol* 569: 59-74.
220. Nemzou NR, Bulankina AV, Khimich D, Giese A, Moser T (2006) Synaptic organization in cochlear inner hair cells deficient for the CaV1.3 ( $\alpha 1D$ ) subunit of L-type  $Ca^{2+}$  channels. *Neuroscience* 141: 1849-1860.
221. Nenov AP, Norris C, Bobbin RP (1996) Acetylcholine response in guinea pig outer hair cells. II. Activation of a small conductance  $Ca^{2+}$ -activated  $K^{+}$  channel. *Hear Res* 101: 149-172.
222. Nishikawa M, Munakata M, Akaike N (1994) Muscarinic acetylcholine response in pyramidal neurones of rat cerebral cortex. *Br J Pharmacol* 112: 1160-1166.
223. Nomura J, Hosoi T, Okuma Y, Nomura Y (2003) The presence and functions of muscarinic receptors in human T cells: the involvement in IL-2 and IL-2 receptor system. *Life Sci* 72: 2121-2126.
224. Nomura Y, Gacek RR, Balogh K (1965) Efferent innervation of vestibular labyrinth: histochemical demonstration of acetylcholinesterase activity in the guinea pig inner ear. *Arch Otolaryngol* 81: 335-339.
225. Norris CH, Housley GD, Williams WH, Guth SL, Guth PS (1988) The acetylcholine receptors of the semicircular canal in the frog (*Rana pipiens*). *Hear Res* 32: 197-206.
226. Norris CH, Ricci AJ, Housley GD, Guth PS (1992) The inactivating potassium currents of hair cells isolated from the crista ampullaris of the frog. *J Neurophysiol* 68: 1642-1653.
227. North RA, Slack BE, Surprenant A (1985) Muscarinic M1 and M2 receptors mediate depolarization and presynaptic inhibition in guinea-pig enteric nervous system. *J Physiol* 368: 435-452.

228. O'Rourke ST, Vanhoutte PM (1987) Subtypes of muscarinic receptors on adrenergic nerves and vascular smooth muscle of the canine saphenous vein. *J Pharmacol Exp Ther* 241: 64-67.
229. Ohmori H (1978) Inactivation kinetics and steady-state current noise in the anomalous rectifier of tunicate egg cell membranes. *J Physiol* 281: 77-99.
230. Ohmori H (1984) Studies of ionic currents in the isolated vestibular hair cell of the chick. *J Physiol* 350: 561-581.
231. Ohmori H (1990) Mechano-electrical transduction and muscarinic cholinergic responses in the chick hair cell. *Neuroscience Research - Supplement* 12: S51-S62.
232. Ohtani M, Devau G, Lehouelleur J, Sans A (1994) Cholinergic agonists increase intracellular calcium concentration in frog vestibular hair cells. *Hear Res* 80: 167-173.
233. Ona A (1993) The mammalian vestibular ganglion cells and the myelin sheath surrounding them. *Acta Otolaryngol Suppl* 503: 143-149.
234. Park WS, Han J, Earm YE (2008) Physiological role of inward rectifier K(+) channels in vascular smooth muscle cells. *Pflugers Arch*.
235. Pattillo JM, Yazejian B, DiGregorio DA, Vergara JL, Grinnell AD, Meriney SD (2001) Contribution of presynaptic calcium-activated potassium currents to transmitter release regulation in cultured *Xenopus* nerve-muscle synapses. *Neuroscience* 102: 229-240.
236. Pemberton KE, Jones SV (1995) Enhancement of an L-type calcium current in AtT-20 cells; a novel effect of the m4 muscarinic receptor. *Pflugers Arch* 429: 699-707.
237. Pemberton KE, Jones SV (1997) Inhibition of the L-type calcium channel by the five muscarinic receptors (m1-m5) expressed in NIH 3T3 cells. *Pflugers Arch* 433: 505-514.
238. Peralta EG, Ashkenazi A, Winslow JW, Smith DH, Ramachandran J, Capon DJ (1987a) Distinct primary structures, ligand-binding properties and tissue-specific expression of four human muscarinic acetylcholine receptors. *EMBO J* 6: 3923-3929.

239. Peralta EG, Winslow JW, Peterson GL, Smith DH, Ashkenazi A, Ramachandran J, Schimerlik MI, Capon DJ (1987b) Primary structure and biochemical properties of an M2 muscarinic receptor. *Science* 236: 600-605.
240. Petersen KR, Nerbonne JM (1999) Expression environment determines K<sup>+</sup> current properties: Kv1 and Kv4 alpha-subunit-induced K<sup>+</sup> currents in mammalian cell lines and cardiac myocytes. *Pflugers Arch* 437: 381-392.
241. Plaster NM, Tawil R, Tristani-Firouzi M, Canun S, Bendahhou S, Tsunoda A, Donaldson MR, Iannaccone ST, Brunt E, Barohn R, Clark J, Deymeer F, George AL, Jr., Fish FA, Hahn A, Nitu A, Ozdemir C, Serdaroglu P, Subramony SH, Wolfe G, Fu YH, Ptacek LJ (2001) Mutations in Kir2.1 cause the developmental and episodic electrical phenotypes of Andersen's syndrome. *Cell* 105: 511-519.
242. Pochet S, Metioui M, Grosfils K, Gomez-Munoz A, Marino A, Dehaye JP (2003) Regulation of phospholipase D by muscarinic receptors in rat submandibular ductal cells. *Cell Signal* 15: 103-113.
243. Prestwich SA, Bolton TB (1995) G-protein involvement in muscarinic receptor-stimulation of inositol phosphates in longitudinal smooth muscle from the small intestine of the guinea-pig. *Br J Pharmacol* 114: 119-126.
244. Raiteri M, Marchi M, Costi A, Volpe G (1990) Endogenous aspartate release in the rat hippocampus is inhibited by M2 'cardiac' muscarinic receptors. *Eur J Pharmacol* 177: 181-187.
245. Ramanathan K, Michael TH, Jiang GJ, Hiel H, Fuchs PA (1999) A molecular mechanism for electrical tuning of cochlear hair cells. *Science* 283: 215-217.
246. Rennie KJ, Correia MJ (1994) Potassium currents in mammalian and avian isolated type I semicircular canal hair cells. *J Neurophysiol* 71: 317-329.
247. Rennie KJ, Correia MJ (2000) Effects of cationic substitutions on delayed rectifier current in type I vestibular hair cells. *J Membr Biol* 173: 139-148.
248. Rennie KJ, Weng T, Correia MJ (2001) Effects of KCNQ channel blockers on K(+) currents in vestibular hair cells. *Am J Physiol Cell Physiol* 280: C473-C480.
249. Reuveny E, Jan YN, Jan LY (1996) Contributions of a negatively charged residue in the hydrophobic domain of the IRK1 inwardly rectifying K<sup>+</sup> channel to K(+)-selective permeation. *Biophys J* 70: 754-761.

250. Reuveny E, Slesinger PA, Inglese J, Morales JM, Iniguez-Lluhi JA, Lefkowitz RJ, Bourne HR, Jan YN, Jan LY (1994) Activation of the cloned muscarinic potassium channel by G protein beta gamma subunits. *Nature* 370: 143-146.
251. Ricci A, Rennie KJ, Cochran SL, Kevetter GA, Correia MJ (1997) Vestibular type I and type II hair cells. 1: Morphometric identification in the pigeon and the gerbil. *J Vestib Res* 7: 393-406.
252. Ricci AJ, Rennie KJ, Correia MJ (1996a) A delayed rectifier conductance shapes the voltage response of type I hair cells. *Ann N Y Acad Sci* 19;781: 690-692.
253. Ricci AJ, Rennie KJ, Correia MJ (1996b) The delayed rectifier, IK1, is the major conductance in type I vestibular hair cells across vestibular end organs. *Pflugers Arch* 432: 34-42.
254. Rimmaudo LE, de la TE, Sacerdote dL, Sales ME (2005) Muscarinic receptors are involved in LMM3 tumor cells proliferation and angiogenesis. *Biochem Biophys Res Commun* 334: 1359-1364.
255. Rio DC, Clark SG, Tjian R (1985) A mammalian host-vector system that regulates expression and amplification of transfected genes by temperature induction. *Science* 227: 23-28.
256. Roberts WM (1994) Localization of calcium signals by a mobile calcium buffer in frog saccular hair cells. *Journal of Neuroscience* 14: 3246-3262.
257. Rossi ML, Prigioni I, Valli P, Casella C (1980) Activation of the efferent system in the isolated frog labyrinth: effects on the afferent EPSPs and spike discharge recorded from single fibres of the posterior nerve. *Brain Res* 185: 125-137.
258. Rouse ST, Levey AI (1996) Expression of m1-m4 muscarinic acetylcholine receptor immunoreactivity in septohippocampal neurons and other identified hippocampal afferents. *J Comp Neurol* 375: 406-416.
259. Rouse ST, Levey AI (1997) Muscarinic acetylcholine receptor immunoreactivity after hippocampal commissural/associational pathway lesions: evidence for multiple presynaptic receptor subtypes. *J Comp Neurol* 380: 382-394.
260. Sah P, McLachlan EM (1992) Potassium currents contributing to action potential repolarization and the afterhyperpolarization in rat vagal motoneurons. *J Neurophysiol* 68: 1834-1841.

261. Salathe M, Bookman RJ (1995) Coupling of  $[Ca^{2+}]_i$  and ciliary beating in cultured tracheal epithelial cells. *J Cell Sci* 108 ( Pt 2): 431-440.
262. Samandari F, Bogusch G (1981) [Medullated ganglion cells in the guinea pig labyrinth]. *Acta Anat (Basel)* 109: 149-156.
263. Sandmann J, Peralta EG, Wurtman RJ (1991) Coupling of transfected muscarinic acetylcholine receptor subtypes to phospholipase D. *J Biol Chem* 266: 6031-6034.
264. Scarfone E, Dememes D, Perrin D, Aunis D, Sans A (1988) Alpha-fodrin (brain spectrin) immunocytochemical localization in rat vestibular hair cells. *Neurosci Lett* 93: 13-18.
265. Schacht J., Zenner H.P. (1986) The Phosphoinositide cascade in isolated outer hair cells: possible role as second messenger for motile responses. *Hear Res* 22: 94.
266. Schacht J, Zenner HP (1987) Evidence that phosphoinositides mediate motility in cochlear outer hair cells. *Hear Res* 31: 155-159.
267. Schmidt M, Fasselt B, Rumenapp U, Bienek C, Wieland T, van Koppen CJ, Jakobs KH (1995) Rapid and persistent desensitization of m3 muscarinic acetylcholine receptor-stimulated phospholipase D. Concomitant sensitization of phospholipase C. *J Biol Chem* 270: 19949-19956.
268. Schreibmayer W, Dessauer CW, Vorobiov D, Gilman AG, Lester HA, Davidson N, Dascal N (1996) Inhibition of an inwardly rectifying  $K^+$  channel by G-protein alpha-subunits. *Nature* 380: 624-627.
269. Schwarz IE, Schwarz DW, Fredrickson JM, Landolt JP (1981) Efferent vestibular neurons: a study employing retrograde tracer methods in the pigeon (*Columba livia*). *J Comp Neurol* 196: 1-12.
270. Schwindt PC, Spain WJ, Foehring RC, Stafstrom CE, Chubb MC, Crill WE (1988) Multiple potassium conductances and their functions in neurons from cat sensorimotor cortex in vitro. *J Neurophysiol* 59: 424-449.
271. Selyanko AA, Hadley JK, Wood IC, Abogadie FC, Jentsch TJ, Brown DA (2000) Inhibition of KCNQ1-4 potassium channels expressed in mammalian cells via M1 muscarinic acetylcholine receptors. *J Physiol* 522 Pt 3: 349-355.

272. Shapiro RA, Scherer NM, Habecker BA, Subers EM, Nathanson NM (1988) Isolation, sequence, and functional expression of the mouse M1 muscarinic acetylcholine receptor gene. *J Biol Chem* 263: 18397-18403.
273. Shen W, Hamilton SE, Nathanson NM, Surmeier DJ (2005) Cholinergic suppression of KCNQ channel currents enhances excitability of striatal medium spiny neurons. *J Neurosci* 25: 7449-7458.
274. Shepherd GM, Barres BA, Corey DP (1989) "Bundle blot" purification and initial protein characterization of hair cell stereocilia. *Proceedings of the National Academy of Sciences of the United States of America* 86: 4973-4977.
275. Sheridan RD, Sutor B (1990) Presynaptic M1 muscarinic cholinceptors mediate inhibition of excitatory synaptic transmission in the hippocampus in vitro. *Neurosci Lett* 108: 273-278.
276. Shieh RC (2000) Mechanisms for the time-dependent decay of inward currents through cloned Kir2.1 channels expressed in *Xenopus* oocytes. *J Physiol* 526 Pt 2: 241-252.
277. Shieh RC, Lee YL (2001) Ammonium ions induce inactivation of Kir2.1 potassium channels expressed in *Xenopus* oocytes. *J Physiol* 535: 359-370.
278. Shigemoto T, Ohmori H (1990) Muscarinic agonists and ATP increase the intracellular Ca<sup>2+</sup> concentration in chick cochlear hair cells. *J Physiol* 420: 127-148.
279. Shigemoto T, Ohmori H (1991) Muscarinic receptor hyperpolarizes cochlear hair cells of chick by activating Ca(2+)-activated K<sup>+</sup> channels. *J Physiol* 442: 669-690.
280. Skinner LJ, Enee V, Beurg M, Jung HH, Ryan AF, Hafidi A, Aran JM, Dulon D (2003) Contribution of BK Ca<sup>2+</sup>-activated K<sup>+</sup> channels to auditory neurotransmission in the Guinea pig cochlea. *J Neurophysiol* 90: 320-332.
281. Slepecky N, Chamberlain SC (1985) Immunoelectron microscopic and immunofluorescent localization of cytoskeletal and muscle-like contractile proteins in inner ear sensory hair cells. *Hear Res* 20: 245-260.
282. Small DH, Reed G, Whitefield B, Nurcombe V (1995) Cholinergic regulation of neurite outgrowth from isolated chick sympathetic neurons in culture. *J Neurosci* 15: 144-151.

283. Sobin A, Flock A (1983) Immunohistochemical identification and localization of actin and fimbrin in vestibular hair cells in the normal guinea pig and in a strain of the waltzing guinea pig. *Acta Otolaryngol* 96: 407-412.
284. Sobko A, Peretz A, Shirihai O, Etkin S, Cherepanova V, Dagan D, Attali B (1998) Heteromultimeric delayed-rectifier K<sup>+</sup> channels in schwann cells: developmental expression and role in cell proliferation. *J Neurosci* 18: 10398-10408.
285. Soneoka Y, Cannon PM, Ramsdale EE, Griffiths JC, Romano G, Kingsman SM, Kingsman AJ (1995) A transient three-plasmid expression system for the production of high titer retroviral vectors. *Nucleic Acids Res* 23: 628-633.
286. Standen NB, Stanfield PR (1979) Potassium depletion and sodium block of potassium currents under hyperpolarization in frog sartorius muscle. *J Physiol* 294: 497-520.
287. Standen NB, Stanfield PR (1980) Rubidium block and rubidium permeability of the inward rectifier of frog skeletal muscle fibres. *J Physiol* 304: 415-435.
288. Stanfield PR, Nakajima S, Nakajima Y (2002a) Constitutively active and G-protein coupled inward rectifier K<sup>+</sup> channels: Kir2.0 and Kir3.0. *Rev Physiol Biochem Pharmacol* 145: 47-179.
289. Stanfield PR, Nakajima S, Nakajima Y (2002b) Constitutively active and G-protein coupled inward rectifier K<sup>+</sup> channels: Kir2.0 and Kir3.0. *Rev Physiol Biochem Pharmacol* 145: 47-179.
290. Steinacker A, Rojas L (1988) Acetylcholine modulated potassium channel in the hair cell of the toadfish saccule. *Hear Res* 35: 265-269.
291. Stengel PW, Gomeza J, Wess J, Cohen ML (2000) M(2) and M(4) receptor knockout mice: muscarinic receptor function in cardiac and smooth muscle in vitro. *J Pharmacol Exp Ther* 292: 877-885.
292. Sugai T, Yano J, Sugitani M, Ooyama H (1992) Actions of cholinergic agonists and antagonists on the efferent synapse in the frog sacculus. *Hear Res* 61: 56-64.
293. Sugihara I (1994) Calcium-activated potassium channels in goldfish hair cells. *J Physiol* 476: 373-390.
294. Suh BC, Hille B (2006) Does diacylglycerol regulate KCNQ channels? *Pflugers Arch* 453: 293-301.



295. Suh BC, Hille B (2007) Regulation of KCNQ channels by manipulation of phosphoinositides. *J Physiol* 582: 911-916.
296. Thomas P, Smart TG (2005) HEK293 cell line: a vehicle for the expression of recombinant proteins. *J Pharmacol Toxicol Methods* 51: 187-200.
297. Tietje KM, Goldman PS, Nathanson NM (1990) Cloning and functional analysis of a gene encoding a novel muscarinic acetylcholine receptor expressed in chick heart and brain. *J Biol Chem* 265: 2828-2834.
298. Tilney LG, DeRosier DJ, Mulroy MJ (1980) The organization of actin filaments in the stereocilia of cochlear hair cells. *J Cell Biol* 86: 244-259.
299. Tilney MS, Tilney LG, Stephens RE, Merte C, Drenckhahn D, Cotanche DA, Bretscher A (1989) Preliminary biochemical characterization of the stereocilia and cuticular plate of hair cells of the chick cochlea. *Journal of Cell Biology* 109: 1711-1723.
300. Tokimasa T, Hasuo H, Koketsu K (1981) Desensitization of the muscarinic acetylcholine receptor of atrium in bullfrogs. *Jpn J Physiol* 31: 83-97.
301. Torskaia IV, Goloborod'ko VN (1977) [Acetylcholinesterase in the glial elements of the cat spinal cord]. *Neirofiziologiya* 9: 48-51.
302. Van der Zee EA, Luiten PG (1999) Muscarinic acetylcholine receptors in the hippocampus, neocortex and amygdala: a review of immunocytochemical localization in relation to learning and memory. *Prog Neurobiol* 58: 409-471.
303. Van Koppen CJ, Nathanson NM (1990) Site-directed mutagenesis of the m2 muscarinic acetylcholine receptor. Analysis of the role of N-glycosylation in receptor expression and function. *J Biol Chem* 265: 20887-20892.
304. Varro A, Balati B, Iost N, Takacs J, Virag L, Lathrop DA, Csaba L, Talosi L, Papp JG (2000) The role of the delayed rectifier component IKs in dog ventricular muscle and Purkinje fibre repolarization. *J Physiol* 523 Pt 1: 67-81.
305. Viana F, Bayliss DA, Berger AJ (1993) Multiple potassium conductances and their role in action potential repolarization and repetitive firing behavior of neonatal rat hypoglossal motoneurons. *J Neurophysiol* 69: 2150-2163.
306. Vilaro MT, Palacios JM, Mengod G (1990) Localization of m5 muscarinic receptor mRNA in rat brain examined by in situ hybridization histochemistry. *Neurosci Lett* 114: 154-159.

307. Wackym PA, Chen CT, Ishiyama A, Pettis RM, Lopez IA, Hoffman L (1996) Muscarinic acetylcholine receptor subtype mRNAs in the human and rat vestibular periphery. *Cell Biol Int* 20: 187-192.
308. Wackym PA, Popper P, Lopez I, Ishiyama A, Micevych PE (1995) Expression of alpha 4 and beta 2 nicotinic acetylcholine receptor subunit mRNA and localization of alpha-bungarotoxin binding proteins in the rat vestibular periphery. *Cell Biol Int* 19: 291-300.
309. Wackym PA, Popper P, Ward PH, Micevych PE (1991) Cell and molecular anatomy of nicotinic acetylcholine receptor subunits and calcitonin gene-related peptide in the rat vestibular system. *Otolaryngol Head Neck Surg* 105: 493-510.
310. Wang H, Shi H, Lu Y, Yang B, Wang Z (1999) Pilocarpine modulates the cellular electrical properties of mammalian hearts by activating a cardiac M3 receptor and a K<sup>+</sup> current. *Br J Pharmacol* 126: 1725-1734.
311. Wangemann P, Liu J, Scherer EQ, Herzog M, Shimosono M, Scofield MA (2001) Muscarinic receptors control K<sup>+</sup> secretion in inner ear strial marginal cells. *J Membr Biol* 182: 171-181.
312. Wei AD, Butler A, Salkoff L (2005) KCNQ-like potassium channels in *Caenorhabditis elegans*. Conserved properties and modulation. *J Biol Chem* 280: 21337-21345.
313. Weiner DM, Levey AI, Brann MR (1990) Expression of muscarinic acetylcholine and dopamine receptor mRNAs in rat basal ganglia. *Proc Natl Acad Sci U S A* 87: 7050-7054.
314. Weng T, Correia MJ (1999) Regional distribution of ionic currents and membrane voltage responses of type II hair cells in the vestibular neuroepithelium. *J Neurophysiol* 82: 2451-2461.
315. Wersall J (1956) Studies on the structure and innervation of the sensory epithelium of the cristae ampullares in the guinea pig; a light and electron microscopic investigation. *Acta Otolaryngol Suppl* 126: 1-85.
316. Wess J (1996) Molecular biology of muscarinic acetylcholine receptors. *Crit Rev Neurobiol* 10: 69-99.
317. Wess J, Duttaroy A, Gomeza J, Zhang W, Yamada M, Felder CC, Bernardini N, Reeh PW (2003a) Muscarinic receptor subtypes mediating central and peripheral

antinociception studied with muscarinic receptor knockout mice: a review. *Life Sci* 72: 2047-2054.

318. Wess J, Duttaroy A, Zhang W, Gomeza J, Cui Y, Miyakawa T, Bymaster FP, McKinzie L, Felder CC, Lamping KG, Faraci FM, Deng C, Yamada M (2003b) M1-M5 muscarinic receptor knockout mice as novel tools to study the physiological roles of the muscarinic cholinergic system. *Receptors Channels* 9: 279-290.
319. Wess J, Liu J, Blin N, Yun J, Lerche C, Kostenis E (1997) Structural basis of receptor/G protein coupling selectivity studied with muscarinic receptors as model systems. *Life Sci* 60: 1007-1014.
320. Wessler I, Kirkpatrick CJ, Racke K (1998) Non-neuronal acetylcholine, a locally acting molecule, widely distributed in biological systems: expression and function in humans. *Pharmacol Ther* 77: 59-79.
321. Wilson GF, Chiu SY (1990) Potassium channel regulation in Schwann cells during early developmental myelinogenesis. *J Neurosci* 10: 1615-1625.
322. Wischmeyer E, Doring F, Karschin A (1998) Acute suppression of inwardly rectifying Kir2.1 channels by direct tyrosine kinase phosphorylation. *J Biol Chem* 273: 34063-34068.
323. Wotta DR, Wattenberg EV, Langason RB, El Fakahany EE (1998) M1, M3 and M5 muscarinic receptors stimulate mitogen-activated protein kinase. *Pharmacology* 56: 175-186.
324. Wu BN, Luykenaar KD, Brayden JE, Giles WR, Corteling RL, Wiehler WB, Welsh DG (2007) Hyposmotic challenge inhibits inward rectifying K<sup>+</sup> channels in cerebral arterial smooth muscle cells. *Am J Physiol Heart Circ Physiol* 292: H1085-H1094.
325. Yamada M, Basile AS, Fedorova I, Zhang W, Duttaroy A, Cui Y, Lamping KG, Faraci FM, Deng CX, Wess J (2003) Novel insights into M5 muscarinic acetylcholine receptor function by the use of gene targeting technology. *Life Sci* 74: 345-353.
326. Yamada M, Lamping KG, Duttaroy A, Zhang W, Cui Y, Bymaster FP, McKinzie DL, Felder CC, Deng CX, Faraci FM, Wess J (2001a) Cholinergic dilation of cerebral blood vessels is abolished in M(5) muscarinic acetylcholine receptor knockout mice. *Proc Natl Acad Sci U S A* 98: 14096-14101.

327. Yamada M, Miyakawa T, Duttaroy A, Yamanaka A, Moriguchi T, Makita R, Ogawa M, Chou CJ, Xia B, Crawley JN, Felder CC, Deng CX, Wess J (2001b) Mice lacking the M3 muscarinic acetylcholine receptor are hypophagic and lean. *Nature* 410: 207-212.
328. Yang B, McCaffrey TV (1996) The roles of muscarinic receptor subtypes in modulation of nasal ciliary action. *Rhinology* 34: 136-139.
329. Yang D, MacCallum DK, Ernst SA, Hughes BA (2003) Expression of the inwardly rectifying K<sup>+</sup> channel Kir2.1 in native bovine corneal endothelial cells. *Invest Ophthalmol Vis Sci* 44: 3511-3519.
330. Yoshida N, Shigemoto T, Sugai T, Ohmori H (1994) The role of inositol trisphosphate on ACh-induced outward currents in bullfrog saccular hair cells. *Brain Research* 644: 90-100.
331. Yu SP, Kerchner GA (1998) Endogenous voltage-gated potassium channels in human embryonic kidney (HEK293) cells. *J Neurosci Res* 52: 612-617.
332. Zagoory O, Braiman A, Gheber L, Priel Z (2001) Role of calcium and calmodulin in ciliary stimulation induced by acetylcholine. *Am J Physiol Cell Physiol* 280: C100-C109.
333. Zenner HP (1988) Motility of outer hair cells as an active, actin-mediated process. *Acta Otolaryngol* 105: 39-44.
334. Zhang H, Craciun LC, Mirshahi T, Rohacs T, Lopes CM, Jin T, Logothetis DE (2003) PIP(2) activates KCNQ channels, and its hydrolysis underlies receptor-mediated inhibition of M currents. *Neuron* 37: 963-975.
335. Zhang Q, Pacheco MA, Doupnik CA (2002a) Gating properties of GIRK channels activated by Galpha(o)- and Galpha(i)-coupled muscarinic m2 receptors in *Xenopus* oocytes: the role of receptor precoupling in RGS modulation. *J Physiol* 545: 355-373.
336. Zhang W, Yamada M, Gomeza J, Basile AS, Wess J (2002b) Multiple muscarinic acetylcholine receptor subtypes modulate striatal dopamine release, as studied with M1-M5 muscarinic receptor knock-out mice. *J Neurosci* 22: 6347-6352.
337. Zhu G, Zhang Y, Xu H, Jiang C (1998) Identification of endogenous outward currents in the human embryonic kidney (HEK 293) cell line. *J Neurosci Methods* 81: 73-83.

338. Zhu Y, Kong WJ, Xia J, Zhang Y, Cheng HM, Guo CK (2008) [Properties of cholinergic receptor-mediated ion channels on type I vestibular hair cells of guinea pigs.]. *Sheng Li Xue Bao* 60: 375-381.

## Vita

NAME: Gang Qiang Li, M.D.

### PRESENT POSITION AND ADDRESS:

Pre-doctoral Fellow (Manning J. Correia Ph.D. mentor)  
Department of Otolaryngology, Neuroscience and Cell Biology  
University of Texas Medical Branch  
301 University Blvd.  
Galveston, TX 77555-1063  
Tel: (409) 772-2721  
E-mail: ganli@utmb.edu

### BIOGRAPHICAL:

Father:	Yongzhao Li
Mother:	Runlan Fang
Wife:	Jian W. Fu
Child:	Juliana W. Li
Date of Birth:	Aug. 28, 1972
Place of Birth:	Peixian, Jiangsu Province, China
Home Address:	710 Ferry RD, #314, Galveston, TX 77550
Tel:	(409) 763-7029

### EDUCATION:

8/2002-present	Neuroscience, Ph.D. Candidate (Manning J. Correia Ph.D. supervisor) Dec. 2008 graduation expected Department of Otolaryngology, Neuroscience & Cell Biology, UTMB, Galveston, TX
9/1991-8/1996	Clinical Medicine, M.D. Fourth Military Medical University, Xi'an, China
9/2003-12/2003	Certificate Course: Science, Law and Society University of Houston Health Law & Policy Institute and UTMB

### PROFESSIONAL WORK HISTORY AND TRAINING EXPERIENCE:

9/1996-8/2002	Otolaryngologist and Research Assistant Institute of Space Medico-Engineering, Beijing, China
9/1997-8/1998	Otolaryngologist Department of Otolaryngology at TongRen Hospital, Beijing, China

#### RESEARCH PROJECT:

The muscarinic acetylcholine receptor expression on pigeon vestibular hair cells and its modulation of ionic channels, especially one of the inward rectifier potassium channels, Kir2.1.

#### ANNUAL SEMINAR PRESENTATION:

- 2004 Muscarinic Receptors in the Vestibular Epithelium and Their Modulation of Ion Channels
- 2005 Muscarinic Receptor Subtype Expression on Avian Vestibular Hair Cells
- 2006 Expression of mAChR Subtypes on Vestibular Peripheral Neurons
- 2007 Modulation of pKir2.1 by Muscarinic Receptor Activation

#### MEMBERSHIP IN SCIENTIFIC SOCIETIES:

- 2005-present The American Physiological Society
- 2008 The Society for Neuroscience

#### HONORS:

- 2007 Curtis W. Lambert Scholarship
- 2007 George Sealy Research Award in Neurology
- 2006 Who's Who Among Students in American Universities & Colleges
- 2002 Scientific and Technical Award: The Third Prize

#### PUBLISHED:

##### A. ARTICLES IN JOURNALS:

Li GQ, Kevetter GA, Leonard RB, Prusak DJ, Wood TG, Correia MJ. Muscarinic acetylcholine receptor subtype expression in avian vestibular hair cells, nerve terminals and ganglion cells. *Neuroscience*. 2007 Apr 25;146(1):384-402. Epub 2007 Mar 27. (*Figure 4 was selected for the cover of this issue*).

##### B. MEETINGS:

1. Li, G.Q., Leonard, G. K., Leonard R. B., and. Correia M. J. Muscarinic Receptor Subtype Expression in Avian Vestibular Hair Cells and Nerve Terminals. 2005 Experimental Biology Meeting abstracts. The FASEB Journal, 19, Abstract 681.13. 2005.
2. Li, G.Q., Correia, M.J., The Inhibitory Effects of Carbachol on Pigeon Inwardly Rectifying Potassium Channel (pKir) Expressed in Transfected tsA-201 Cells and Native Type II Vestibular Hair Cells, Society of Neuroscience Annual Meeting, Abstract 47.7. 2005.
3. Schloesser Ryan, Li, G. Q., Correia M.J. Fluorescent Labeling of Ion Channels in Pigeon Vestibular Hair Cells, Tri-Beta National Honor Society Regional Convention, 2006.
4. Li, G.Q., Correia, M.J., The Inhibitory Effects of Carbachol on Pigeon Inwardly Rectifying Potassium Channel (pKir) Expressed in Transfected tsA-201 Cells and

Native Type II Vestibular Hair Cells, National Student Research Forum 48<sup>th</sup> Annual Meeting, 2007.

C. ABSTRACTS:

1. Li, G.Q., Leonard, G. K., Leonard R. B., and. Correia M. J. Muscarinic Receptor Subtype Expression in Avian Vestibular Hair Cells and Nerve Terminals. 2005 Experimental Biology Meeting abstracts. The FASEB Journal, 19, Abstract 681.13. 2005.
2. Li, G.Q., Correia, M.J., The Inhibitory Effects of Carbachol on Pigeon Inwardly Rectifying Potassium Channel (pKir) Expressed in Transfected tsA-201 Cells and Native Type II Vestibular Hair Cells, Society of Neuroscience Annual Meeting, Abstract 47.7. 2005.
3. Schloesser R.W., Li, G.Q., Rae, J.L., Correia, M.J., KCNQ Family Member Protein on Type I and Type II Pigeon Vestibular Hair Cells, Society of Neuroscience Annual Meeting, 2006.

D. REPORT:

Yongzhi Li, Yuanliang Wu, Hong Zhang, Gang Q. Li. Requirement analysis of Medical Administration and Medical Experiment for Mid-long Term Manned Space Flight, 2002.

RESEARCH SKILLS:

- A. Inner ear surgery of pigeon, gerbil, and chicken
- B. Confocal microscope operation (~300hrs logged on confocal microscope (LSM 510))
- C. Tissue fixation
- D. Frozen section preparation
- E. Immuno-fluorescent histochemistry and cytochemistry
- F. Protein Blotting techniques (Western Blot)
- G. Patch clamp techniques (whole cell ruptured & perforated patch)
- H. Isolation of vestibular hair cells and ganglia
- I. Tissue Slice preparation (sliced vestibular end organs for hair cell patch clamp)
- J. Knowledge and use of Adobe® Photoshop®, Adobe® Illustrator®, Origin, Clampfit software

Permanent address: EnJiLi XiaoQu, 32-1-103, HaiDian District, Beijing 100036, China  
This dissertation was typed by the author.